Optimization of wind farm power production using innovative control strategies

Duc, Thomas; Giebel, Gregor; Göçmen, Tuhfe; Korpås, Magnus ; Coupiac, Olivier

Publication date:
2017

Document Version
Publisher's PDF, also known as Version of record

Optimization of wind farm power production using innovative control strategies

Department of Wind Energy Master Report

Thomas Duc

DTU Wind Energy-M-0161

June 2017

DTU Wind Energy
Department of Wind Energy

Authors: Thomas Duc

Title: Optimization of wind farm power production using innovative control strategies

DTU Wind Energy-M-0161
June 2017

Project Period:
January – June 2017

ECTS: 30

Education: Master of Science

Supervisors:

Gregor Giebel
Tuhfe Göcmen
DTU Wind Energy

Magnus Kopås
NTNU

Olivier Coupiac
ENGIE Green

Remarks:
This report is submitted as partial fulfillment of the requirements for graduation in the above education at the Technical University of Denmark.

DTU Wind Energy is a department of the Technical University of Denmark with a unique integration of research, education, innovation and public/private sector consulting in the field of wind energy. Our activities develop new opportunities and technology for the global and Danish exploitation of wind energy. Research focuses on key technical-scientific fields, which are central for the development, innovation and use of wind energy and provides the basis for advanced education at the education.

We have more than 240 staff members of which approximately 60 are PhD students. Research is conducted within nine research programmes organized into three main topics: Wind energy systems, Wind turbine technology and Basics for wind energy.

Technical University of Denmark
Department of Wind Energy
Frederiksborgvej 399
4000 Roskilde
Denmark

www.vindenergi.dtu.dk

Abstract

Wind energy has experienced a very significant growth and cost reduction over the past decade, and is now able to compete with conventional power generation sources. New concepts are currently investigated to decrease costs of production of electricity even further. Wind farm coordinated control is one of them; it is aimed at increasing the efficiency of a wind farm and decreasing the fatigue loads faced by wind turbines by reducing aerodynamic interactions between them. These objectives are achieved considering two different strategies: curtailing an upwind turbine to reduce the wind speed deficit caused by the wake downstream, or yawing the turbine to deflect the wake away from the downwind turbine.

Simulation results found in the literature indicate that an increase in overall power production can be obtained. However they underline the high sensitivity of these gains to incoming wind conditions. It is therefore not known to what extent these gains can be reproduced in a real wind farm where wind conditions are very fluctuating. The French national project SMARTEOLE constitutes one of the first attempts of implementing these strategies on a full scale wind farm. A ten month measurement campaign was realized in 2016 in which different scenarios were tested. In this master thesis the experimental data from this field test are analyzed and used to calibrate two different models. An optimization process is then performed based on these models to find the maximum power production of two aligned wind turbines.

The experimental results show that the scenarios implemented during the first measurement campaign did not achieve an increase in overall power production, which confirms the difficulty to realize wind farm power optimization in real operating conditions. In the curtailment field test, the down-regulation of the upwind turbine was probably too high to expect the downstream wind turbine to compensate for that loss. Total losses were quite low though, meaning that a significant part of the upwind turbine lost energy is regained downstream by the second turbine. Regarding the yaw offset strategy, no wake deflection could be detected at the downstream turbine and therefore no conclusion be drawn about the impact of yaw misalignment of the upstream turbine. In both cases, unfavorable wind conditions and an incomplete knowledge of the wind turbine behavior in the farm considerably reduced the amount of usable data in the wake sector.

However the data recorded during this campaign could still be used to calibrate models. First a wake deficit model was obtained by re-calibrating the well known Jensen model. Contrary to the original Jensen model, where the wake expansion coefficient is assumed to be constant for the whole wind farm, in this new proposed model it is calculated at each wind turbine based on the local measurement of turbulence intensity. In that way the wake added turbulence intensity can be taken into account and thus the wind speed deficit caused by wind turbines in the wake of other turbines further upstream is not over-estimated. This model proved to be in very good agreement with the measured power deficit in the wind farm. Second, a Ct model giving variation of wind turbine thrust coefficient during down-regulation could be derived from the analysis of guaranteed power curves and validated using experimental data.

The combined power production of two aligned wind turbines was finally maximized considering a curtailment strategy and using these two models. The results from the optimization process in full wake conditions show that the more important gains are obtained in the wind speed range $6 - 10$ m/s, i.e. when both the Cp and the Ct of the wind turbines are high. The maximum expected increase in combined power production is found to be in the order of 2 to 3% for a particular wind speed bin, however when averaged over the complete wind speed range these gains represent only 0.3 to 0.5%. The width of the wind direction sector in which the coordinated control is profitable could also be assessed to 10°, centered on the full wake direction. These results confirm the high sensitivity of coordinated control to incoming wind conditions, and that gains that are to be expected considering two wind turbines only are small. New scenarios based on the results found during this thesis are supposed to be implemented during the second field test campaign of SMARTEOLE planned for the second semester of 2017.

Acknowledgement

As this master thesis was carried out in a company, ENGIE Green, a lot of people were involved in my work in both the DTU and the ENGIE sides and I would like to thank them here.

On the DTU side, I would like to thank particularly Tuhfe Göçmen and Gregor Giebel for the guidance all along the thesis and the very fruitful feedbacks received regularly during the Skype meetings. I also thank Jonas Kazda for having kindly sent me his files containing the data for the Cp and Ct surfaces of the NREL 5 MW wind turbine and for the useful papers that helped me to built the bibliography.

On the ENGIE Green side, I would like to thank warmly Olivier Coupiac for the day to day supervision of my work and all the advice provided during these five months. Many thanks also to Arthur Petit for the help in getting starting with R and in processing the data, and to Nicolas Girard, Sophie Guignard, Aurélien Proust, Lucas Alloin and all the other people that are involved in the SMARTEOLE project.

Thanks also to Magnus Korpås from NTNU for having accepted to co-supervise the thesis despite his very busy timetable.

In a larger scale I would like to thank all the people involved in the organization of my Joint Nordic Master "Innovative Sustainable Energy Engineering" in all universities involved in the project, and in particular Ida Johanne Ulseth at NTNU for the organization of the Winter School and the great help in dealing with all the administrative issues.

Last but not least, I would also like to thank especially my colleagues from the Wind Energy track, Meadhbh Ní Chléirigh, Feng Guo, Sayantan Chattopadhyay and Luis Guajardo for the amazing two years we had together. Hopefully we will find some time in the future to organize again some other *Moon Cake Sessions*!

Contents

1 | Introduction

Energy is one of the main challenges of the 21st century. The demand keeps increasing, led by the strong growth in emerging countries while at the same time conventional fossil fuel resources are depleting. In order to cope with this problem, and also to limit as much as possible greenhouse gases emissions, a huge development of renewable energies is needed as they represent a clean and inexhaustible source of production.

There are many different ways of producing energy from a renewable resource, but among those wind energy and solar photovoltaic are the ones showing the best promises and currently experiencing the highest growth rate. Their main advantage bears on the fact that unlike other type of green energies (like hydropower or geothermal energy), they are evenly distributed around the world. This makes them attractive for many countries and therefore explains their significant expansion over the last decade.

In particular, the total installed capacity of wind energy in Europe has been more than tripled during the past ten years (from 41 GW in 2005 to 154 GW in 2016) and is now the second most important power generation capacity after natural gas, as illustrated on Figure 1.1 [1]. The share of wind energy in the total European Union (EU) electricity consumption represented 10.4% in 2016, but in some countries the penetration rate of wind is much higher. It was for example 37% in Denmark, 27% in Ireland and 25% in Portugal [1].

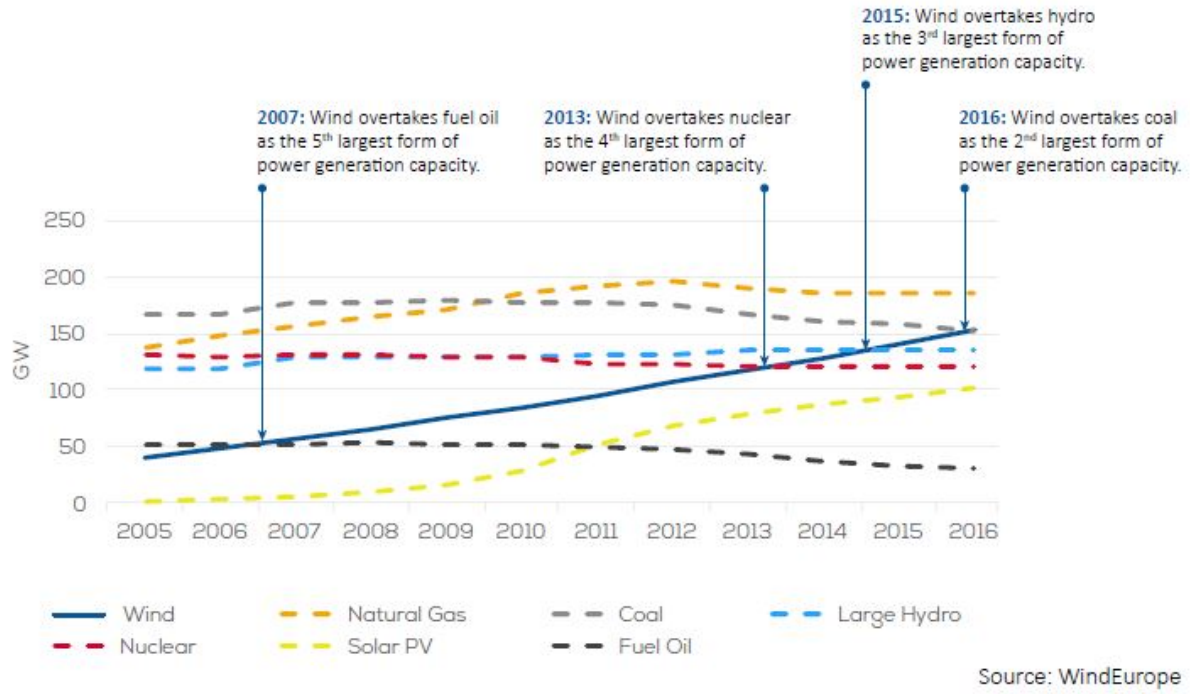

Figure 1.1: *Cumulative power capacity in the European Union between 2005 and 2016. From [1]*

This growth was first boosted by support mechanisms implemented in different states of the EU, but over the years wind energy has become a very competitive source of producing energy. The Levelized Cost of Energy (LCoE) of onshore wind energy is now ranged between 52 to 110 €/MWh, which is in the same order of magnitude of conventional power generation sources [2].

In order to decrease further the LCoE of wind energy and makes it even more competitive, new concepts are currently being studied. The French national project SMARTEOLE is a perfect example as it is investigating innovative control strategies meant to improve sustainability and efficiency of wind energy at three different scales: the blade, the wind turbine and the farm.

The work presented here is closely related to SMARTEOLE as it was carried out in one of the companies involved in the project, ENGIE Green. It is focused only on wind farm coordinated control whose main objectives are to increase the efficiency of a wind farm and decrease the fatigue loads faced by the wind turbines. This goal is achieved by controlling the wind turbines in such a way that aerodynamic interactions between them are reduced.

Contents and Aim of the Thesis

This master thesis was written between February and June 2017 and is based on the results from the first field test campaign of SMARTEOLE realized between December 2015 and September 2016. The two different wind farm strategies that are studied, the curtailment strategy and the yaw offset strategy, were implemented during this first campaign. The objective of the thesis were thus to analyze the experimental data recorded during the field tests to quantify the impact of these strategies, use these data to calibrate different models, and from these models derive optimal wind turbine settings in order to prepare he second campaign planned in the second semester of 2017. It is mainly concentrated on the optimization of the wind farm power production, consequences about wind turbine loading are sometimes discussed but not thoroughly investigated.

First, basics about aerodynamics of wind turbine wake and wind turbine control are quickly exposed in Chapter 2. A literature review of the main results about wind farm coordinated control is also provided. Then, in Chapter 3, the context of the SMARTEOLE project is presented and the experimental setup used during the field tests described.

A significant work of data analysis was carried out in this thesis in order to process the huge quantity of data recorded by the different sensors in the wind farm. In particular, the data had to be filtered and corrected for different bias and offsets. Part of this work had already been realized in 2016 during the first months of the campaign by another student. This thesis completes this first analysis by providing a correction of the wind speed through the derivation of a nacelle transfer function using nacelle lidars. Then several studies are led to analyze in details the performance of the wind farm under normal operating conditions. The efficiency of the farm and the turbulence intensity distribution are measured, and an alternative way of assessing the incoming wind speed is also discussed. All these issues are developed in Chapter 4.

The Chapter 5 is focused on the wake modeling. Two well known wake models, the Jensen and the Larsen models, were implemented and compared to experimental data. A re-calibrated Jensen model is chosen and validated considering a particular wake event in the farm.

Finally, results of the experimental field tests for both the curtailment and the yaw offset strategies are analyzed in Chapter 6 and Chapter 7, respectively. Regarding the curtailment strategy, a Ct model is derived from the analysis of the wind turbine guaranteed power curves to assess variations of the thrust coefficient with down-regulation. This model is validated using the available experimental data, and used in association with the re-calibrated Jensen model to optimize the combined power production of two aligned wind turbines.

2 | Theoretical Background and Literature Review

In this chapter are quickly explained the most important principles about wind turbine wake and control, needed to fully understand the concepts addressed in this thesis. Then a short literature review is provided about wind farm coordinated control for optimized operation.

2.1 Wind Turbine Wake

The extraction of the wind kinetic energy by a wind turbine rotor has two main consequences on the flow downstream: the wind speed decreases and the flow becomes more turbulent. These issues create repercussions on the downstream wind turbines which are affected by an upstream emitted wake. The wind speed deficit causes a decrease in the produced power, while the increased turbulence is responsible for a rise in the fatigue mechanical loads [3]. It is therefore recommended to space as much as possible the wind turbines in a wind farm, however due to technical and economical constraints, an important spacing is sometimes difficult to achieve. Furthermore, the influence of a wind turbine wake has been measured up to 15 D (diameters) [4]. This distance is much greater than the usual values used in practice, i.e. 6 to 10 D in the prevailing wind directions and around 3 D in crosswind directions [3]. As a consequence it can be expected that wake will be present for any wind farms.

When studying wind turbine wake, a distinction must be made between the near wake and the far wake [5]. A very close link exists between these two notions but they account for a different behavior of the aerodynamics inside the wake. The near wake is the region located just behind the rotor and is therefore greatly influenced by its geometry. Due to high gradient of wind speed and pressure between the wake and the undisturbed flow, a shear layer is created and grows with the distance from the rotor. In this layer an important sheared-generated turbulence can be found, which helps in the transfer of momentum between the wake and the surrounding flow [6]. As the high velocity fluid is mixed outside the wake is mixed with the low velocity fluid inside it, the wake expands, as illustrated on Figure 2.1 [3]. Once the shear layer has reached the center of the wake, the near wake region ends and the far wake region begins. The length of the near wake region is mainly dependent on the ambient turbulence intensity and the thrust coefficient of the wind turbine, which indicates the fraction of kinetic energy which is extracted from the wind. A semi-empirical expression can be derived from these two parameters to compute the length of the near wake [7], but in most cases the transition from near wake to far wake happens between 2 and 5 D [8].

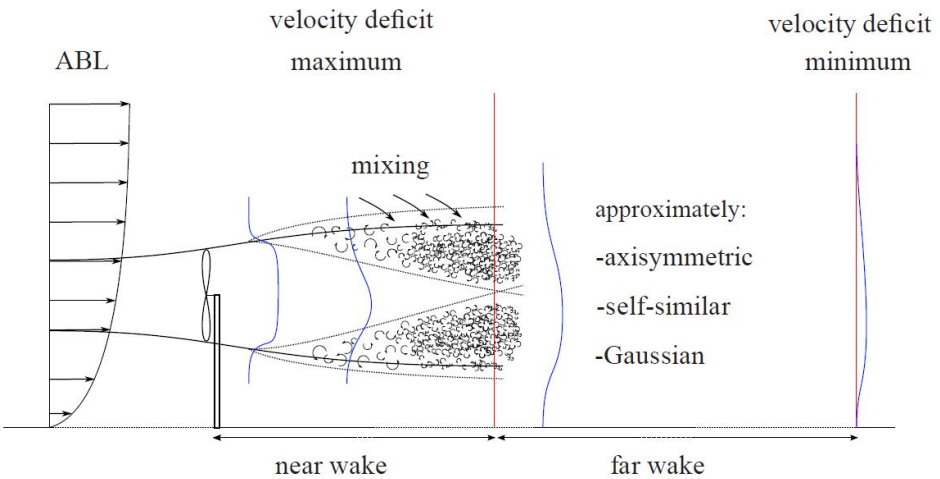

Figure 2.1: *Development of a Wind Turbine Wake. From [3]*

In the far wake region, the wind speed deficit and turbulence intensity profiles can be considered in first approximation as axisymmetric and have self-similar distributions on the cross direction of the wake [8]. The geometry of the rotor is not as important as in the near wake region, and the thrust on the turbine and the wake added turbulence are enough to characterize the flow. It is in this region that are generally located downwind turbines in a wind farm, the attention is therefore put on the wake and turbulence models, interaction between multiple wakes and effects from the topography [5]. As this thesis is aiming at reducing the impact of wake on the downwind turbines, the work realized is mainly focused on this particular region and some key elements about the far wake are provided here.

As already mentioned above, a wind turbine wake can have noticeable effects at very significant distances downstream. However it is admitted that these persistent effects are generally related to the increased turbulence in the flow, as the decay of velocity deficit is more rapid than the decay of added turbulence intensity [5]. In first approximation, they can be approached respectively by $x^{-2/3}$ and $x^{-1/3}$ (with x the downstream distance), while the wake width increases with $x^{1/3}$ [8].

Stronger wakes can be found when both wind speed and ambient turbulence intensity are low. This is because the two parameters that mainly influence the recovery of the wake are the thrust coefficient and ambient turbulence intensity. Indeed, the former is indicating the ratio of kinetic energy extracted from the wind. When it decreases, typically at high wind speed when the power of the rotor is limited to its rated value, the downstream flow is left more energetic and thus the impact of the wake is smaller. Regarding the latter, a higher ambient turbulence provides a better mixing between the two flows and therefore allows a faster restoration of the initial velocity [3].

An important consequence from this observation is that when several turbines are aligned in a row, the wake emitted from one turbine downstream is recovering quicker than from one upstream. Indeed, the downstream turbine is submitted to an increased turbulence due to the upstream wake. It is generally found for multiple wake events that the wind speed deficit is only important for the first turbine exposed to the wake, for the other ones the deficit increases only slightly and finally reaches an equilibrium value when the turbulence seems to be saturated [5]. This is also noticed on the loading of the downstream wind turbines, where no appreciable differences can be found between the loading from single and multiple wake events [8].

Finally, a last remark is made about a phenomenon called wake meandering. This consists of high scale movement of the wake, due to the presence of large eddies [3]. However, as this issue was not considered in this thesis, this topic in not developed here. In any case, the time scale of the meandering effects are expected to be much larger than the one considered for the coordinated control, which should be implement on a second-wise basis.

2.2 Wind Turbine Control

Wind turbine control can be related either to the electrical control or the mechanical control. In the electrical control, the turbine is seen as a generator connected to the grid, and the issues addressed are generally related to the stability of the network, e.g. ensuring a good quality of the output electrical power, the reactive power capability, the behavior during fault [9], etc. However, the problems discussed in this thesis are more linked with the mechanical control of wind turbines and thus the electrical control will not be developed further.

The two main objectives of mechanical control are to control the aerodynamic power extracted from the wind and to limit the loads exerted on the wind turbine structure. Modern wind turbines are now in most cases variable speed and variable pitch controlled wind turbines. This configuration allows to govern two parameters, the rotor speed (through the control of the generator torque) and the blade pitch angle, and ensures a smooth and optimized control of the output power.

A more detailed presentation of the different regions considered in the control, focused on the wind turbines studied in this thesis, will be provided later in Section 3.2.2, but the main basics are first explained here. At low wind speed the rotor speed of the turbine is adapted to track the optimal operation point which guarantees a maximum extraction of wind energy. When the turbine reaches rated

power, the electrical power is controlled thanks to the generator torque and the variation of the blade pitch angle maintains the rotor speed around its rated value [10]. Fluctuations of wind speed can be smoothed using the rotor speed. During a sudden increase, the extra energy from the wind can be stored as kinetic energy in the rotor to maintain constant the electrical power. When the wind speed decreases, this energy is restored to the generator as the rotor speed drops. In the case of a constant increase in the wind speed, then the blade pitch angle is changed to reduce the aerodynamic properties of the wind turbine and prevent the rotor from accelerating further. A sketch of the various mechanisms involved in the system can be found on Figure 2.2 below.

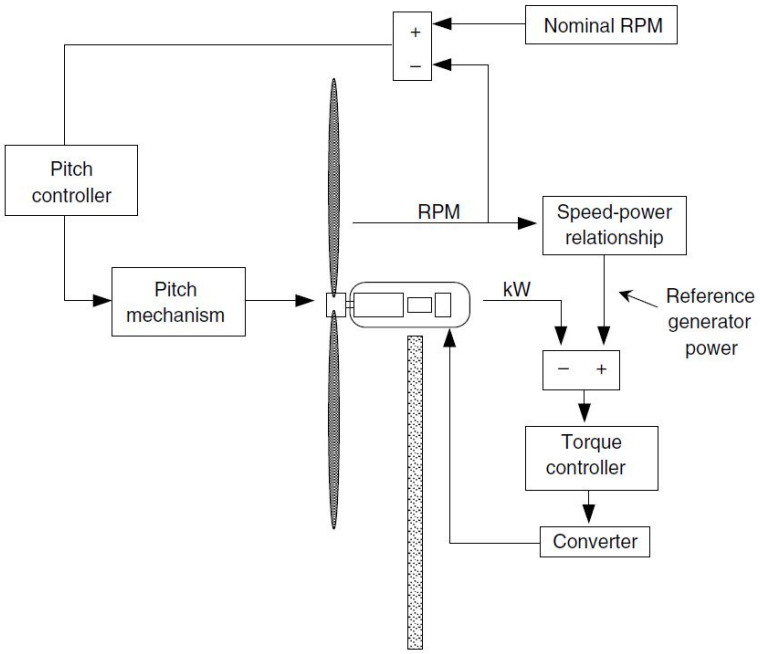

Figure 2.2: *Overview of the mechanisms involved in the control of a modern wind turbine. From [10]*

A main concern regarding wind turbine control is the loading. Wind turbines are designed to face a certain amount of extreme and fatigue loads during their lifetime (the design requirements are developed in [11]), and therefore they must be controlled in a way ensuring that these conditions will not be exceeded. Loads on wind turbines are caused by several reasons, the most commons being the wind shear, the tower shadow, the wind turbulence, and the wake from an upwind turbine. Some control strategies, such as a damping of resonances or an individual pitch control, can be developed at wind turbine scale to reduce these loads [12]. Other strategies can be implemented at a wind farm scale in order to decrease the overall loading of all wind turbines. These issues are discussed on the next section.

2.3 Wind Farm Coordinated Control

There are two categories in the area of wind farm coordinated control [13]. The first one is related to the electrical engineering and deals with the questions of quality of generated power and stability of the grid. The other one is more related to mechanical engineering and corresponds to the study of aerodynamic interactions between the wind turbines of a farm. So far, most of the research based on wind farm control has been focused on the first category; nonetheless, the second category has become increasingly important over the past few years [14].

This thesis is focused on this second kind of wind farm control, therefore questions about electrical engineering are not developed further. Principles and objectives behind mechanical wind farm control are first explained, and then the results presented in the literature about the two control strategies studied in this thesis, the curtailment (or down-regulation or derating) strategy and the yaw offset strategy, are briefly reviewed.

2.3.1 Reasons and Objectives

Wind turbines are generally aggregated in wind farms in order to reduce overall costs, such as engineering, grid connection and operation and maintenance costs. However this creates wake interactions between the turbines, whose causes and consequences have already been developed in Section 2.1. To reduce the impact of wake, the best practice consists in locating the turbines in a way that minimize those interactions. However in reality, due to a certain number of constraints imposed on the development of wind farms, it is very difficult to respect these conditions. This can lead to wind farm layout where the spacing between the wind turbines is particularly small, such as in the Lillgrund offshore wind farm and *La Sole du Moulin Vieux* wind farm which will be presented later in this paper. In general the spacing between wind turbines is in the order of 6 – 10 D for prevailing wind directions and around 3 D in the crosswind directions [3]. Even at this distances there might still be wake interactions, especially in offshore wind farms where wakes are more persistent.

Once the wind turbines of the farm have been installed, the only remaining possibility to reduce wake interaction is wind farm coordinated control. In the traditional single wind turbine control, presented above in Section 2.2, each wind turbine maximizes its own power production without taking into account the presence of downwind wind turbines. This is no longer the case in wind farm coordinated control: the particular layout of the farm is now included in the analysis and all the outputs are considered at a wind farm scale. Different objectives can be investigated: overall power maximization, following a wind farm power reference and fatigue reduction [14]. To achieve these objectives, two strategies are generally considered in the literature: in the curtailment strategy the upwind turbines are down-regulated to leave more energy for the downwind turbines, and in the yaw offset strategy the upwind turbines are yawed to deflect the wake away from the downwind turbines. Some papers also mention the possibility of a tilt control [15, 16], where the rotor of the upwind turbine is tilted forward so that the wake is deflected towards the ground. However, tilt control is not implemented yet in modern wind turbines, and moreover tilting the rotor forward would also reduce the blade tower clearance.

Finally it must be emphasized that these two strategies are highly dependent on the incoming wind conditions. An optimal power curve will allow a gain for a certain wind direction but might cause a loss if the wind changes even of a few degrees. To be implemented correctly, these incoming conditions must be known very accurately in real time, and the wind farm control must adapt very quickly to maximize the possible gains and reduce the losses. These strategies have probably a better potential in offshore wind farms: the wind turbines are generally organized in grids and therefore are affected by wake in all directions, and they are furthermore exposed to stronger wake effects.

2.3.2 Principle of the Curtailment Strategy and Results

As developed in Section 2.1, the wind speed deficit and added turbulence intensity caused by a wind turbine wake is closely related to the thrust coefficient Ct of the upwind wind turbine. This thrust coefficient is itself dependent on the aerodynamic efficiency of the wind turbine, and thus on its power performance through the performance coefficient Cp. Hence the principle of the curtailment strategy is fairly simple: decreasing the aerodynamic properties of the upwind wind turbine to reduce the impact generated by its wake. The power loss induced by the diminution of the upwind Cp is expected to be regained at the wind turbines downstream thanks to a smaller wind speed deficit.

A theoretical model was proposed in the framework of the "Heat and Flux" project developed at the Energy Center of the Netherlands [17]. Considering two turbines modeled by actuator disks and BEM theory [6], it was found that a gain of 4.8% in overall production could be obtained when reducing the axial induction factor from 1/3 to 1/5. This is because the Cp curve around the Betz limit is very flat, while the Ct curve is steeper and therefore decreasing the axial induction factor reduces the Ct more than the Cp, as illustrated on Figure 2.3. It was also found that the optimal induction factor of the k^{th} wind turbine in a row of n turbine was given by $\frac{1}{2(n-k)+3}$.

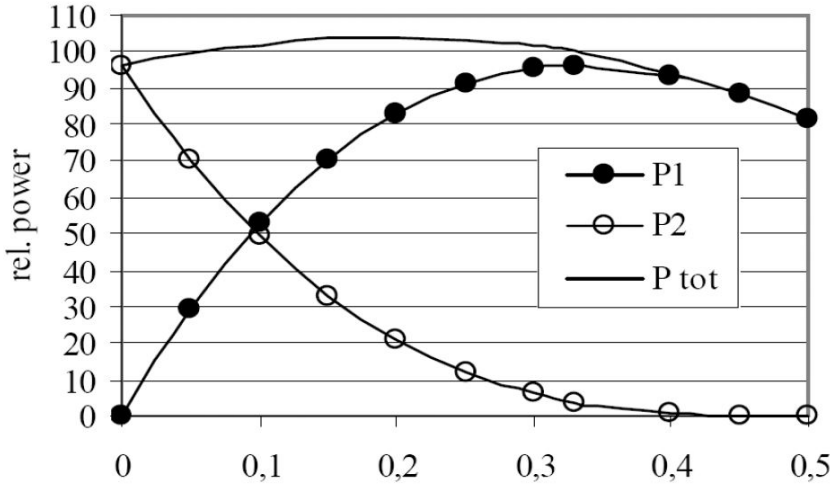

Figure 2.3: *Evolution of the combined relative power of two wind turbines as a function of the upwind turbine induction factor. From [17]*

Most of the results developed so far are based either on simulations or wind tunnel experiments. They report indeed an increase in combined power production, but this increase remains small, around 4 to 6% for the most critical wind conditions (depending on the number of wind turbines considered), and around $0.5 - 1\%$ when averaged over all wind speed and directions [14]. In [18] a gain up to 40% at low wind speed is found but this is only because the curtailment of the upwind wind turbine reduces the wake deficit at the downwind wind turbines just enough to go above the cut-in wind speed. These results must also been taken cautiously since [19] observed that the choice of the wake model has a great influence on the results.

Simulations realized in [20] also underlines the impact of atmospheric conditions on the result of the curtailment strategy. It was found a gain of 3% at low turbulence level but this gain decreases down to 1% and -14% when considering medium and high turbulence, respectively. This underlines the difficulty to reproduce the results obtained in simulation and wind tunnels, where the incoming conditions can be controlled very accurately, into actual full scale wind farms, submitted to highly fluctuating conditions. There is apparently only one full scale test of this curtailment strategy realized at the EWTW wind farm [21] in the scope of the "Heat and Flux" project, considering 5 Nordex80 2.5 MW with 3.8D spacing. Pitching the upwind wind turbine by 2° was allowing a gain on the combined power production of the two most upwind turbines, while the remaining 3 were not really influenced by the change [17].

The impact on wind turbine loading is not developed much here since this thesis is more focused on power optimization. In general, it can be expected that the static loading on the wind turbine affected by down-regulation is decreased due to the reduced aerodynamic properties. On the contrary, the static loading at the downwind turbine is expected to increase since it operates at a higher power setpoint [22]. However, this increase in static loading will probably be compensated by the decrease in fatigue loading allowed by the reduced wake-added turbulence intensity.

2.3.3 Principle of the Yaw Offset Strategy and Results

When a wind turbine is not facing directly the wind, and therefore has a certain yaw error, the wake that develops downwind is deflected with a certain angle. This principle is illustrated on Figure 2.4 below.

The yaw offset strategy consists thus to create an artificial yaw error on the upwind turbine in order to deflect the wake away of the downstream turbine. In [15], simulations are performed on the NREL 5MW reference wind turbine [23] using a CFD tool (SOWFA) and confirm that yawing a turbine can indeed deflect its wake: at 7 D downstream the wake is deflected by 0.5 D for a yaw angle of 35°. The effect of this strategy on the fatigue loads (for the blade, drivetrain, tower and yaw bearing loads) and power production of the upwind wind turbine is also investigated using FAST. It seems that all fatigue loads considered are decreasing by 10 to 20% for the same yaw angle of 35°, however the active power is also reduced by more than 30%.

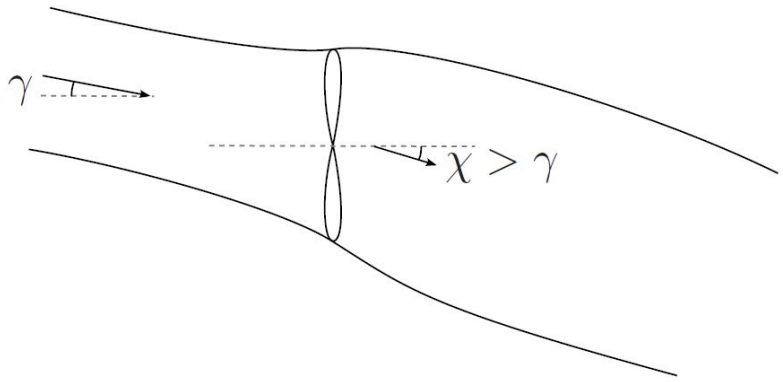

Figure 2.4: *Deflection of wind turbine case due to the turbine yaw error. From [3]*

In a related paper, the impact of this wake deflection on the downwind turbine is studied using the same tools [16]. The reference conditions was taken as the downstream wind turbine being under the full wake of the upstream turbine. The results show an increase of 4.6% in the combined power production of the two turbines for a yaw angle of 25°. However the fatigue loads on the downstream turbine seem to increase, especially for the blades and the drivetrain. This is mainly explained the fact that due to the wake deflection the downwind turbine goes from full wake conditions to partial wake conditions which causes a greater fluctuation in the blade cycle and thus an increased fatigue. Individual pitch control is shown to be able to decrease the blade loading, without changing much the power production. Experiments in wind tunnel [24] shows that a 12% increase in combined power production of two turbines (separated by a distance of 3D) can be achieved by yawing the upstream turbine by angle of 30°.

Similarly as for the curtailment strategy, they are very few full scale experiments available in the literature, and the only that could be found were also led at the ECN. In [25] is studied the impact of yawed operation on the power production and the blade loading considering the same Nordex wind turbines of the EWTW wind farm. It is found that the decrease in power production of the turbine is more important at high tip-speed ratio, but a very important scatter of the data is found between the different wind turbines. Blade loads are found to be increased especially in the flapwise direction since the edgewise loads are mainly driven by gravity forces.

The use of the yaw offset strategy in order to increase the power production of a wind farm was investigated through the concept "Controlling Wind" in ECN's scaled wind farm [26]. The wind turbines considered in this test are only 10 kW wind turbines (7.5 m hub height, rotor diameter of 7.6 m). Unfortunately, an important scatter in the recorded data could not allow any clear conclusions about the possibility of achieving increased wind farm power production thanks to this concept. Nevertheless, some promising results were obtained for small wind speed (around 4 m/s) and low yaw angles (below 10°).

2.3.4 Summary

As a conclusion, it can be said that wind farm coordinated control for minimizing aerodynamic interactions between the wind turbines is a relatively new concept that has been investigated over the last decade. It is aimed to decrease the levelized cost of energy on wind energy by increasing the power production of a wind farm and/or reducing the loads faced by the turbines.

Two strategies have been mainly considered so far: the curtailment and the yaw offset strategies. They basically consist in acting on the upstream wind turbine to decrease or deflect the wake on the downstream wind turbine. Assessing accurately the incoming wind conditions is an essential condition to achieve these objectives as these strategies appear to be very sensitive to both wind speed and direction.

Most of the results obtained so far are based on simulations and seem to highlight potential for increased power production and/or load reduction. However there is a lack of experimental data to confirm these tendencies, and they are generally limited to wind tunnel experiments where the flow can be controlled

closely. The real wind conditions that are facing wind turbines are known to be much more fluctuating, therefore it is really difficult to assess to what extent the results obtained in simulations and wind tunnel can be reproduced in a full scale wind farm.

The French national project SMARTEOLE, presented on the next chapter, is aiming at giving some answers to this question as these two strategies are implemented on an operating onshore wind farm.

3 | The *SMARTEOLE* Project

In this chapter is developed the context in which this thesis is written. This work is carried out as a part of a national project called SMARTEOLE and gathering several French research organizations and companies who have an interest in wind energy. A brief description of the actors and objectives of SMARTEOLE is first provided in Section 3.1, then the experimental setup used during the project is described in Section 3.2. Finally, the first results obtained in the first twenty months of the project are quickly presented in Section 3.3.

3.1 Project Members and Objectives

As developed in the previous chapter, the need for an improved control of wind turbines is getting more and more important and research on this topic is very dynamic. As a perfect example, a national project has been launched in France in 2014 between several industrial actors and research institutions. The name of the project is "*Smart Rotors to Improve Wind Energy Efficiency and Sustainability*", and is summarized under the acronym SMARTEOLE [27]. This project is supported by the *Agence Nationale pour la Recherche* who funds 800 k€ from the 2.2 M€ budget. It is supposed to last 42 months, between January 2015 and June 2018, and aims at designing control solutions in order to improve wind energy efficiency and sustainability, based on real time measurement of the incoming wind flow conditions.

The two following sections presents the different actors taking part in the project and its more detailed objectives.

3.1.1 Project Partners

The SMARTEOLE project is gathering six different institutions, two of them coming from the world of industry, the other ones being research organizations. A quick presentation of each of them and their different research areas is provided here.

ENGIE Green

ENGIE Green (EG) was born on December 1st 2016 from the merging of two smaller companies, Futures Energies and MAÏA Eolis (the SMARTEOLE project was initiated by the latter). It is a subsidiary company of the big French energy company ENGIE, originally specialized on natural gas but having developed its mix towards renewable energies over the last few years.

ENGIE Green owns a capacity of 860 MW which is 100% renewable and mainly bears on onshore wind energy (810 MW) and solar photovoltaics (50 MW). Some minor remaining capacity consists of hydroelectric power plants, and currently some offshore wind energy project are being developed. ENGIE Green is part of the Business Unit *France Renouvelables* which gathers other renewable energy companies in France completely or partly owned by the group and represents an installed capacity of almost 6 GW. In particular, it is in France the first onshore wind energy producer (1550 MW), the first solar photovoltaics producer (600 MW) and the second hydroelectric producer (3550 MW).

Avent Lidar Technologies

Avent Lidar Technologies (ALT) is a French company that was created in 2009 from a joint investment of Leosphere (specialized on ground-based lidars) and Renewable NRG Systems (wind measurement technology). The company develops, manufactures and sells lidars (Light Detection And Ranging), remote sensing instruments used to measure the atmospheric conditions. Compared to conventional wind measurement sensors (cup or sonic anemometers placed on a met-mast), they offer a certain flexibility and new possibilities that makes them very interesting for wind energy.

Leosphere and ALT are dedicating 20% of their expenses on R&D projects intended to increase the reliability of lidar measurement and to find innovative solutions involving their combined use with wind turbines to improve the efficiency and sustainability of wind energy.

PRISME

The *Laboratoire pluridisciplinaire de recherche en ingénierie des systèmes* (PRISME) is dependent of the University of Orléans. It is a multidisciplinary laboratory that studies engine combustion, aerodynamics and mechanics, signal processing, automatics and robotics.

In terms of wind energy, the PRISME is particularly interested in aerodynamics of rotor systems and transport mechanisms in the atmospheric boundary layer. Therefore, a great attention is paid to wind turbine wakes which explains their involvement in the SMARTEOLE project.

IFPEN

The *Institut français du pétrole Energies nouvelles* (IFPEN) is a research organism which is co-funded by the state and by private investments. Its main goals are to bring innovative solutions to the climate and energy challenges of the 21st century, and to develop technologies that can be used directly by the industry.

Regarding wind energy, the IFPEN is developing a control system called WiSE-Control which aims at reducing greatly the loads faced by wind turbines based on the anticipation of the incoming wind speed provided by a nacelle lidar measurement. This system is currently tested during the SMARTEOLE project.

LAAS

The *Laboratoire d'analyse et d'architecture des systèmes* (LAAS) is an unit from the CNRS (National Center for Scientific Research) located in Toulouse. Their research area covers a wide range of topics related to critical information processing, networks and communications, robotics, decision and optimization, micro- and nano-systems RF and optics, nano-engineering and integration, energy management, micro-nano- and bio-technologies.

LHEEA

The *Laboratoire de recherche en Hydrodynamique, Energétique et Environnement Atmosphérique* (LHEEA) is another unit of the CNRS attached to the *Ecole Centrale de Nantes*. Their scientific thematic is focused on free surface hydrodynamics, fluid-structure aerodynamics, dynamics of the atmosphere and system approach for ground and marine propellants. In particular, one of their objectives is the development of Marine Renewable Energies (offshore wind, tidal and wake energy) and the laboratory has several wind tunnels; one of them is used in the framework of the SMARTEOLE project.

3.1.2 Objectives

As already mentioned above, the main objectives of SMARTEOLE are to design innovative control solutions meant to improve the efficiency and the sustainability of the wind turbines. These control solutions are developed at three different scales: the blade, the wind turbine and the wind farm; and they are tested through several experiments realized both in laboratory (wind tunnel) and in the field (two full scale field tests performed in an operating wind farm owned by ENGIE Green).

At blade scale, the objective is to control the aerodynamic performance of the blade through a modification of the pressure distribution (a modification of circulation) with fluidic and/or plasma actuators distributed along the blade. These studies are done at lab scale in wind tunnels and involve PRISME, LAAS and LHEEA.

At wind turbine scale, the objective is to design a feed-forward pitch controller anticipating the incoming wind conditions measured using a nacelle lidar minimizing the loading of the wind turbine, and to confront this new optimized controller with the conventionnal pitch control strategies implemented in the wind turbines used for the field test. This part is directed by IFPEN, in cooperation with ALT and EG.

At wind farm scale, new strategies of distributed production are investigated and tested during two field measurement campaigns. The objective is to gain a better understanding of wake interactions between the different wind turbines, and to demonstrate an increase in overall farm production for one or several of the strategies tested. The impact of a possible increased loading of the wind turbines due to these control strategies is also studied. Being the owner of the wind farm used during the campaign, EG is particularly interested in these topics, whereas ALT and PRISME are investigating the use of lidar technology for wind turbine wake tracking.

3.2 Experimental Setup

In this section is presented the wind farm which is considered in the SMARTEOLE project, with its layout and wind turbines, and also all the different devices used during the field tests. Other experiments are carried out in wind tunnels, however as they are not related to this particular thesis their setups are not developed here.

3.2.1 La Sole du Moulin Vieux Wind Farm

La Sole du Moulin Vieux (SMV) is a wind farm owned by ENGIE Green and located in the North of France, between the two cities of Ablaincourt-Pressoir and Vermandoviliers, in the county of Somme (province Haut-de-France). It consists of 7 Senvion REpower MM82 2050 kW wind turbines (80 m hub height), and was commissioned in two different steps by MAÏA Eolis: the first five wind turbines (SMV1 to SMV5) were put in operation in March 2009. while the two last ones (SMV6 and SMV7) were installed as an extension of the farm under the name *Les Kerles* four years later, in 2013. The Figure 3.1 shows the layout of the wind farm with the inter-distances between the wind turbines and the main direction angles.

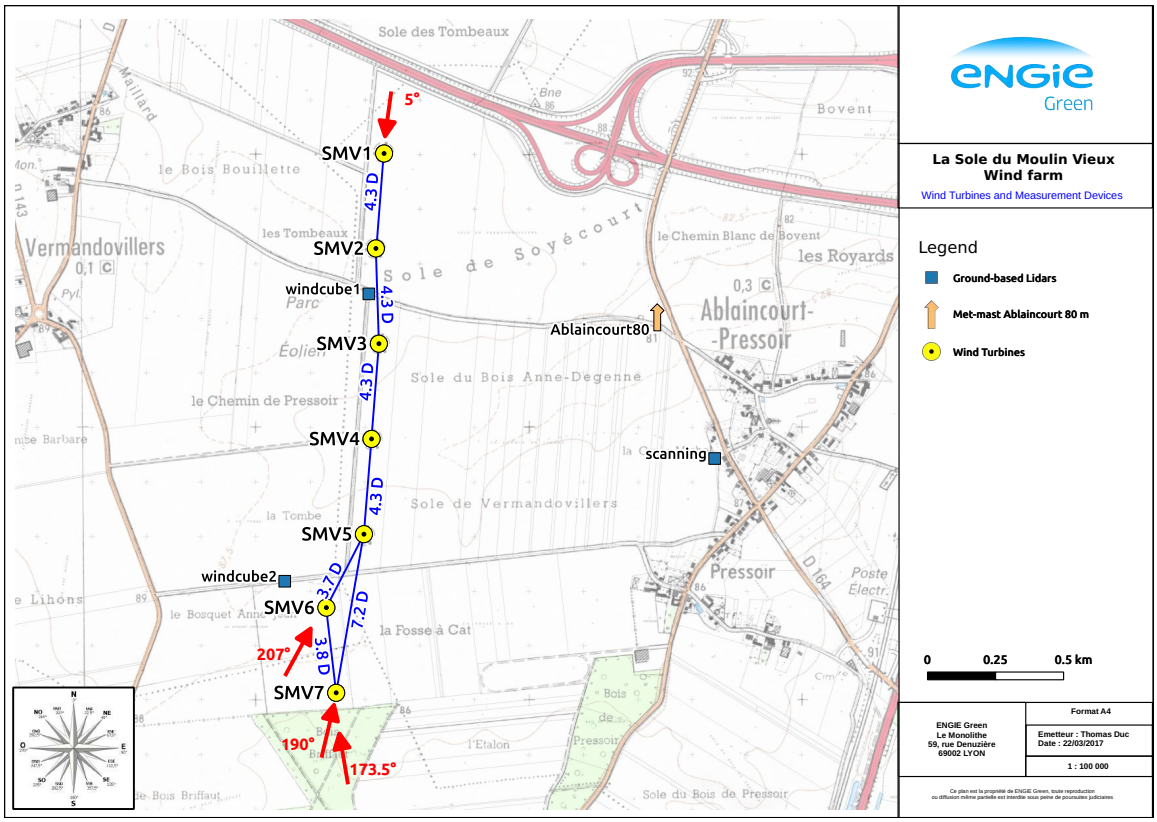

Figure 3.1: *Layout of the SMV wind farm with turbine inter–distances and main direction angles and position of wind measurement devices*

The prevailing wind direction for this particular site follow an axis South-West / North-East, which is quite typical in this region of France and explains the North / South axis on which are oriented the

wind turbines. However, due to development constraints, the two last wind turbines from the wind farm extension were installed slightly outside this axis, shifting the direction angle between the wind turbines SMV6 and SMV5 closer to the prevailing wind directions. This, combined with the very small distance between these two turbines (only 305 m, i.e. 3.7 D), makes the study of the wake from SMV6 to SMV5 of huge interest and explains why this wind farm was chosen for the SMARTEOLE project.

The surrounding terrain is very flat and consists only of grass and lands. The only exception is made by the small wood located on the South of the farm, at proximity of SMV7.

3.2.2 Available Measurement Sensors

A very extensive set of measurement devices are used during the field test of the SMARTEOLE project, including several lidars, a met-mast and strain gauges. In this section are summarized their locations and the main informations about them.

Ablaincourt Met-Mast

A 80 m high lattice met-mast is located just outside the city of Ablaincourt, some 1 km east of the wind farm as shown on the wind farm map. It was installed in 2010 to serve as supervision instrument for the wind farm and was originally equipped with some traditional cup anemometers and wind vanes (Thies First Class) at different heights, with also thermometers. However only the cup anemometer at 80 m and the wind vane at 30 m were giving usable data for the SMARTEOLE project.

The instruments were replaced between March 29th 2016 and May 31st 2016 with 4 sonic anemometers Metek USA at 80, 60, 40 and 20 m, a Thies First Class cup anemometer at 80 m, a Thies First Class wind vane at 70 m, and Campbell thermometers at 78, 58, 38, and 20 m. Unfortunately, some communication problems occurred during the summer 2016 and data was lost after August 9th 2016.

Ground-based Lidars

Two ground-based lidars were used in the SMARTEOLE project: a Windcube and a scanning lidar Windcube 200S.

The Windcube is used to measure the wind conditions at the precise wind farm location. It was first installed between the wind turbines SMV2 and SMV3 (see label 'windcube1' on the map) but then was moved on May 2016 closer to SMV6 (label 'windcube2'). However it faced some electric supply problems during the summer (the cable was first cut and then stolen), therefore there are some holes in the data. It was finally removed on October 2016. An autonomous windcube will be used for the next field test campaign. The wind speed and direction is measured at 9 different altitudes going from 40 to 200 m, the default altitude considered in this thesis is 80 m corresponding to the hub height of the wind turbines.

The scanning lidar was installed at Ablaincourt-Pressoir, 1.3 km east of the two turbines SMV6 and SMV5. Three Plan Position Indicators (PPI) have been programmed at 2.5°, 3.8°, 5.2° elevation angles. These values have been chosen in order to cover a large section of the of the rotor swept area of SMV5, as seen on Figure 3.3b. The studied azimuth angle range is 248° to 278°, covering the turbines SMV4, SMV5, SMV6. This scanning lidar is used to study the wake properties from the wind turbines SMV6 and SMV5, and his results are mainly processed by the PRISME who takes a deep interest in this topic.

Figure 3.2: *The Windcube lidar at the bottom of SMV6. Picture taken by ENGIE Green*

(a) *Picture of the scanning lidar, taken by ENGIE Green*

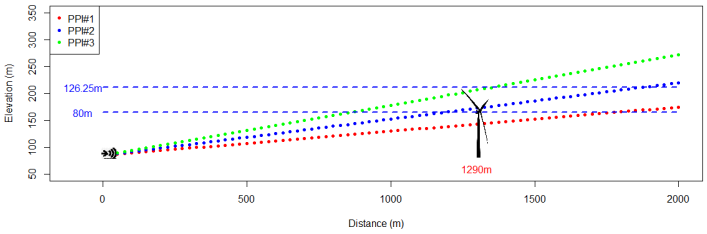

(b) *Scanning lidar PPI scenarios*

Figure 3.3: *The scanning lidar Windcube 200S at Ablaincourt-Pressoir and the PPI programmed*

Nacelle-mounted Lidars

Two nacelle lidars were installed for the field test campaign on the two wind turbines of study SMV5 and SMV6.

A lidar Wind Iris was mounted on top of SMV5 between October 2015 and April 2016. He was used to study the performance of the wind turbine and did not face any particular problems during this period. The upwind wind speed measured by this lidar is reconstructed from the result of two horizontal radial wind speed measurements. This reconstruction is assuming an homogeneity of the wind speed field, therefore as soon as one of the two beams of the lidar is in the wake of another wind turbine, the measure is not consistent. The lidar measures the wind speed for 10 different ranges going from 80 m to 400 m upstream of SMV5; but most of the studies in this report are focused on the 200 m range corresponding to 2.5 D.

Figure 3.4: *The Wind Iris lidar on top of SMV5. Picture taken by ENGIE Green*

A 5-beam nacelle lidar Wind Orion was installed on top of SMV6. It has been operating between November 26th 2015 and removed on April 1st 2016 (but faced technical issues between January 1st and February 23rd) for the curtailment field test and then between June 29th 2016 and December 22nd 2016 for the yaw misalignment experiment. In addition to the measurement of the upstream wind speed which is of course of great use for analyzing the power performances of the wind turbine, this lidar is also capable of measuring the horizontal and vertical wind shears at 10 different ranges upstream (from 80 m to 400 m). This data is mainly used by the IFPEn for the development of control strategies intended to minimize the loading on the turbine.

Wind Turbine Characteristics and SCADA Data

All the wind turbines in the SMV wind farm have a supervisory control and data acquisition system (SCADA) which is used to store information about the wind turbine status (e.g. grid availability, active and reactive power production, rotor speed, pitch angle or nacelle position) but also the weather conditions measured by the instrumentation located on top of the nacelle (giving the external temperature, the wind speed and relative wind direction compared to the wind turbine, although these two last measurements are really noisy as they are placed just behind the rotor).

For this particular project SCADA data was available as 10-min average values for all wind turbines, and the wind turbines SMV5 and SMV6 were also instrumented to store 1-sec values. A quick analysis of these 10-min values for rotor speed and pitch for the different wind turbines in the farm led to the Figure 3.5 showing the MM82 characteristic curves. In this graph the power, Cp and Ct curves represented corresponds to guaranteed curves given by the manufacturer Senvion.

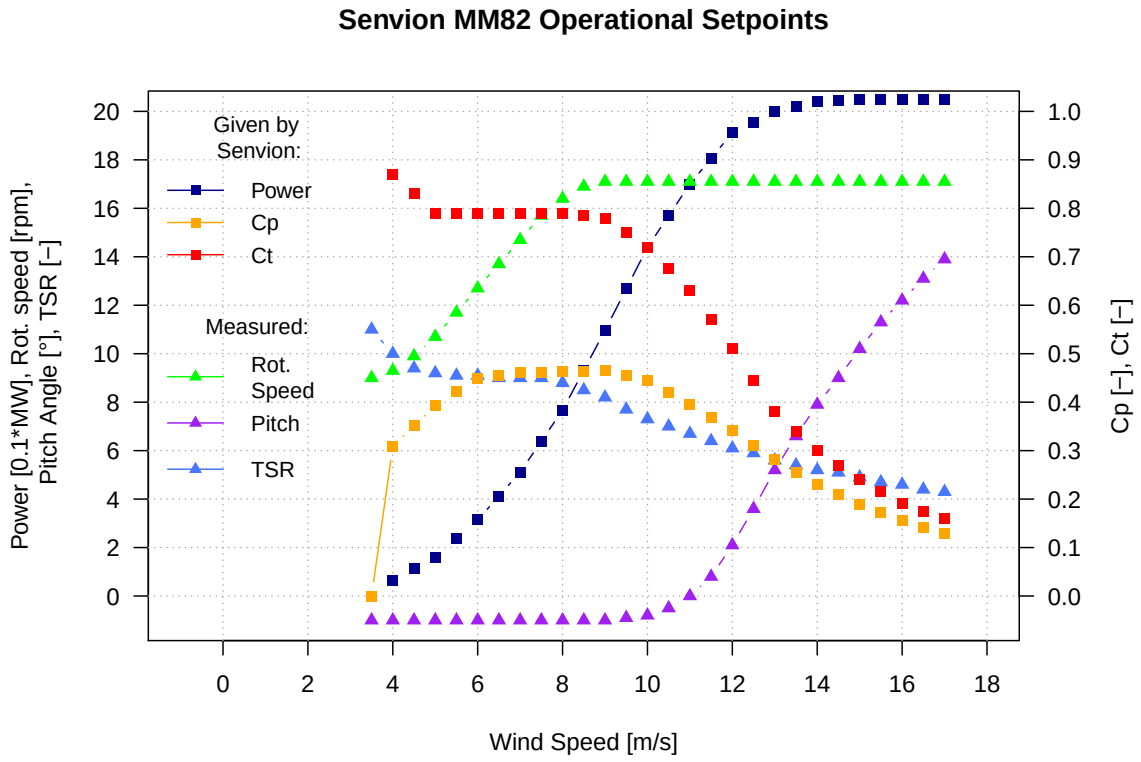

Figure 3.5: *Senvion MM82 2050 kW operational points (△) and guaranteed performance (□)*

From these curves three different control regions can be seen. The first region, between 4 and 9 m/s is the variable speed region. The rotor speed is regularly increasing with the wind speed in order to maintain the turbine at the tip-speed-ratio (TSR) that ensures the best aerodynamic properties and thus the best performance coefficient Cp (the pitch angle being kept as its optimal value of -1°); as a consequence the energy extraction from the wind is maximum and the thrust coefficient Ct symbolizing the wind force exerted on the turbine is also very high.

The third region, occurring after the turbine has reached its nominal power (at 12.5 m/s) and until the cut-out wind speed (25 m/s), is the constant power region. The power extraction from the wind is regulated and kept at its nominal value of 2050 kW by pitching the blades to decrease the aerodynamic efficiency of the turbine. As the pitch angle of the blades increases, the performance of the turbine decreases as well as the thrust coefficient.

In between these two regions, from 9 m/s to 12.5 m/s, is the second region: the constant speed region. The wind turbine has reached its nominal speed (17.1 rpm) and therefore cannot maintain the optimal TSR as the wind speed increases, but as not reached the nominal power yet. In this region the performance and thrust coefficients are decreasing slightly with the increasing wind speed, while the blades are starting to be pitched (this is done in order to avoid going over the nominal power because of the wind speed fluctuation).

MERRA Data

MERRA stands for Modern-Era Retrospective analysis for Research and Applications. It is a database made available free of charge by the NASA that provides access to weather conditions which are obtained thanks to satellite observation. The grid spatial resolution is about 50 km x 50 km (1/2° in latitude and 2/3° in longitude) and values are given on a hourly basis.

The MERRA data used in this project are taken from the grid point located at (E3.125°, N50°). This data is mainly used to get the air pressure at the wind farm site, which is needed to assess the air density

(the temperature being provided by the SCADA signal of the wind turbines). From this data is also calculated the Monin-Obukhov length L through the following equation [28]:

$$L = \frac{\Theta_v}{\kappa g} \frac{u_*^3}{\overline{w'\Theta'_v}} \tag{3.1}$$

where Θ_v is the virtual potential temperature, κ the Von-Karmann constant, g the gravity constant, u_* the friction velocity and w the vertical velocity. This length is used to assess the atmospheric stability based on the following conditions [29]:

- $L < 0$: the atmosphere is unstable
- $L > 0$: the atmosphere is stable
- $|L| = \infty$: the atmosphere is neutral

Strain Gauges

Strain gauges were installed at the blade root of the wind turbines SMV5 and SMV6. Their purpose was to measure the variations of the fatigue loads of these two turbines when curtailing or yawing the upwind wind turbine. Indeed, raising the combined power production of the farm is not of great interest if the lifetime of the wind turbines is decreased much more because of an increased fatigue. On the other keeping the production more or less constant but reducing significantly the loads would already be a great improvement.

The strain gauges installed were Fiber Bragg Grating based sensors, developed by FiberSensing. Depending on the strain exerted on the fiber optic, it will reflect the light differently and therefore the strain can be seen as a linear function of the shift in the wavelength reflected. This measurement is also dependent on the ambient temperature which must then be assessed very accurately. The Strain gauges were installed at each blade root of the wind turbines, in a location were the strain is expected to be maximum and sensitive to all modes of deformation. In all cases, two strain gauges were installed, one used to measure the strain and the second one to measure the temperature.

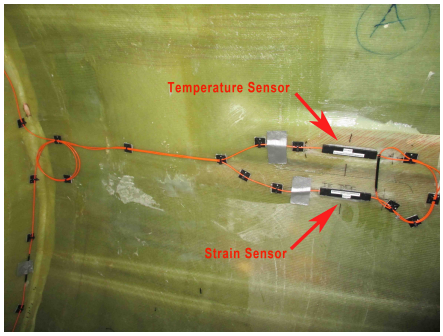

Figure 3.6: *The strain gauges installed on one of the blade roots*

The strain gauges were only installed between April and May 2016, i.e. in the middle of the field test campaing. However, due to time constraints the results from these strain gauges could not be processed and analyzed during this thesis.

3.3 SMARTEOLE Project - First Results

In this section are quickly summarized the first results obtained in the first phase of the SMARTEOLE project. They were presented at the TORQUE conference of Munich in October 2016.

At blade scale, two strategies were implemented and investigated to control the flow and the lift coefficient (Cl) of a given airfoil. The objective is to design a close loop system that will maintain a constant Cl despite the fluctuating wind conditions faced by the turbine. The strategies studied to achieve this goal were based on jet flow control [30] and plasma actuators [31]. Wind tunnel experiments led on the PRISME facilities show that the lift coefficient could indeed be controlled using both strategies. The increment in the Cl was measured to 0.06 for the plasma actuators and up to 0.11 for the jet flow [32]. The objective is now to be able to implement the close-loop system in order to control the flow for fluctuating conditions.

At wind turbine scale, the studies led by the IFPEn on the 5 beam lidars measurements from the first field test campaign of the project led to the development of an algorithm used to reconstruct the incoming wind field from lidar data [33]. The control strategy previously developed was also improved to take into account pitch actuators dynamics and anticipate the future pitch set-points thanks to the reconstructed wind field. Simulations realized on FAST with a Senvion MM82 wind turbine model show a significant reduction in the tower top fore-aft moments (both in terms of extreme and fatigue loading). The objective is now to implement this innovative control strategy in a real wind turbine during the second field test campaigns.

Finally at wind farm scale, the results from the scanning lidar were analyzed by the PRISME and that led to the development of an algorithm used to detect the wake position based on the lidar data [34]. The results about the implementation of a curtailment strategy for power optimization were also partly published in [35]. However, a more extensive analysis of these experimental results, both for the curtailment and the yaw offset strategy, will be provided in this thesis in Chapters 6 and 7, respectively.

4 | Wind Farm Performance Analysis Under Normal Operation

As it can be expected from the very extensive experimental setup installed for the field test analysis, a huge quantity of data was recorded from all instruments during the 10 months of the measurement campaigns (December 2015 - September 2016). In order to use this data properly, it must be checked and corrected for various bias and offsets. This work is done in Section 4.1. Afterwards, in Section 4.2 an assessment of the performance of the wind turbines and the farm is provided to highlight the potential for a coordinated control. An alternative way of measuring the wind speed is provided and discussed in Section 4.3, and the on-site turbulence intensity conditions are finally studied in Section 4.4.

4.1 Data Analysis and Correction

The measurement sensors being all calibrated independently from each other, they all have particular bias that must be corrected. Here is developed a simple method used to recalibrate the wind direction signals from all instruments. The correlation between the different wind speed sensors is also investigated, and finally a Nacelle Transfer Function (NTF) is computed from nacelle lidar measurements in order to be able to use reliably the nacelle wind speed signal provided by the SCADA during the project.

4.1.1 Data Availability

The data availability for the two parts of the measurement campaign, the curtailment field test (between December 2015 and April 2016) and yaw offset field test (between May 2016 and September 2016) are shown below on Figure 4.1 and Figure 4.2, respectively.

It must be noted that regarding the lidars, only the used ranges are taken into account in these graphs (80 m height for the Windcube, 200 m upwind for the nacelle-mounted lidars) and that the instrument is considered as available whenever a wind measure is present. However, for all the studies led in this chapter, the lidar measurement will also be filtered in "Measure availability". The criteria used for this 90%, i.e. 90% of the second-wise measurements must be available over the 10-min period.

As seen on the graphs, the availability of the wind measurement devices was not very good due to technical issues, especially during the yaw offset campaign (moreover the data from the 5 beam lidar for this campaign was only obtained from the project partner Leosphere in late April 2017, i.e when most of the data analysis was already done). Therefore it has been decided to rely mostly on the SCADA measurements of wind speed and direction. This approach is also relevant because wind farms generally do not have lidars or met-mast installed nearby and can only rely on SCADA to optimize their production. However, SCADA wind measurements are known to be very noisy since they are located behind the rotor and thus in a region with a highly distorted flow [36]. To make these indicators as reliable as possible, they were calibrated to correct their errors that might be caused by the increased turbulences in the flow.

4.1.2 Wind Direction Offset Calibration

In this section is developed the correction of the direction offset. The wind direction is calculated by summing the nacelle position signal with the (relative) wind direction signal given by the wind vane on the top of the nacelle.

The offset is mainly caused by the error when indicating the location of the North as seen by the wind turbine which is used as the 0° value for the calculation of the wind speed signal. The relative wind direction signal acts as a perturbation but its average value should be zero since the control of the wind turbine is made such that the rotor is always facing upwind.

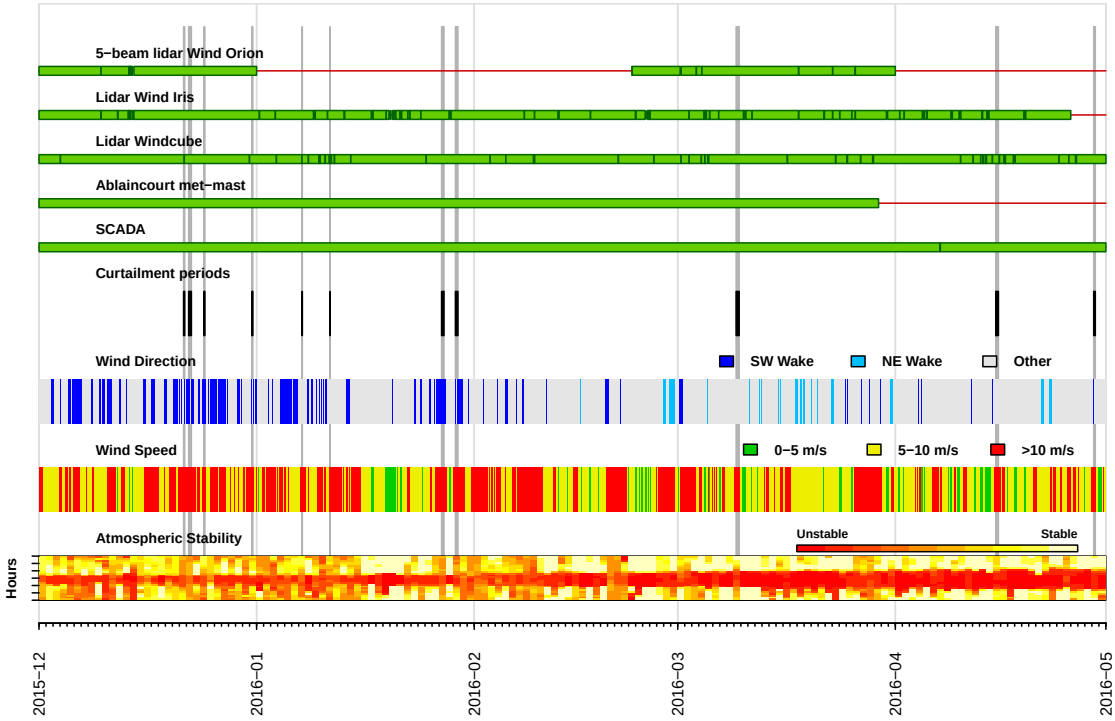

Figure 4.1: *Data Availability and External Conditions during the curtailment field test*

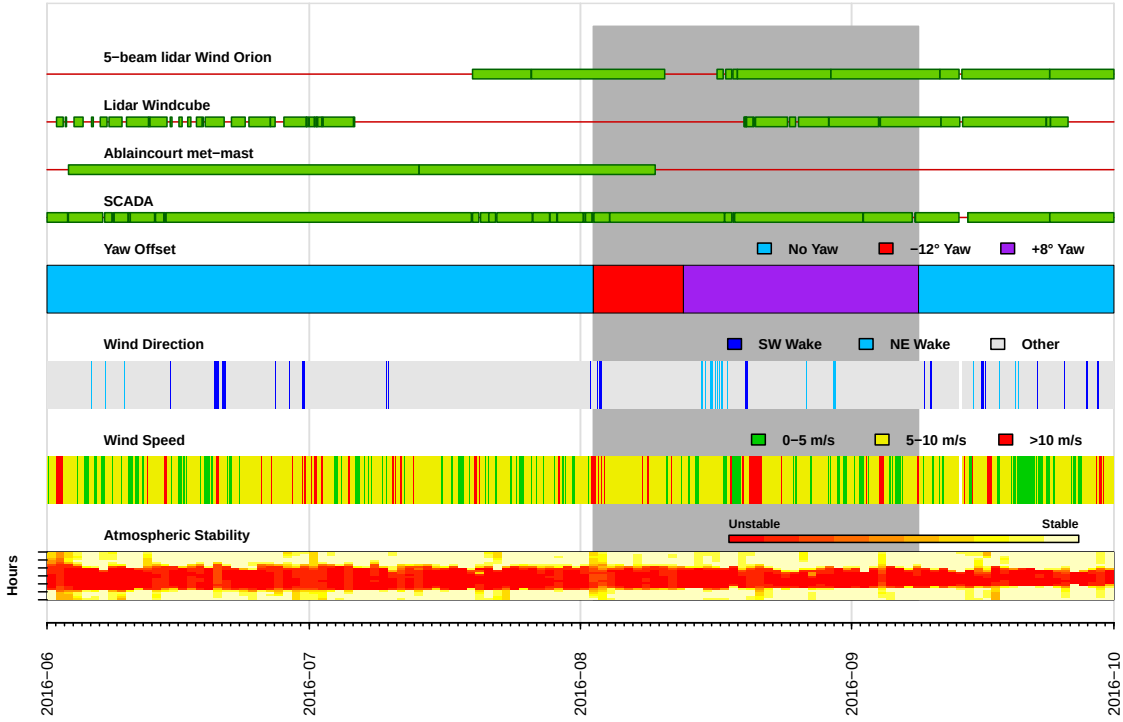

Figure 4.2: *Data Availability and External Conditions during the Yaw Offset field test*

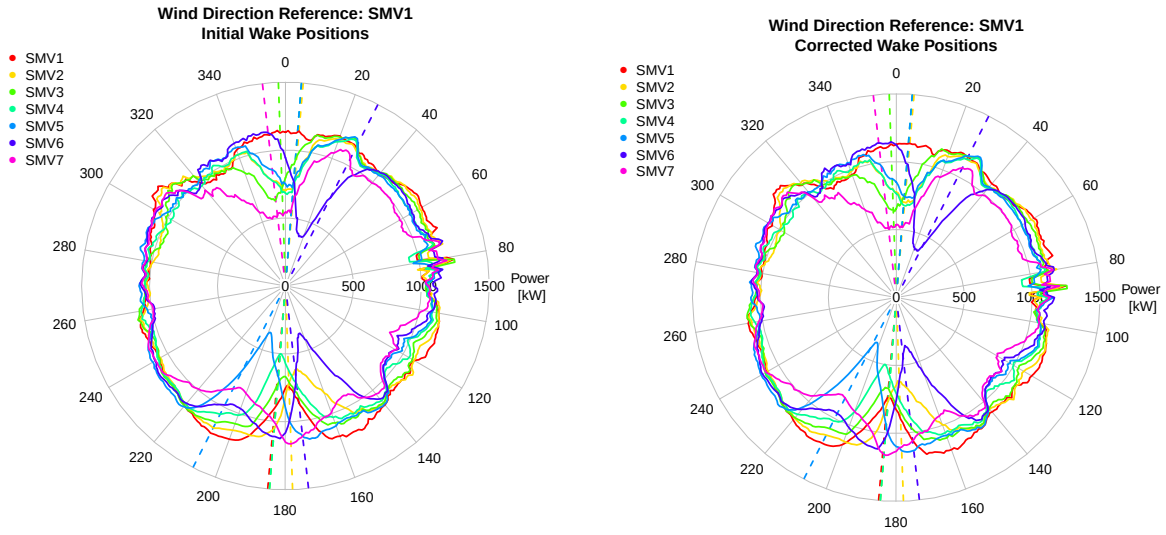

(a) *SMV1 initial wake positions*

(b) *SMV1 final wake positions*

Figure 4.3: *SMV1 direction offset calibration*

The wind direction indicators were corrected by comparing the location of the different wakes in the wind farm with their expected values (derived from the wind turbine coordinates), using the following procedure:

1. The data considered corresponds to 1 year of SCADA measurements (10-min average values from 01.08.2015 to 01.08.2016) which is filtered to keep only the periods when all wind turbines have the same operation conditions (no change in the pitch and vane settings, and all curtailment periods have also been removed).

2. These data are then filtered again to keep only 10-min periods for which the maximum power from one of the wind turbine inside the wind farm is between 1 and 1,5 MW. This is done to consider only the steepest section of the power curve, for which the Ct of the wind turbine is maximum and thus the wake is the strongest.

3. Then to correct the wind direction sensor of wind turbine SMVi, the power production of all wind turbines inside the wind farm is plotted against the wind direction given by SMVi, as represented on Figure 4.3a for SMV1 in particular. The curves are obtained by realizing a moving average of the values over 10 degrees.

4. The location of the wakes are obtained by considering the minimal values for each peaks on all the signals, the errors compared to their theoretical values are computed. Their might be some issues when two different wakes are located close to each other and thus only a resulting double wake peak can appear with no correspondence with the theoretical position. However due to the very simple configuration of this wind farm there is no such issues except for the wake on SMV7 from SMV6 and SMV5, which is hence left out of the study.

5. The offset correction factor to be applied to SMVi is determined by doing the average of these errors for the wakes when SMVi is not disturbed by the wake of another wind turbine (i.e. the wake from SMV2 to SMV3 is not taken into account to correct the wind direction of SMV4 because for those wind directions SMV4 is in the wake of SMV3 and thus the wind vane might be influenced). As a consequence the correction is mainly based on the wakes SMV5 to SMV6, SMV6 to SMV5 and SMV7 to SMV6 since these wakes are very visible due to the smaller distances between these turbines and they are also positioned slightly away from the North-South alignment of the wind farm.

6. After application of this correction factor, the differences between the observed wake location and its theoretical value are computed again for each turbine and each wake to know precisely the residual

errors occurring when considering a particular wake with a particular wind direction reference. The final graph for the wind direction SMV1 can be found on Figure 4.3b; for the other wind turbines and wind sensors (windcube, met-mast) please refer to Appendix A.1.

In the following sections of the report the wind directions will be corrected with the offsets indicated in Table 4.1 unless stated otherwise.

Table 4.1: *Summary of offsets for all instruments*

Reference Sensor	Offset [°]
SMV1	-5.5
SMV2	-8.0
SMV3	-22.5
SMV4	-16.0
SMV5	-21.0
SMV6	-17.5
SMV7	-20.0
Met-mast	-10.5
Wincube (position1)	-18.5

4.1.3 Wind Speed Sensors Comparison

After having corrected the offsets of the different wind measurement devices, the wind speed measurements are now compared. Correlations between the on-site ground-based lidar windcube and the met-mast, and between the windcube and the two nacelle-mounted lidars are performed to make sure that all the wind speed measurements are consistent.

Windcube vs Met-mast

The data from the met-mast located at Ablaincourt are first compared with wind speed data obtained from the lidar Windcube located between the turbines SMV2 and SMV3 (position 1). This is to make sure that the windcube gives a consistent measurement compared with the measure of the mast. The two sensors studied is the cup anemometer at 80 m on the met-mast and the wind speed measurement from the windcube at 80 m. The reference wind direction is taken from the windcube measurement and corrected with the value derived in the previous section.

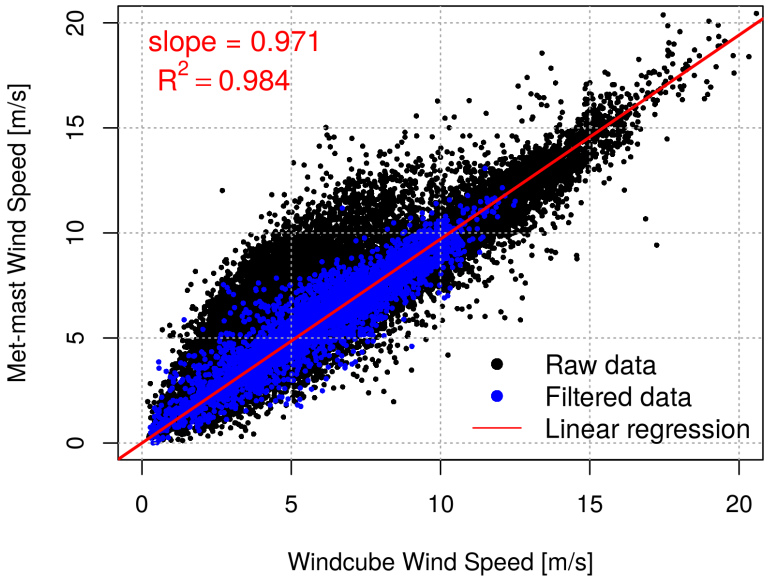

Figure 4.4: *Comparison of wind speed measurements between the lidar Windcube and the met-mast*

The combined available data for the two sensors consists of 31541 data-points (10-min average wind speed measurements recorded between 16.06.2015 and 29.03.2016). However this data set is filtered in direction to dismiss data recorded when one of the sensor is disturbed (e.g. when the windcube or the mast are in the wakes of the wind turbines). The selected combined valid sector for these two sensors is identified as [55°; 140°]. The data set is now reduced to 4765 points accounting for $\sim$ 800 hours of measurement (this wind direction is not really prevailing). A linear regression with a fixed intercept of 0 is performed on this reduced data set (indicated as "filtered data" in blue) and shown on Figure 4.4. The mention "raw data" in black accounts for the complete combined data set between the two instruments.

There is quite an important scatter of the raw data, mainly due to the disturbed sectors: when the windcube is in the wakes of the wind turbines SMV2 or SMV3 (when wind comes from 10° or 170° $\pm$30°, respectively), the wind speed it measures is artificially low compared to the met-mast. On the other hand, when the wind comes from the west, the met-mast is in the wakes of the different wind turbines and there is also a wind speed deficit (although smaller than for the windcube since the distance between the turbines and the met-mast is much larger than the one between the windcube and the turbines).

On the filtered data, which should be outside any disturbed sectors, the linear regression leads to a slope of 0.971. However, even though the line is mainly fitted for low wind speeds (between 5 and 10 m/s), it also seems to be valid for higher wind speeds outside the measurement sectors. The difference to the value of 1 might be explained by the important distance between the two sensors, and thus a possible influence of the topography. Also lidars are measuring wind speed over a volume while cup anemometer is a point measurement.

Windcube vs lidar Wind Iris

The data from the lidar windcube are compared to the data from the lidar Wind Iris, mounted on the nacelle of the turbine SMV5 (hub height 80 m). The sensors considered is the wind speed measurement at 80 m from the windcube and the upwind wind speed measured by the Wind Iris at a range of 200 m (basically 2,5 D upwind). The reference wind direction is taken from the windcube.

The combined available data set consists of 20255 points recorded between 28.10.2015 and 25.04.2016. This is filtered on the following valid sectors: [55°; 140°] & [220°; 330°]. The reduced data set is made of 9624 points accounting for $\sim$ 1600 hours. Data and linear regression is shown on Figure 4.5a.

There is a much better correlation between the two sensors. This might be explained by a smaller distance between them and also by the widening of the valid measurement sector allowing much more more data in the undisturbed sectors.

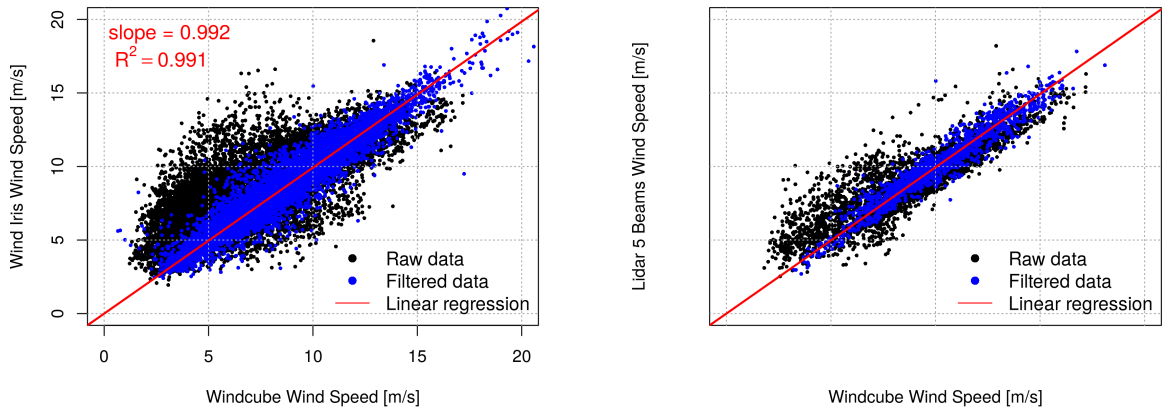

(a) Windcube vs Wind Iris *(b) Windcube vs 5 beams lidar Wind Orion*

Figure 4.5: *Comparison Wincube wind speed measurement with the nacelle mounted lidars*

Windcube vs lidar 5 beams Wind Orion

The data from the lidar windcube are compared to the data from the 5 beams lidar, mounted on the nacelle of the turbine SMV6 (hub height 80 m). The sensors considered is the wind speed measurement at 80 m from the windcube and the upwind wind speed measured by the 5 beams lidar at a range of 200 m. The reference wind direction is taken from the windcube.

The combined available data set consists of 4624 points recorded between 26.11.2015 and 01.04.2016 (with a break between 01.01.2016 and 23.02.2016). This is filtered on the following valid sectors: [55°; 140°] & [220°; 330°]. The reduced data set is made of 1391 points accounting for $\sim$ 230 hours. Data and linear regression is shown on Figure 4.5b (axes have been removed for confidentiality issues).

Again, the correlation between the sensors is much much better than it is with the mast, even though there is a lack of data compared with the wind iris lidar. In general nacelle lidars seems to provide a very consistent value of the wind speed as long as the turbines they are mounted on are not in the wake of another wind turbine. It is thus relevant to use these lidars to identify the Nacelle Transfer Functions for the nacelle anemometers.

4.1.4 Derivation of a Nacelle Transfer Function using Nacelle Lidars

SCADA wind speed measurements are known to be very noisy since the nacelle anemometers are located behind the rotor and thus in the wake of the wind turbine. To correct the errors that might be caused by the increased turbulence in the flow and make them as reliable as possible, a Nacelle Transfer Function (NTF) is computed based on the free wind speed measurements given by the nacelle lidars.

NTFs are used as an alternative mean to derive a wind turbine power curve, following the procedure described in the IEC standard 61400-12-2:2013 [37]. The Annex D explains the different steps needed to obtain the NTF. In this particular case, these steps were followed as much as possible; the main difference with the recommendations of the standard comes from the fact that the free wind speed is measured using a nacelle lidar and not a neighboring met-mast.

The NTF for three different wind turbines were derived: SMV5 using the nacelle lidar wind iris, SMV6 using the 5 beams lidar, and SMV2 using the lidar windcube located nearby. In the two first cases, the chosen range for the wind speed measurement was 200 m upstream (corresponding to 2.5 D, which is the distance recommended by the standard for the location of the met-mast). For the last one, the distance from SMV2 to the windcube is also $\sim$ 200 m but the wind measured is not always coming upstream. In each case a proper wind direction sector was defined for which the free wind speed measurement was not disturbed by the wake of other wind turbines. To read the detailed procedure followed to derive these three NTFs, including the selection of these undisturbed sectors (and the values chosen for the computation of the uncertainties), please refer to Appendix A.2.

On Figure 4.6a is presented the result for the wind turbine SMV5. Similarly to the previous sections, the raw data in black corresponds to the complete combined data set between the nacelle lidar and scada measurement, while the filtered data in blue is the valid data used for the derivation of the NTF, shown as the red squares. The error bars represent the 95% confidence interval.

The Figure 4.6b compares the NTFs obtained for the three different wind turbines. They all show a very similar behavior, which is comforting regarding their consistency. Compared to the 1:1 linear trend, the NTF are slightly curved especially in the region 5 – 10 m/s, which is also clearly visible on the valid dataset. This region corresponds to the variable speed region of the wind turbine which is operating at maximum Ct. The wind speed deficit after the wind turbine is thus maximal and that is why the free wind speed appears higher than the nacelle wind speed. After rated wind speed (around 12 m/s) the wind turbine begins to pitch and thus Ct decreases. Therefore the wind speed deficit also decreases and the nacelle measured wind speed gets closer to the free wind speed.

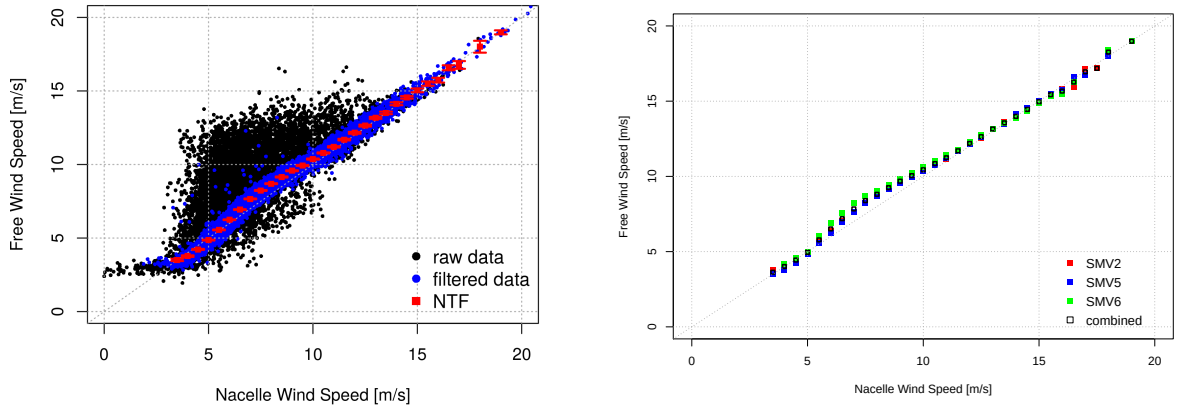

(a) Case of SMV5

(b) Comparison of all three NTFs

Figure 4.6: *Derivation of Nacelle Transfer Functions*

4.1.5 Air Density Correction and Conclusion

In the following chapters of this report, the wind speed used in the different graphs will always be taken from a nacelle wind speed signal and corrected with a NTF, unless stated otherwise. If the wind turbine is SMV2, SMV5 or SMV6, the proper computed NTF is used. For any other turbine, the NTF used is obtained by the average value of the three computed NTFs for each wind speed bin. Following the recommendations of the IEC standard, linear interpolation is used between each bin, and no extrapolation is performed outside the measured range (i.e. the wind speeds below 3.5 m/s and above 19 m/s are not corrected, which is not a big problem since the cut-in wind speed of the wind turbine is 3.5 m/s and wind speeds above 19 m/s are very rare).

When needed, the air density is computed from the temperature signal given in the SCADA and the pressure measurement taken from the MERRA data (and thus constant over one hour). For the power curves, the wind speed is normalized to sea-level air density using Equation (4.1):

$$V_{norm} = V_{meas} \left(\frac{\rho_{meas}}{\rho_0} \right)^{\frac{1}{3}} \tag{4.1}$$

where $\rho_0 = 1.225\ kg.m^{-3}$ is the sea-level air density.

In the remaining sections of this chapter and in Chapter 5, the data set used mainly bears on SCADA measurements recorded between 15.06.2015 and 01.08.2016. The data are properly filtered for grid availability and the curtailment periods are left outside the study.

4.2 Wind Farm Performance

Before trying to find the best strategy to optimize the wind farm production, it is necessary to analyze the performance of the wind farm under normal operation conditions in order to identify properly the regions where its efficiency is lower and thus favorable to improvement using coordinated control. This is done in this section. A special attention is paid to the wind turbines SMV5 and SMV6 as the wake event SMV6 - SMV5 is particularly studied in the SMARTEOLE project, and then the efficiency of the total wind farm is analyzed.

4.2.1 Wind Turbines SMV5 and SMV6

The power curves of the wind turbines SMV5 and SMV6 out of any disturbing sectors are are shown on Figure 4.7. They are calculated using the nacelle anemometer wind speed and corrected with the NTFs. As it can be seen, the wind turbine SMV6 is seen to be under-producing slightly compared to SMV5

and the MM82 ideal power curve guaranteed by Senvion. This cannot be explained by differences in the surrounding terrain, the presence of the wood South of the farm is indeed increasing the turbulence intensity for SMV6 and thus reducing its performance (see later on Figure 4.16 in Section 4.4), but this sector has been filtered out of the study. On the remaining sectors, SMV5 and SMV6 are facing very similar turbulence intensity. A more probable explanation might be that the wind turbine has a small yaw error that decreases its performance. This point will be discussed in more details later.

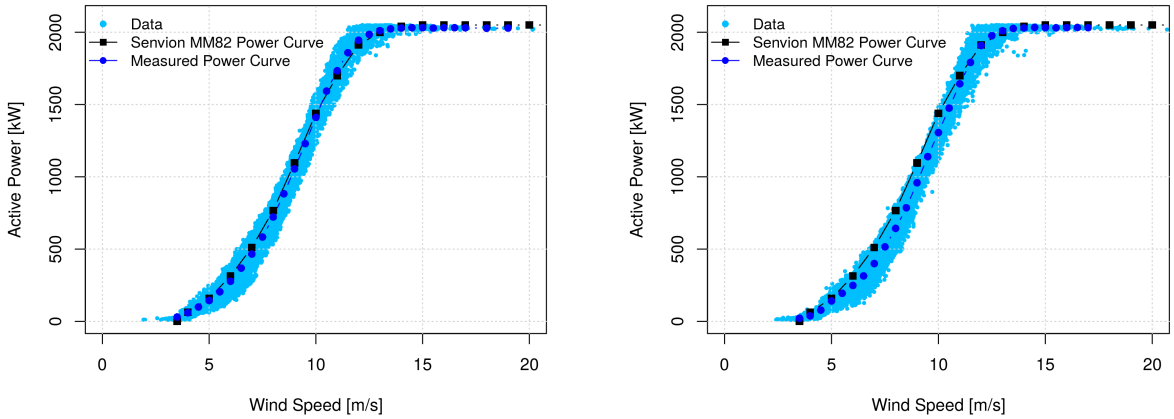

(a) *For the wind turbine SMV5* ***(b)*** *For the wind turbine SMV6*

Figure 4.7: *Measured power curves of the wind turbines outside of any disturbing sectors*

The wake event between SMV6 and SMV5 is now investigated in more details, as it is the one considered for the SMARTEOLE project due to the very short distance between the wind turbines and their orientation close to the prevailing wind directions. On Figure 4.8a is represented the power curves of SMV6 and SMV5 on the wake sector [180°; 220°]. The impact of the wake is seen to be particularly important for wind speeds varying between 6 and 13 m/s. Referring to Figure 3.5, it corresponds to the region where the performance and thrust coefficients of the turbine are both very high. When the wind speed increases further, the upwind wind turbine is not harvesting as much power from the wind since it is limited to rated power and thus leaves a more energetic flow for the downwind wind turbine.

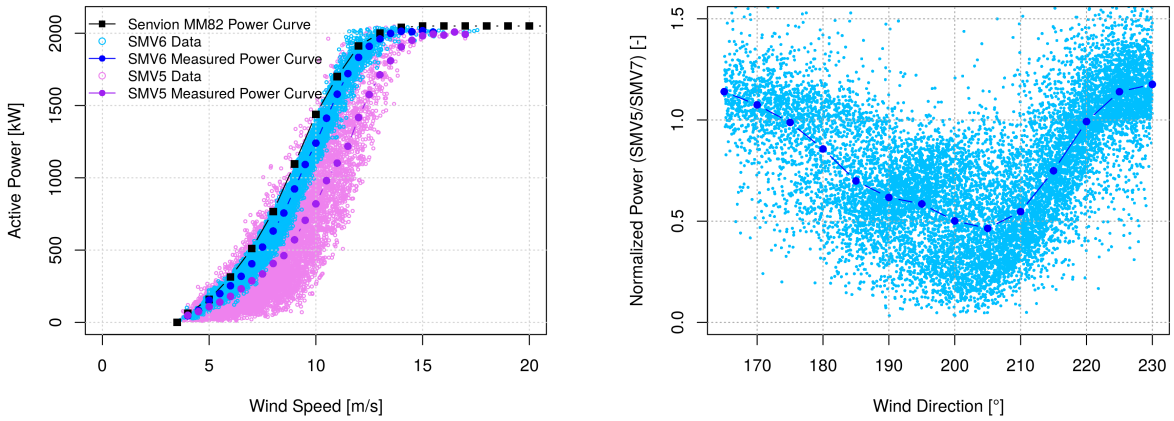

(a) *SMV5 and SMV6 power curves in the whole wake sector [180°; 220°]* ***(b)*** *SMV5 normalized power against wind direction, for the complete wind speed range*

Figure 4.8: *Study of the SMV6 (+SMV7) - SMV5 wake*

On Figure 4.8b is represented the SMV5 normalized power as a function of the wind direction (with 5° bins). The reference power is taken from SMV7 because until 190° SMV6 is still in the wake of SMV7 and thus produces less than SMV5. However, the SMV7 wind turbine is slightly under-producing due to the presence of the wood, that explains why the normalized power goes around 1.2 outside of the wake.

The important scatter of the data is due to the fact that no particular wind speed filtering is performed before binning the data against wind direction. On this graph is clearly seen the huge impact of the wake on SMV5 performance, as under full wake conditions (205°) the power is reduced in average by 50%. This deficit is mainly due to the wind turbine SMV6 and can be explained by the very short distance between the two turbines.

The graph presented on Figure 4.7a is derived from the whole wake sector (and respectively from the complete wind speed range for Figure 4.8b), and changes in power looks very regular. However, when the same analysis is realized on a smaller direction sector or on particular wind speed ranges, things are not that simple and underline a strange behavior of the wind turbines. This is done on Figure 4.9. On Figure 4.9a is shown three power curves corresponding to the three different wake sectors under the influence of SMV6: 190 - 200° (left half-wake), 200 - 210° (full wake) and 210 - 220° (right half-wake). Similarly on Figure 4.9b is represented the wake for different power ranges. A moving average of data points (over 10°) is now used instead of bins to identify more precisely the location of the wake minimum.

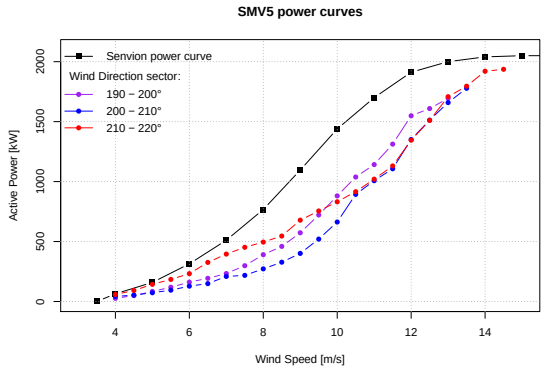

(a) SMV5 power curves as a function of the wind direction

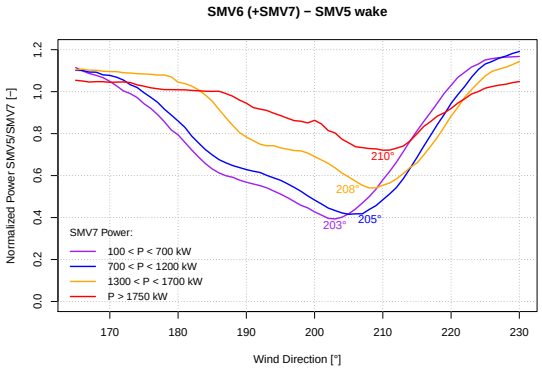

(b) SMV5 normalized power against wind direction for several power ranges

Figure 4.9: *Study of the SMV6 (+SMV7) - SMV5 wake*

A clear change in the wake behavior can be seen. At low power ranges, the SMV6 wake is centered around 203°, but this wake position is slightly moving towards higher values as the wind speed (and the power) increases to finally reach $\sim 210°$ at nominal power. This is also seen on the directional power curves. At low wind speeds, the power curve in the sector [210°; 220°] (in red) shows a much better performance compare to the other half-wake sector [190°; 200°] (in purple). However, as the wind speed increases this tendency is inverted and finally the purple power curve gets better than the red one, which presents more or less the same power deficit as for the full wake sector.

This wake deflection could be related to an increased yaw error of the upwind wind turbine. In Figure 4.10 is represented the yaw error of the wind turbines SMV5 and SMV6 as a function of the active power. These yaw errors were calculated from the horizontal wind direction signal coming from the nacelle lidars installed on these turbines, i.e. the Wind Iris lidar on top of SMV5 and the 5 beam lidar on top of SMV6. Therefore they might contain a certain bias of a few degrees related to the uncertainty in the alignment of the lidar with the turbine. A similar behavior can be seen in both case: from 800 kW, the yaw error of the turbine is regularly increasing towards positive values. This increase seems more important for SMV6 and this might be the reason why this wind turbine has a lower performance than SMV5. In any case, it is surely responsible for the wake deflection.

It must be noticed that this increase in the yaw error is not detected by the wind turbine: the vane angle signal in the SCADA remains centered around the value 0° for every power ranges. ENGIE Green has noticed this particularity in another Senvion wind turbine from a nearby wind farm, so it may be a default inherent to the control of the wind turbine, in particular the way the nacelle flow angle (and thus the wind vane) is affected by the wind speed or the yaw angle, as underlined in [36]. However this makes the optimization of the combined power production of the two wind turbines more complicated as the wake is no longer seen at a fixed direction but is in reality changing with the wind speed.

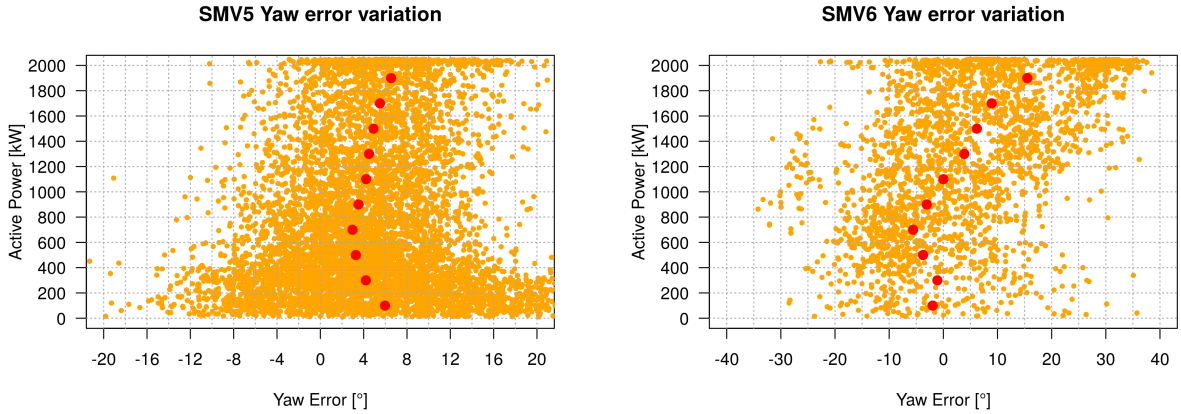

Figure 4.10: *Yaw error of the wind turbines as a function of the active power production*

4.2.2 Wind Farm Efficiency

Finally the total efficiency of the farm is studied as a function of the wind direction. Two different power ranges are considered: between 500 kW and 1200 kw, corresponding to high Ct and thus strong wake effects, and above 1600 kW corresponding to smaller Ct and wake effects. After this power filtering, the active power of each wind turbine is binned against wind direction (10° bins). For each bin, the most producing wind turbine is then considered as a reference and the efficiency of the farm computed using this reference power. This is represented on Figure 4.11 below.

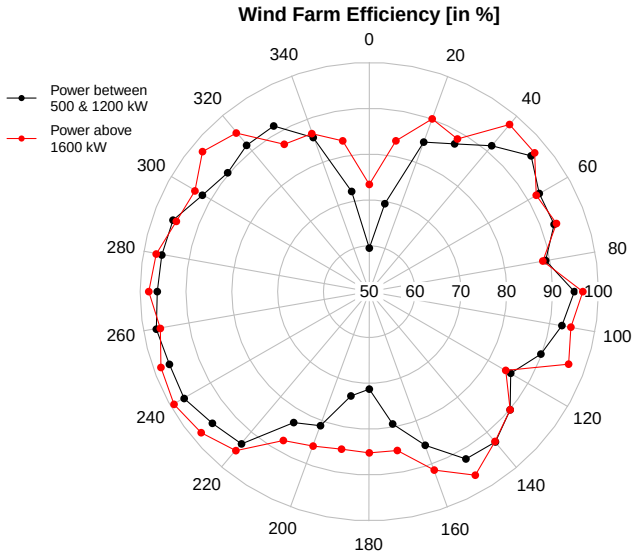

Figure 4.11: *Efficiency of the wind farm as a function of wind direction*

Not surprisingly, the efficiency is particularly low for northerly and southerly winds as the wind turbines are oriented along this particular direction. In the strong wake case, it is reduced to approximately 60% and 70% for wind direction of 0° and 180°, respectively. When the power increases, the impact of the wakes are seen to decrease as the efficiency the wake sectors increase of about 15%. The impact of the SMV6 - SMV5 wake can be seen in the sector [200°; 220°] where the efficiency is lower compared to the symmetric sector [140°; 160°].

4.3 Rotor Effective Wind Speed

As developed in Section 4.1.4 and Section 4.2, nacelle wind speed signal can prove fairly reliable once properly corrected when it comes to assessing power production of wind turbines based on 10-min average values. However, an efficient wind turbine control must bear on real-time observation of wind conditions, i.e. second-wise measurements. In that case the nacelle wind speed signal might prove too noisy to provide an efficient input to a controller, even with a low-pass filter. Wind speed measurements based on power production are better, but they cannot be used when the turbine has reached its nominal power or when it is curtailed or yawed. Therefore an alternative way of measuring wind speed must be found combining both accuracy and reliability.

The concept of Rotor Effective Wind Speed (REWS) was introduced in the PossPOW project as an answer for this problem [38]. It is based on SCADA measurement of rotor speed and pitch angle which are inputs into a Cp model shown on Equation (4.2).

$$\begin{aligned} C_p(\lambda,\theta) &= c_1\left(\frac{c_2}{\lambda_i} - c_3\theta - c_4\theta^{c_5} - c_6\right) exp\left(\frac{-c_7}{\lambda_i}\right) \\ \lambda_i &= \left[\left(\frac{1}{\lambda + c_8\theta}\right) - \left(\frac{c_9}{\theta^3+1}\right)\right]^{-1} \end{aligned} \tag{4.2}$$

where θ is the pitch angle and λ the tip-speed-ratio (TSR). This model was originally set up by [39], but later the coefficients were changed by [9] and [40] to fit for variable wind speed turbines. The values used in this section are indicated in Table 4.2. They are taken directly from the PossPOW project which proved to be working very well for different wind turbine models with rated power around 2 - 3 MW and located in offshore wind farms [41]. This is the first time that they are being tested for onshore wind turbines though.

Table 4.2: *Coefficients used in the Cp model of Equation* (4.2)

c_1	c_2	c_3	c_4	c_5	c_6	c_7	c_8	c_9
0.47	101	0.4	0.01	1.95	5	16.5	0.089	0.02

The REWS is computed iteratively by inserting Equation (4.2) in the classical active power equation and using the tip-speed-ratio expression between λ, the rotational speed ω and the wind speed U, shown below. A Newton-Raphson algorithm is set up to solve the iteration process. A description of the procedure followed can be found in Appendix B.1.

$$P = \frac{1}{2}\rho\, C_p(\lambda,\theta)\,\pi\, R^2\, U^3 \tag{4.3}$$

$$\lambda = \frac{R\omega}{U} \tag{4.4}$$

1-sec SCADA data from wind turbine SMV5 was processed between 01.12.2015 and 31.03.2016. The REWS was calculated alongside with the nacelle wind speed (NWS) and power curve wind speed (PWS, the wind speed extracted from the instantaneous measured active power and the ideal power curve). In Figure 4.12 are shown two different time series at low and high wind speed. In both cases the REWS is seen to be performing well, especially at low wind speed the REWS signal (as well as the PWS signal) appears much less noisy than the NWS signal: this is because the wind turbine is in variable-speed region and thus the values of pitch angle and TSR remain constant. The REWS and PWS represent an averaged wind speed over the total surface of the rotor, while the NWS is point measurement (and located behind the rotor). When the wind speed increases the values of TSR and pitch are changing at every second and therefore the REWS becomes much noisier.

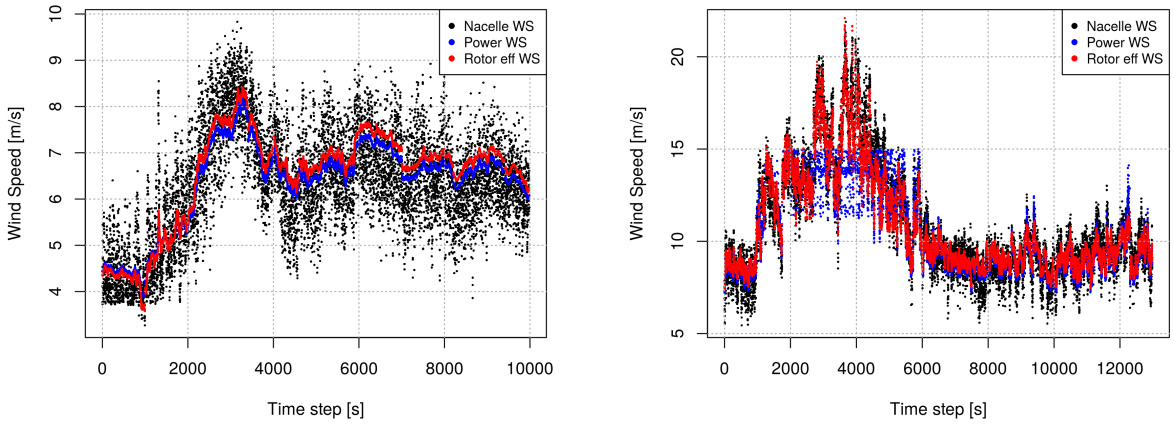

(a) At medium-low wind speed *(b) At high wind speed*

Figure 4.12: *Comparison of the performance of the rotor effective wind speed (REWS) with the nacelle anemometer (NWS) and the power curve wind speed (PWS) @ Wind Turbine SMV5*

The advantage of choosing the REWS rather than the PWS for assessing the free wind speed is partly seen on Figure 4.12b (between 2000 and 6000 sec, the incoming wind speed is above the rated wind speed of the wind turbine and therefore the PWS cannot be used), but it is even more visible on Figure 4.13, corresponding to a time series when the SMV6 turbine is curtailed. The REWS is seen to follow quite accurately the wind speed variations but as the active power of the turbine is limited to a fixed value (1600 kW) the PWS gives a constant and wrong wind speed estimation.

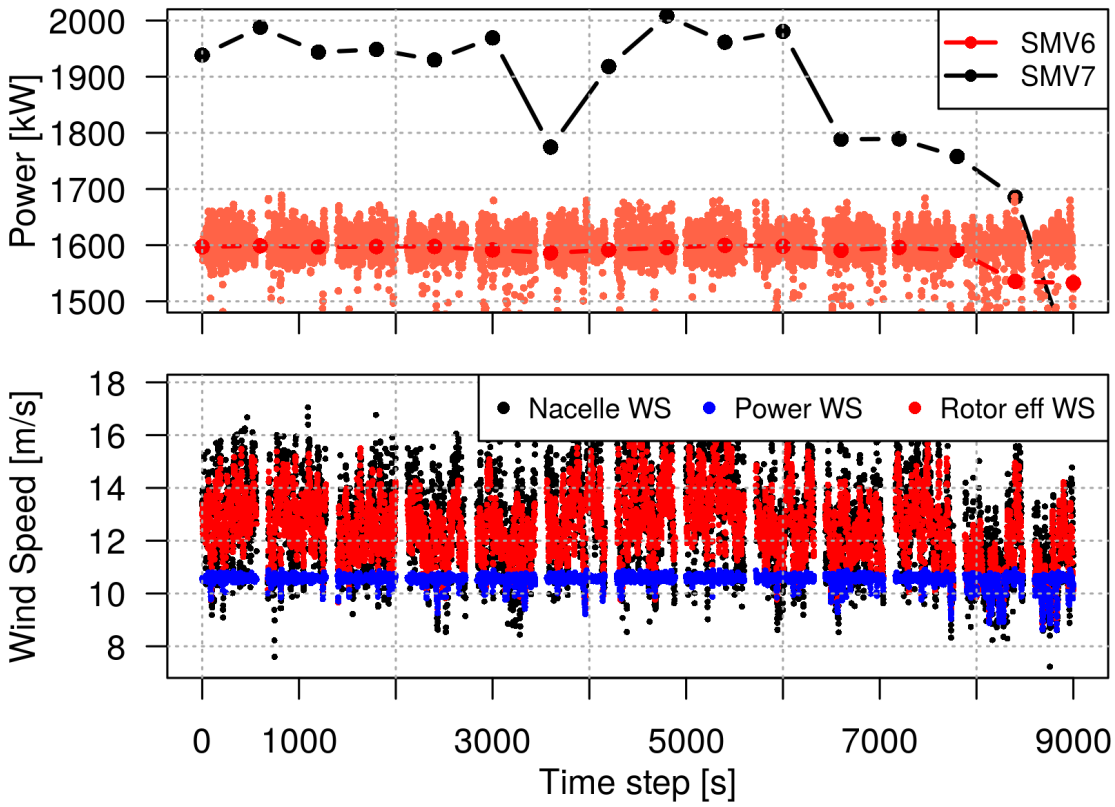

Figure 4.13: *Comparison of the performance of the REWS with the nacelle anemometer NWS and the power curve wind speed PWS @ Wind Turbine SMV6 (down-regulated at 1600 kW)*

In Figure 4.14 are compared the wind speed 10-min average values for these different signals with measurements from other external sensors (the met-mast and the windcube, both at 80 m). No particular sector filtering was done in this study, which explains the huge scatter of the data when either the windcube or the mast are considered. But in any case the results are really similar from the ones obtained in the case of the Lillgrund offshore wind farm and presented in [38]. Compared to this study, the use of a NTF to correct the nacelle anemometer is seen to improve the correlation between the NWS and the REWS. A very good correlation is obtained between the PWS and the REWS (in the wind speed range for which the power curve method is applicable), this is because they both include a geometrical averaging of the wind speed and thus have smaller variations.

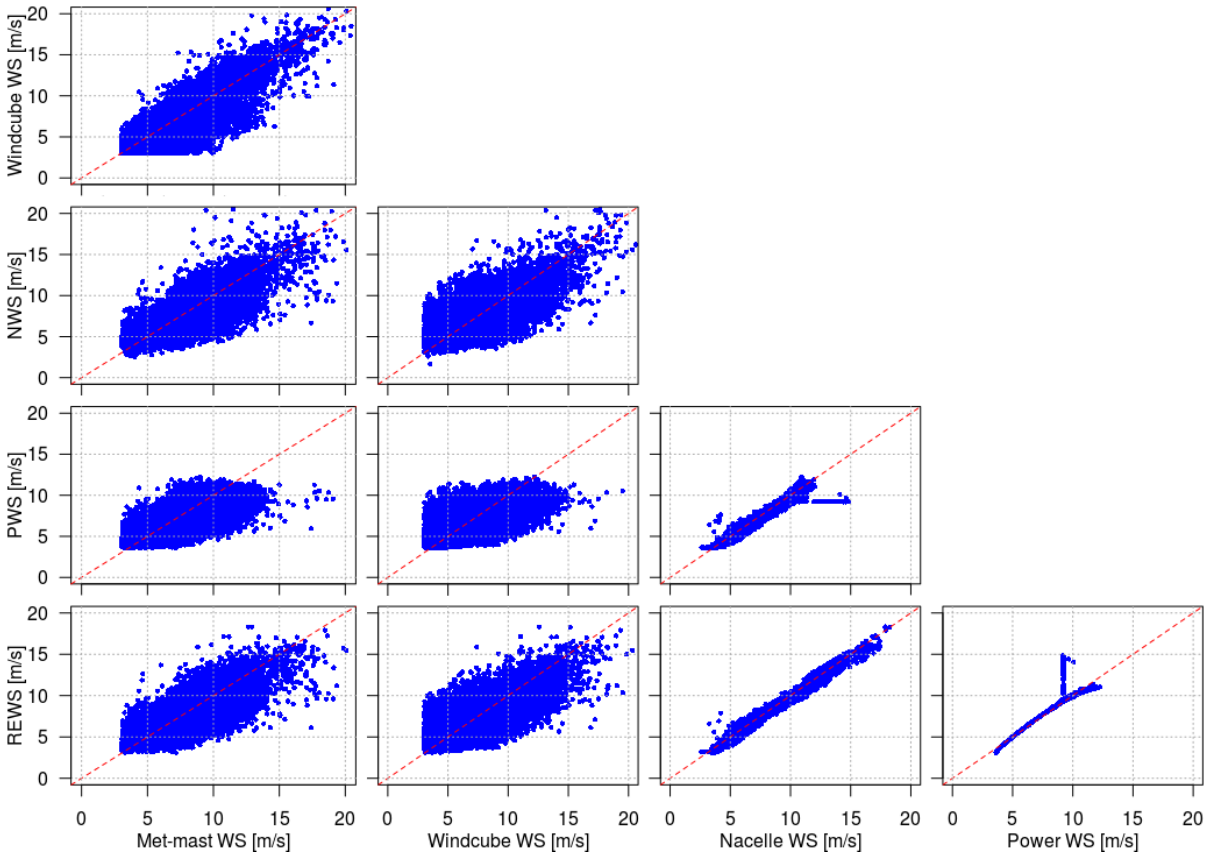

Figure 4.14: *Comparison of the Met-mast wind speed, Windcube wind speed, rotor effective wind speed (REWS), nacelle wind sped (NWS) and power curve wind speed (PWS) @ Wind Turbine SMV5*

4.4 On-site Turbulence Intensity

In this section is studied the on-site turbulence intensity (TI). This parameter is known for having a big influence on wind turbines, in particular on the power production and the fatigue loads. It has also an impact on the wake of the wind turbines, and thus it is needed to calibrate properly most of the wake models. As a consequence, it is of great interest to measure precisely the variations of the TI inside the wind farm.

The TI as seen by the wind turbine SMV5 is first studied using the different wind speed sensors introduced in the section Section 4.3: NWS, PWS and REWS. They are compared with the TI values computed from two external sensors: the met-mast and the windcube (position 1). The study is led on the same time period as previously: from 01.12.2015 to 31.03.2016. Please note that the met-mast measurements stopped on 29.03.2016 and that 10 days of 1-sec SCADA data was lost in the middle of March 2016 due to technical issues. The TI is binned both in wind speed (0.5 m/s bins) and direction (5° bins) and represented on Figure 4.15.

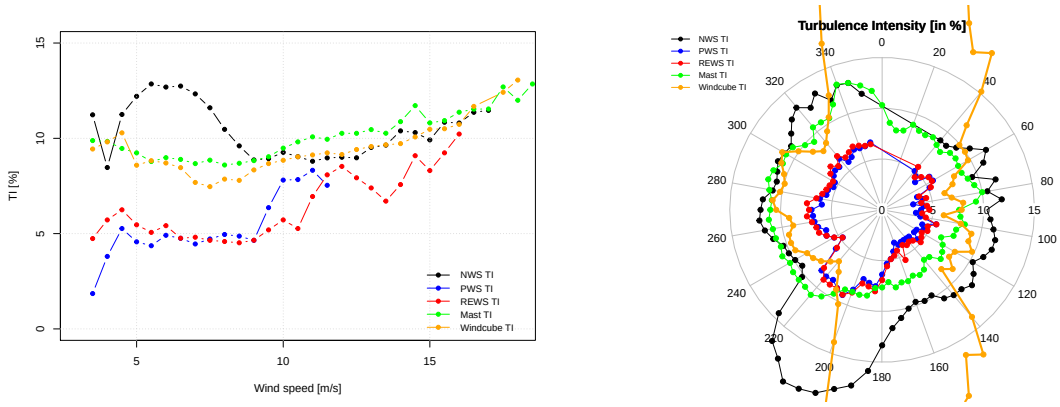

(a) Against wind speed *(b) Against wind direction*

Figure 4.15: *Ambient Turbulence Intensity @ Wind Turbine SMV5*

As it can be seen on Figure 4.15b, the TI seen by the windcube is increasing particularly when the wind comes from 10 or 170° ± 30°, i.e. when the instrument is under the wake of SMV2 and SMV3, respectively. This is due to the fact that lidar needs an homogeneous flow to reconstruct the wind speed from their radial measurements; when one or more of their beams are in the wake of a wind turbine, the wind speed and direction measurement goes wrong and the TI can increase artificially. These particular wind sectors have been filtered out for the lidar signal when plotting Figure 4.15a to avoid having results driven to higher values only because of this measurement problem. Similarly, in the same graph the sector corresponding to the wake from SMV6 has been removed for the sensors located at SMV5. Although the met-mast is in wake of the wind farm in case of westerly winds, they were not filtered because otherwise the dataset would been reduced too much. Thanks to the high distance between the wind turbines and the mast, the impact of the wake is not as strong as for the windcube or the windturbines. It is not negligible though, as seen on the polar plot the TI seen by the mast is 1 or 2% higher when the wind comes from the West rather than the East.

In both graphs it can be seen that the REWS TI and the PWS TI are much smaller than the NWS TI or the met-mast TI. As already mention in the previous section, this is because these wind speeds are averaged over the whole surface of the rotor: the inertia of the rotor decreases the wind speed fluctuations and the smaller eddies are filtered out. On the other hand NWS and met-mast are point measurement and every single variations of the wind speed contributes to increasing the TI. The NWS is also in permanence in the wake of the its own rotor and thus exposed to increased fluctuations. This is particularly visible between 5 and 10 m/s where the wake emitted by the turbine is very strong and consequently the NWS TI signal increases significantly. At higher wind speed the REWS and PWS are both increasing, this is because the operational parameters of the wind turbine (basically TSR and pitch) begin to vary and thus their wind speed signals become noisier, as seen on Figure 4.12b.

In all SMV5 curves, the impact of the SMV6 wake is clearly visible and represented by an increase in TI. As the NWS signal is more sensitive to perturbations, this increase is particularly important on that curve, while on the REWS and PWS the impact is a bit smaller. Based on this example, a Turbulence Intensity rose is computed for each turbines in the wind farm and represented on Figure 4.16. These curves are derived from the 10-min SCADA averaged and standard deviation values of the nacelle wind speed signal, not corrected with the NTF.

In the case of northerly or southerly winds, the turbulence intensity is seen to increase significantly for the first wind turbine in the wake, and then remains more or less constant for the following turbines of the row. This behavior was already observed for offshore wind farms of Lillgrund and Horns Rev [42].

As already mentioned about Figure 4.15b, the TI seen by the met-mast is increasing for westerly winds due to the wake of wind turbines. Other particularities of the terrain can also be discussed. For the wind turbine SMV7 (and partly SMV6), the measured TI is increasing in the sector [160°; 220°] due to presence of the small wood as seen on Figure 3.1. A smaller increase is noticed for the wind turbine SMV1 on the sector [340°; 20°]. It is assumed that this increase is caused by the presence of a motorway at the North of the wind farm, as the met-mast seems also to be affected on the sector [330°; 360°].

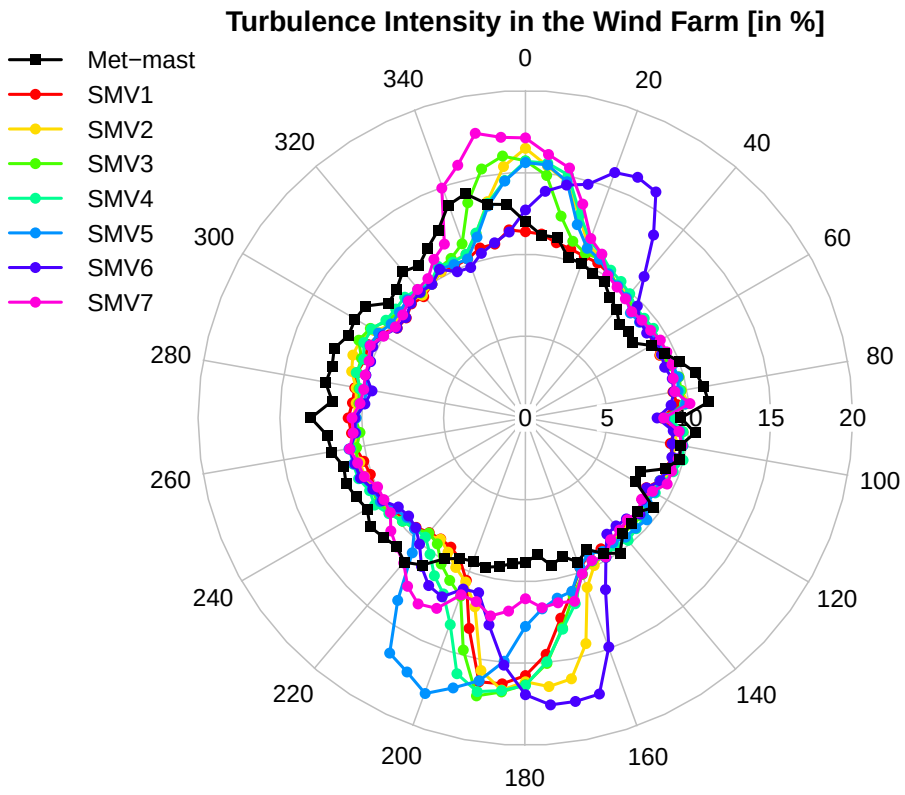

Figure 4.16: *Local TI measured by the wind turbines of the farm*

4.5 Summary

Even though an extensive instrumentation was set up for the field tests of SMARTEOLE, due to some technical issues the recovery of data from sensors proved to be limited. It has therefore been decided to rely mainly on SCADA wind measurements for the rest of the study. These measurements being influenced the distored flow behind the rotor, they have been corrected as accurately as possible to ensure a good enough reliability.

The analysis of the wind farm performance underlined a strange behavior of the two wind turbines of the study, SMV5 and SMV6, which are seen to have an increased yaw error with the increasing wind speed. This is particularly visible on the SMV6 - SMV5 wake and the SMV5 power curves in the wake sector. This behavior need to be taken into account when modeling consistently the power deficit of the wind turbines in the next chapter.

The study of the Rotor Effective Wind Speed confirms the potential of this method for assessing the incoming wind speed for real time wind turbine control. Finally the turbulence intensity in the wind farm could be measured and discussed, this distribution will be used later to improve the wake modeling.

5 | Wake Modeling

In order to run simulations to optimize the overall power production of the wind farm, the behavior of the different components must be described as reliably as possible. Modeling the wake is a key element to be able of predicting the power production of the different wind turbines as a function of the incoming flow conditions.

A review of several wake models developed at the Technical University of Denmark can be found in [43]. The models offering the best representation of the physics phenomenons and the dynamics inside the wake are generally computational fluid dynamics (CFD) models based either on Reynolds Averaged Navier-Stokes (RANS) equations or Large Eddy Simulation (LES), but they are more difficult to calibrate as they need a very accurate description of the atmospheric and flow conditions occurring in the wind farm to perform properly and they are also more costly to run. Here, the computational time is of great importance since the model expected to be used in an optimization process for real time control; and the only parameter considered is the active power of the wind turbines. CFD models are thus not really made for these purposes.

Therefore, it has been decided to focus only on simple but well known and robust wake models; in particular the Jensen [44, 45] and Larsen [46, 47] models which have been used in the research and the industry for years and are implemented in the software WAsP [48] and WindPro [49]. Moreover, the equations involved in those models are fairly simple and thus very easy to implement in any software in a computationally efficient way.

These two models are studied in mode details and calibrated using the experimental data in Sections 5.1 and 5.2. They are then being compared and discussed in Section 5.3. Finally, the chosen model is confronted to experimental data in Section 5.4 to ensure its reliability.

5.1 The Jensen Model

The Jensen model was first introduced by Jensen [44] and Katic [45] during the 80s. It is probably the most well known wake model and has been used for decades on both research and industry. In this model the incoming wind flow U_0 is assumed to be uniform and the wake to expand linearly at a coefficient α, called wake expansion coefficient or wake decay constant, as illustrated on Figure 5.1 and Equation (5.1).

$$R_w = R + \alpha x \tag{5.1}$$

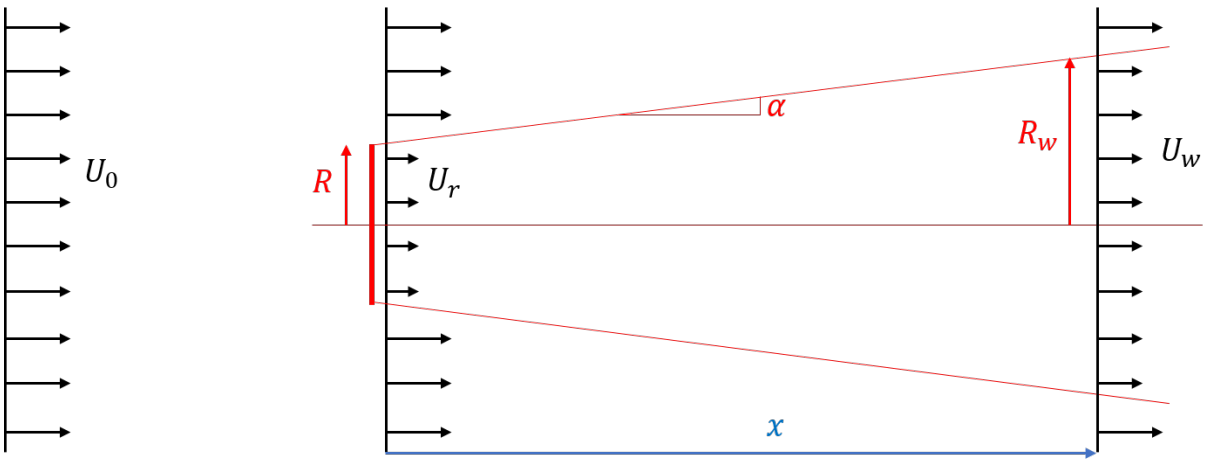

Figure 5.1: *Principle of the Jensen model*

The value of the wind speed at the downwind WT location U_w is derived from the equation of conservation:

$$U_r R^2 + U_0 \left(R_w^2 - R^2\right) = U_w R_w^2 \tag{5.2}$$

noticing that the wind speed at the upwind rotor is linked to the free-flow wind speed through the induction factor $a = 1 - 2\frac{U_r}{U_0}$, which can also be expressed as a function of the thrust coefficient Ct: $a = \frac{1-\sqrt{1-C_t}}{2}$. Combining all those equations leads to the expression of the wind speed deficit coefficient $\delta_w = 1 - \frac{U_w}{U_0}$ presented below.

$$\frac{U_w}{U_0} = 1 - \delta_w = 1 - \frac{1-\sqrt{1-C_t}}{(1+\alpha x/R)^2} \tag{5.3}$$

When summing the wakes from two or more upwind rotors, the wind speed deficit are summed quadratically. Therefore the wake deficit δ_n at the n-th wind turbine can be expressed as:

$$\delta_n = \sqrt{\sum_{i=1}^{n-1} \delta_i^2} \tag{5.4}$$

where δ_i is the wind speed deficit due to wind turbine i.

Wake Decay Constant and Calibration of the Model

In the Jensen model there is only one free parameter to calibrate which is the wake expansion coefficient α (the Ct value being given by the upwind turbine setting). This parameter is dependent on the atmospheric conditions of the wind farm site, and it is recommended to take $\alpha = 0.075$ and $\alpha = 0.05$ for onshore and offshore wind farms, respectively. However, some studies show that these values tend to under-estimate the wake deficits, especially in the case of a flat and homogeneous terrain, with a low roughness (as it is precisely the case for the SMV wind farm) [50]. It is proposed to express α as a function of the roughness length z_0 and atmospheric stability (through the function Ψ_m and the Monin-Obukhov length L) [50]:

$$\alpha = \kappa \left[ln\left(\frac{h}{z_0}\right) - \Psi_m\left(\frac{h}{L}\right)\right]^{-1} \tag{5.5}$$

but it can also be simplified as a linear function of the ambient turbulence intensity, as found in [51]: $\alpha = 0.4\,(TI)_{amb}$. In [52], a modified Jensen model was implemented where the wake decay constant was changed at each wind turbine to take into account the wake added TI, which was itself modeled based on an empirical formula taken from [53], where x_n is the length of the near-wake:

$$\alpha = \frac{1}{6}\,(TI)_{wake} \tag{5.6}$$

$$\text{with } (TI)_{wake} = \sqrt{(TI)_{amb}^2 + (TI)_{added}^2} \tag{5.7}$$

$$\text{and } (TI)_{added} = 5.7\,C_t^{0.7}\,(TI)_{amb}^{0.68}\left(\frac{x}{x_n}\right)^{-0.96} \tag{5.8}$$

The first simulations carried out the data from the SMV wind farm tends to confirm these considerations. As shown on Figure 5.2, which represents the single wake events SMV7-SMV6 and SMV1-SMV2, choosing the recommended value of 0.075 clearly under-estimates the deficit at the downwind turbine. A wake decay constant of approximately 0.05 - 0.6 appears to be much more consistent.

Based on these results and the study of the on-site turbulence intensity presented on Section 4.4, it has finally been decided in this thesis to express the wake decay constant as a linear function of the local turbulence intensity, as in [52], but using directly the measured TI, $(TI)_{meas}$, instead of modeling it:

$$\alpha = k\,(TI)_{meas} \tag{5.9}$$

where k is an empirical parameter to calibrate. From the study of the wake events in the wind farm (presented on Section 5.3 below), this parameter was assessed to $\mathbf{k \simeq 0.55}$, considering the TI distribution of Figure 4.16 which is calculated by the nacelle anemometers and varies around 10 - 12.5% for upwind wind turbines. It must noted that this value is calibrated for a TI derived from a nacelle anemometer

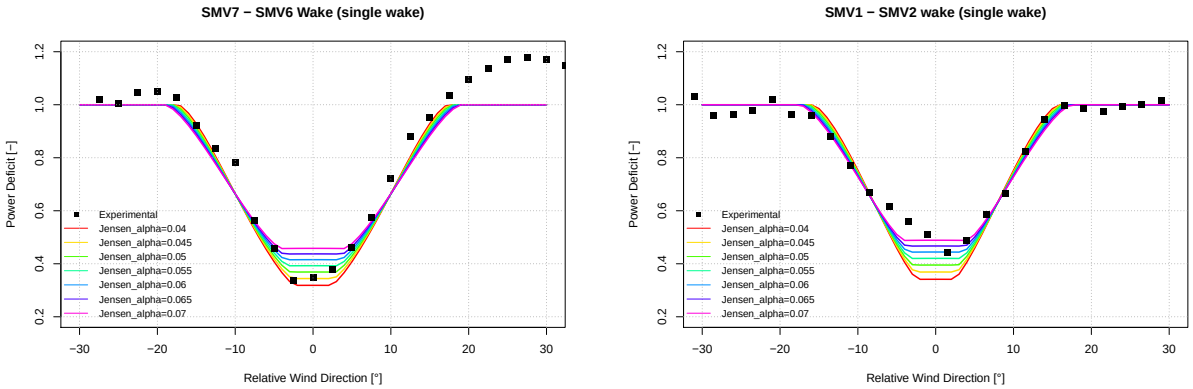

Figure 5.2: *Jensen wake deficit as a function of the value of the wake decay constant*

signal only and contains and additional noise due to the perturbation of the rotor. Using a TI calculated through other signals, for example the power curve method or the REWS, which present a much lower TI (as seen on Figure 4.15), would results in different values for k in order to stay in the same order of magnitude for the final value of α, i.e. approximately $\sim 0.055 - 0.07$.

5.2 The Larsen Model

The Larsen model was first introduced on 1988 as a simple wake calculation procedure [46]. It is more complex than the Jensen model as it is based on the RANS form of the equation of momentum, decomposing the wind speed as the sum of the (averaged) inflow wind speed U_0 and axial (u_x) and radial u_r perturbations.

$$U_0 \frac{\partial u_x}{\partial x} = \frac{1}{r}\frac{\partial}{\partial r}\left(l^2 r \left(\frac{\partial u_x}{\partial r}\right)^2\right) \tag{5.10}$$

where l is the mixinng length from Prandlt's mixing length theory. This model still assumes an axis-symmetric form for the wind speed deficit inside the wake, however this time this deficit is not constant and depends on the radius r from the axis of symmetry.

Solving Equation (5.10) together with the continuity equation and the boundary conditions $U_0 \gg u_x$ and $u_x = 0$ at the boundary of the wake leads to the following expressions for the wake radius R_w, and the axial and radial perturbations:

$$R_w(x) = (35/2\pi)^{1/5}(3c_1^2)^{1/5}(C_t A(x+x_0)^{1/3} \tag{5.11}$$

$$u_x(x,r) = -\frac{U_0}{9}\left(C_t A(x+x_0)^{-2}\right)^{1/3}\left[r^{3/2}(3c_1^2 C_t A(x+x_0))^{-1/2} - \left(\frac{35}{2\pi}\right)^{3/10}(3c_1^2)^{-1/5}\right]^2 \tag{5.12}$$

$$u_r(x,r) = -\frac{U_0}{3}\left(C_t A\right)^{1/3}(x+x_0)^{-5/3} r\left[r^{3/2}(3c_1^2 C_t A(x+x_0))^{-1/2} - \left(\frac{35}{2\pi}\right)^{3/10}(3c_1^2)^{-1/5}\right]^2 \tag{5.13}$$

where A is the rotor swept area and x_0 and c_1 are two empirical constants related to the position of the rotor relatively to the applied coordinate system and the mixing length.

This model was updated later in 2009 [47] considering the analysis of experimental data from full scale wind farm. The new boundary conditions are now fixed on the rotor plane and at fixed frame of

reference located 9.6 D downstream. It also gives rules for calculating wake summation for multiple wake effects inside wind farms (the early version of 1988 was only focus on a single wake case). Two different approaches are considered, a linear approach corresponding to a geometric averaging of the inflow wind speed coming over the rotor area, and a root-mean-square approach which is based on conservation of momentum.

$$\overline{U} = \frac{1}{A_{rot}} \int_{A_{rot}} U dA \tag{5.14}$$

$$\overline{U} = \sqrt{\frac{1}{A_{rot}} \int_{A_{rot}} U^2 dA} \tag{5.15}$$

In this thesis only the linear approach (from Equation (5.14)) is considered. In Appendix B.2.2 is explained the procedure followed for the implementation of the Larsen model. The wake contribution from each wind turbine are summed linearly in the case of multiple wake events.

Calibration of the Model

As seen on Equations (5.11) - (5.13), there are two parameters to calibrate in the Larsen model, c_1 and x_0. In the later version of the model, Larsen provides equations for calculating their values [47]. In those equations, also presented on Appendix B.2.2, the two parameters are obtained from the value of the upwind turbine thrust coefficient and ambient turbulence intensity, using empirical coefficients derived from the wake event at the Vindeby offshore wind farm. In this thesis, these coefficient were kept for the calibration of the model without any modifications.

Considering an ambient turbulence intensity varying around 9 - 10% (depending on the direction sectors) and a thrust coefficient of 0.79 (corresponding to the ideal C_t value in the variable speed region, see Figure 3.5), the obtained values for x_0 and c_1 were varying around 35 m and 0.25, respectively.

5.3 Comparison and Choice of a Wake Model

In this section, the performance of the two wake models presented above is compared using several wake events in the wind farm: the two single wake events SMV7 - SMV6 and SMV1 - SMV2, and the wake event SMV6 (+SMV7) - SMV5 which corresponds to partial summation of two wakes. The data set considered is the same as previously (10-min SCADA data from 15.06.2015 to 01.08.2016) but the data was also filtered to keep only the points when the upwind turbine had an active power between 300 and 1200 kW. This is done to make sure that the upstream wind turbine operation stays in the variable speed region which ensures a constant Ct equal to 0.79. The normalized power and the local TI signals were binned into 2.5° bins, and linear interpolation was used to get the measured TI between each bin.

Three different models are compared here, the *original* Jensen model (considering a constant wake expansion coefficient, taken as 0.06 since it appears to be the best value for the three wake events), the *TI re-calibrated* Jensen model (where α is calculated from the local measurement of the nacelle TI at the upstream wind turbine), and finally the Larsen model (whose coefficients are calculated from the ambient TI measured at the met-mast for each wind direction sector and kept constant for all wind turbines).

The performance of these models is shown on Figure 5.3. In these graphs a very small difference is seen between the two versions of the Jensen model. This is because the TI for the upwind wind turbine is very similar in all cases and gives wake decay constant close to 0.06 using the linear model. On the other hand, the Larsen model is clearly underestimating the power deficit caused by the wake at the downstream wind turbine. With this model the wake recovery happens much faster than in the Jensen model and the results presented here are analogous to the benchmarking study realized in [43] about the Sexbierum and Lillgrund wind farms.

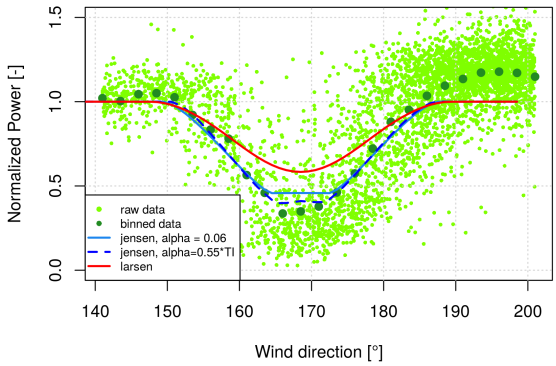

(a) SMV7 - SMV6 wake event (single wake)

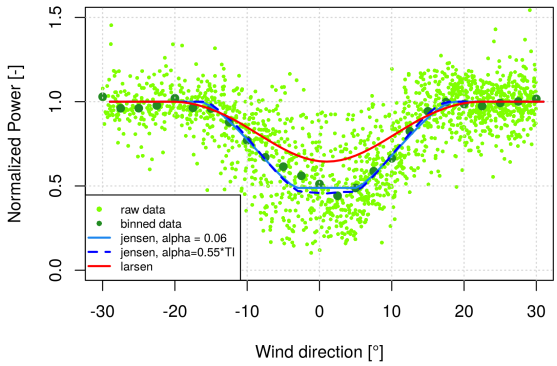

(b) SMV1 - SMV2 wake event (single wake)

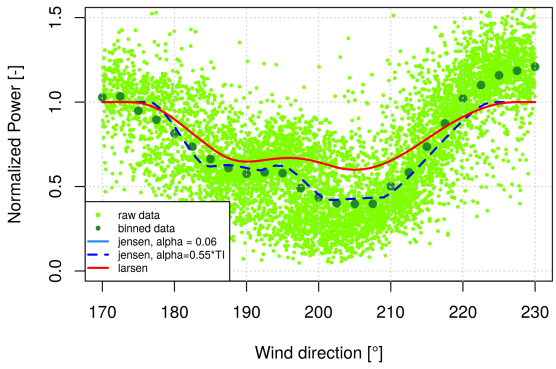

(c) SMV6 (+ SMV7) - SMV5 wake event (double wake)

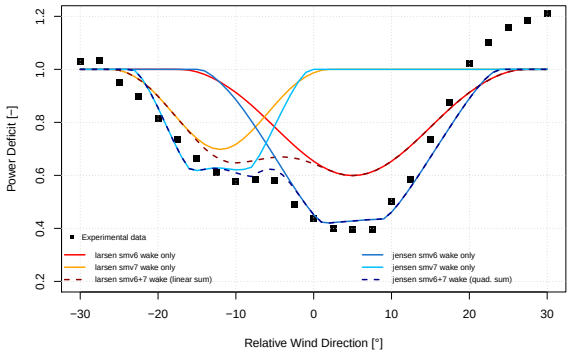

(d) SMV6 (+ SMV7) - SMV5 wake summation

Figure 5.3: *Performance of the wake models*

On Figure 5.4 is studied more specifically the row SMV1 to SMV5. The normalized power is represented against the distance to the most upwind wind turbine (SMV1) for an absolute wind direction of $+5°$ (the corresponding relative wind directions between all wind turbines of the row have been computed and corrected accordingly to give the right input into the wake model). The data is now filtered to keep only the 10-min periods when the active power of SMV1 is between 800 kW and 1200 kW. This is done to ensure that the assumption of a constant Ct still equals to 0.79 remains valid also for the downwind wind turbines, the wake deficit varying around 0.5 in the worst case situation.

The interest of having a TI-dependent wake expansion coefficient for the Jensen model is now particularly visible. Being under the wake of the other wind turbines, SMV2, SMV3 and SMV4 are facing a higher TI, therefore their own wake is expected to recover much quickly due to an increased mixing with the undisturbed flow. It can be seen that considering a linear dependency with TI, α increases from $\simeq 0.07$ at SMV1 to $\simeq 0.1$ at SMV4. Considering a fixed value for α, valid for the most upwind wind turbine, cannot take into account these changes and thus leads to clear over-estimation of the power deficit at the most downwind wind turbines.

The Larsen model is seen to under-estimate the wake for the first two wind turbines, and then over-estimate for the last two. For the former, this is due to the fact that in the Larsen model the wake recovery is faster than in Jensen. The over-estimation is caused by the fact that in this model the wakes are summed linearly and not quadratically as in Jensen. Therefore, the wake contribution from the most upstream wind turbines remains high even at a large distance downstream and after a certain number of contributing turbines the total wake deficit given by Larsen becomes higher than the measured values. This effect would have probably been seen at the third wind turbine too if the three turbines SMV1 - SMV2 - SMV3 were perfectly aligned.

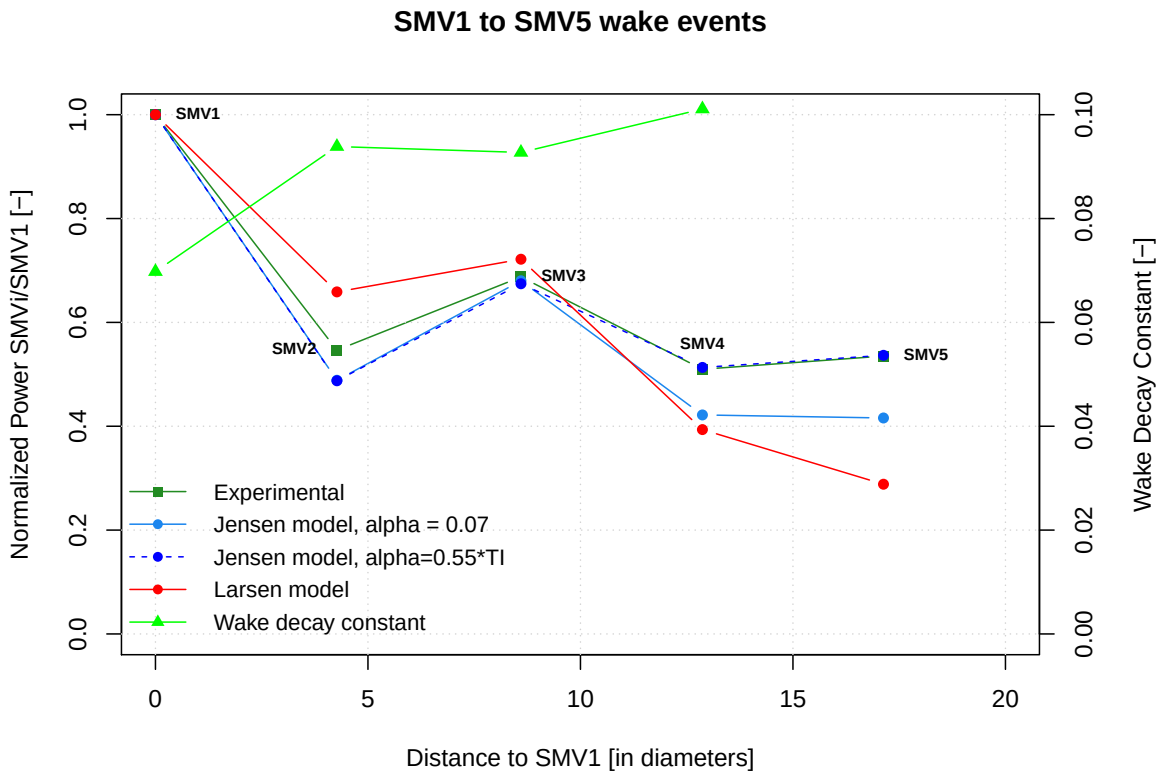

Figure 5.4: *Variation of the power deficit and wake decay constant along the SMV1 - SMV5 row (absolute wind direction of +5°)*

The *TI re-calibrated* Jensen model is therefore the model representing the wake deficits inside the wind farm with the best accuracy, and it also presents the advantage of having a very fast execution. As a consequence this is the model which is chosen for the optimization process realized on the following chapters, using the TI distribution calculated for each wind turbine on Section 4.4.

5.4 Validation of the Wake Model

So far in this section the experimental data has always been filtered to consider only the case of a constant Ct to calibrate and choose properly a wake model. In this sub-section is now studied the case of a varying Ct in order to make sure that the chosen wake model remains consistent in the whole power curve range. The wake event SMV6 - SMV5 is the only one investigated since these are the wind turbines that will be studied in more detail later in Chapters 6 and 7 and also because of their alignment oriented close to the prevailing wind direction that allows a significant number of available data-points for this wake event.

5.4.1 Correction of Inputs into the Model

Before studying the the power curve of the SMV5 wind turbine, it is needed to identify the correct inputs required by the Jensen model. As the wake event considered consists of a summation of two wakes coming from SMV6 and SMV7, this must be done for these two turbines.

There are four varying inputs needed to compute properly the wind speed deficit at the downwind turbine using the Jensen model: the thrust coefficient Ct, the wake expansion decay α, and the relative wind direction (since the distance x between the two turbines is known and remains constant). As in this section the upwind wind turbines are functioning normally, the thrust coefficient can be taken directly

from the guaranteed curve provided by Senvion (see Figure 3.5). As explained in the previous section, the wake decay constant is taken as a linear function of the local TI at each wind turbine. Therefore for both SMV7 and SMV6 the TI was tabulated in terms if wind speed (1 m/s bins) and wind direction (10° bins) which allows to compute a particular value for α for every incoming wind conditions.

However, as observed in Section 4.2, the SMV6 wind turbine is seen to have an increasing yaw error with the increasing wind speed, and consequently its wake is deflected. The SMV6 - SMV5 wake center position measured at the SMV5 wind turbine is varying from $\sim 203°$ at low wind speeds to $\sim 210°$ at rated wind speed (please refer to Figure 4.9). Looking at the SMV7 - SMV6 wake, a similar behavior was observed for SMV7 with an even greater deflection, since the wake center position moves from $\sim 166°$ to $\sim 180°$ between cut-in and rated wind speeds. To take into account these behaviors, the relative wind direction given as input into the wake model is corrected as a function of the wind speed, to make sure that the maximum wake deficit is obtained for the same wind direction as observed in the experimental data.

This correction is presented on Figure 5.5a, while Figures 5.5b to 5.5d illustrate its relevance by looking at the summation of the two wakes. It can be seen that both of them are moving towards higher wind direction with the increasing power production and that the full wake conditions that were happening round 200 - 210° at low wind speeds are shifted around 205 - 215° for higher wind speeds. It also seems that the correction implemented is able to follow this change and capture rightly the power deficit.

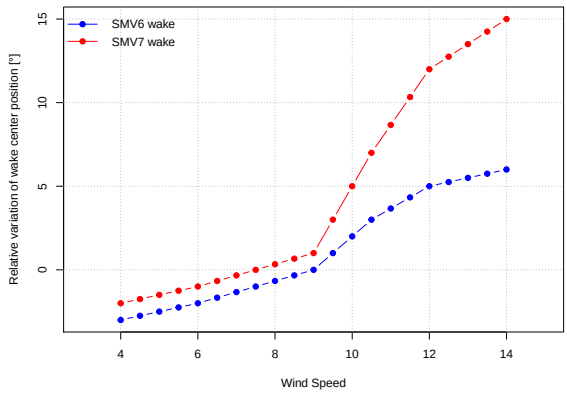

(a) Correction in the relative wind direction to be used for the SMV7 and SMV6 wake events

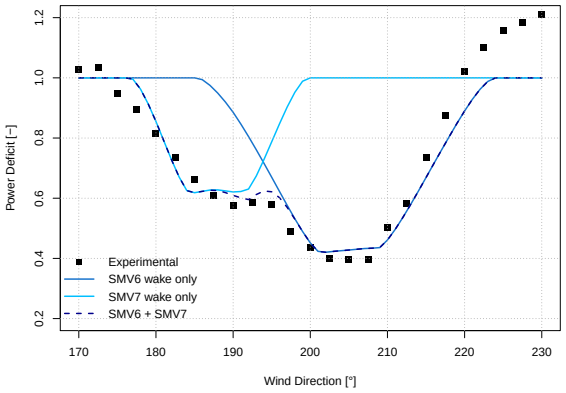

(b) At low wind speeds

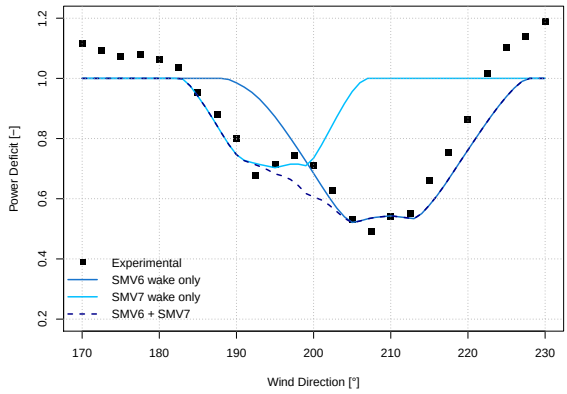

(c) At medium wind speeds

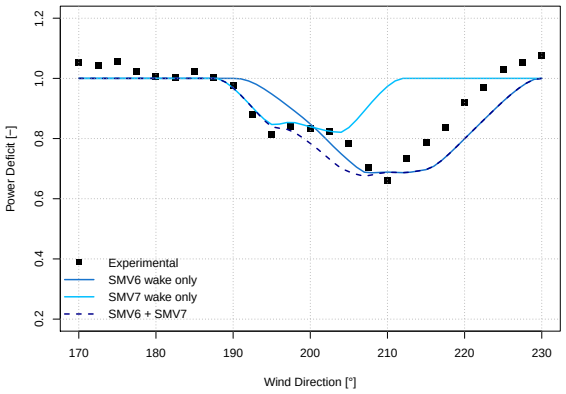

(d) At high wind speeds

Figure 5.5: *Calibration of the relative wind direction used as input into the wake model based on the summation of the SMV6 and SMV7 wakes at different wind speed ranges.*

5.4.2 Comparison of Power Curves and Validation

The modeled power curves of SMV5 are now compared with the experimental data in Figure 5.6 for three different sectors: [190°; 200°], [200°; 210°] and [210°; 220°]. For the experimental data, the wind direction is assessed using the measurement from SMV7 and the power curves are calculated using the nacelle wind speed from SMV6, corrected with the NTF (the SMV7 wind speed proved to be slightly under-estimated due to the presence of the wood nearby).

For the computation of the wind speed deficit at SMV5, the reference wind directions used in the Jensen model for the three considered sectors are taken as 195°, 205°, and 215°, respectively. A relative wind direction is then deduced at each wind speed from the wake deflection correction described above for both SMV6 and SMV7 (the modeled power curve without any wind direction correction is shown in red).

Once the effective wind speed at SMV5 has been determined, it must be converted into a power value using a power curve. The most obvious idea would be to use the SMV5 experimental power curve derived in Section 4.2 and very close from the Senvion ideal curve. However using this power curve always led to an over-estimation of the modeled power, represented in orange. A much better correlation was obtained when using the experimental SMV7 power curve calculated in the same sector. This result is not really explained but provides a very good result for all three sectors as can be seen with the green curve. Therefore, it has been decided to save the SMV7 power curve in each sector for further use when using the wake model for calculating the SMV5 downwind power.

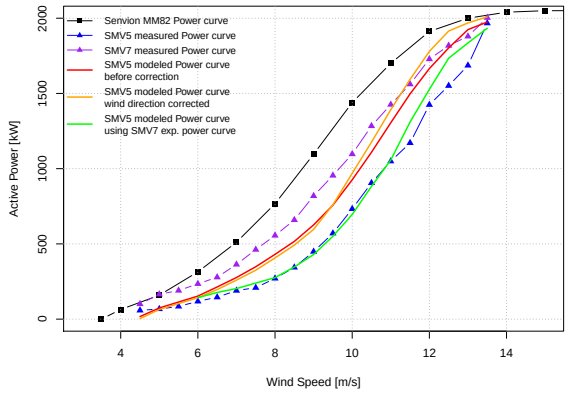

(a) Between 190° and 200°

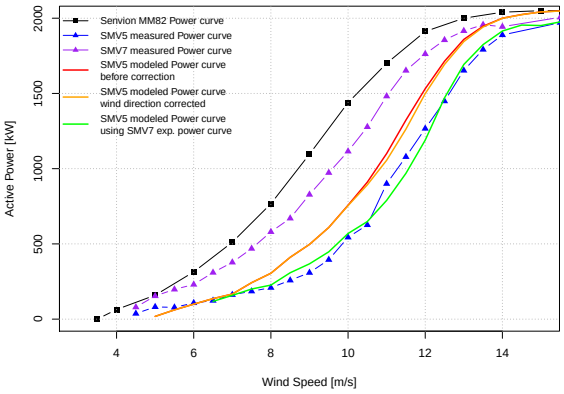

(b) Between 200° and 210°

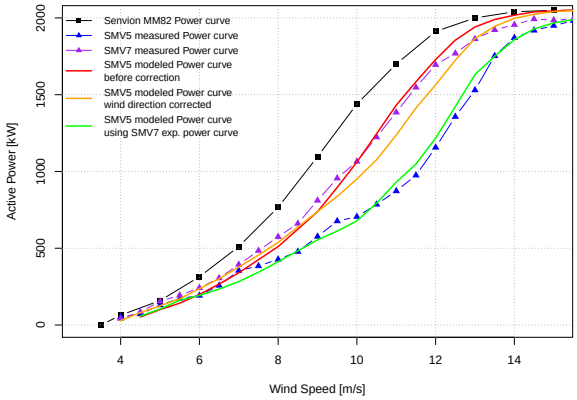

(c) Between 210° and 220°

Figure 5.6: *Comparison of experimental and modeled power curves for three different wind direction sectors*

5.5 Summary

Two different wake models have been reviewed, calibrated and confronted to experimental data. A re-calibrated Jensen model could be derived, where the wake decay constant is calculated at each wind turbine based on the local turbulence intensity measurement. This model proved to be reproducing the different wake deficits inside the wind farm with a very good accuracy, especially along the row SMV1 to SMV5.

In Section 5.4, this model was also validated on the complete wind speed range for the SMV6 - SMV5 wake event. In order to take into account the particular behavior of the SMV6 and SMV7 wind turbines, the relative wind directions to be given as input into the model were corrected based on the measured variation of their respective wake positions. Consequently, the SMV6 - SMV5 wake is now modeled with a great reliability and this modeling can be trusted for the optimization to be performed in Chapter 6.

6 | The Curtailment Strategy

In this chapter is studied very extensively the impact of a curtailment strategy in the combined power production of two wind turbines. The experimental results obtained during the first measurement campaign are first analyzed and suggest a potential for this strategy. Then, a Ct model which is to be an input into the re-calibrated Jensen model, is proposed and validated using the available data from the curtailment field test. Finally, using the combination of this Ct model and the re-calibrated Jensen model, the combined power production of the two wind turbines SMV 5+ SMV6 is optimized.

6.1 Analysis of the Experimental Results

The results from the curtailment field test, realized between December 2015 and April 2016, are studied in this section. The curtailment strategy set up during these tests is first presented, and then the data is analyzed in terms of power production and turbulence intensity.

6.1.1 Curtailment Strategy Implemented during the Field Test

In this first field test of the SMARTEOLE project only the wind turbine SMV6 was curtailed. Only the combined power production of SMV5 and SMV6 is therefore of interest. The wind turbine was down-regulated to a maximum of 20% power in two different steps, based on the reference power given by SMV7 and as expressed on Equation (6.1) and illustrated on Figure 6.1 below.

$$\begin{cases} P_{SMV6} = 1200\ kW & \text{if } 1200 < P_{SMV7} < 1500\ kW \\ P_{SMV6} = 1600\ kW & \text{if } 1600 < P_{SMV7} < 2000\ kW \end{cases} \tag{6.1}$$

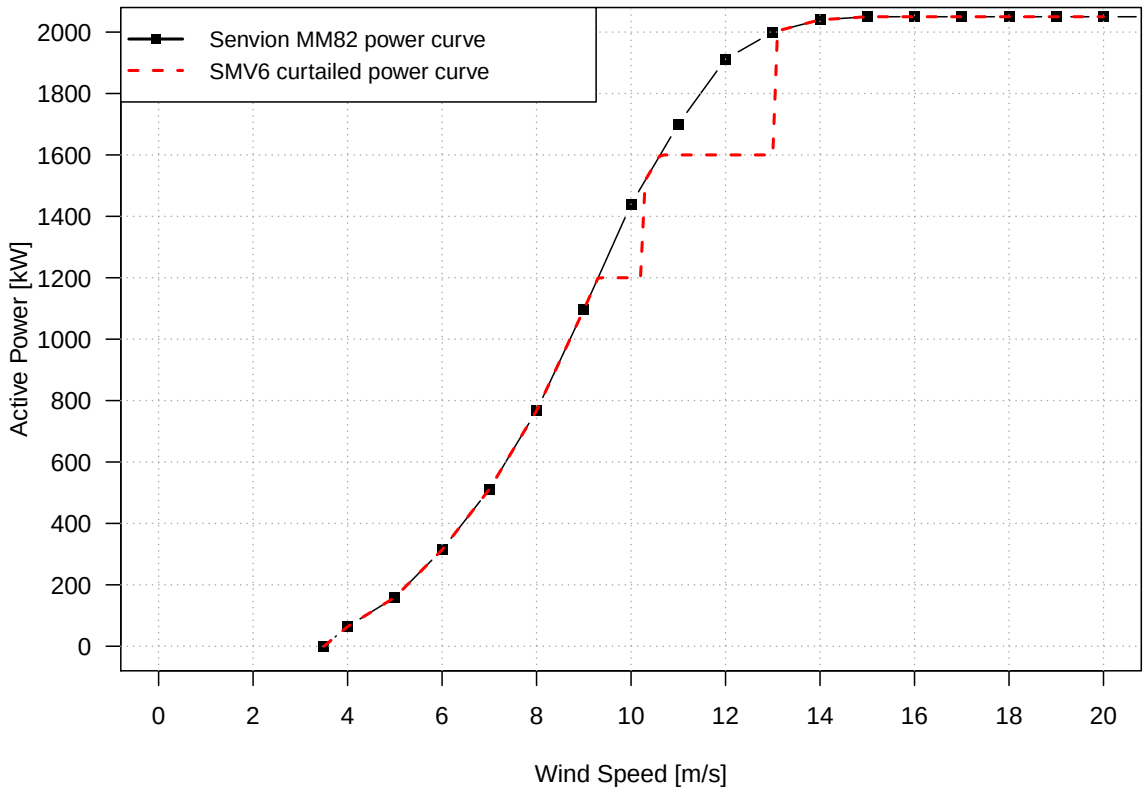

Figure 6.1: *The curtailed power curve implemented in the field test*

This configuration can be qualified as a hard curtailment strategy. A down-regulation of 20% is probably too significant to achieve an increase in the combined power production. The gains are likely to be found when the wind turbine is curtailed for a few percents only [35]. However the technical constraints imposed on the wind turbine control did not allow the implementation a very customized power curve. On the other hand, imposing such a big down-regulation on the upwind turbine makes the analysis of the results easier as the impact of the SMV6 curtailment is expected to be clearly visible on SMV5. Indeed, the objectives of this first campaign were more focused on highlighting some phenomenons about wind turbine wake rather than really achieving an increase in overall power production, and consequently the scenarios implemented were maybe too strong.

The curtailment of SMV6 was manually triggered by the operation and maintenance team of ENGIE Green when the needed external conditions were met: a strong enough wind (above 10 m/s) coming from the South-South-West (180 - 220°). The reference wind direction was taken from the SCADA signal of SMV7. However this was done before this wind direction signal was re-calibrated and due to the error of 20° in this signal the curtailment periods were finally only triggered in the sector [200; 240°]. As a consequence, half of the measures obtained were outside of the sector, and the remaining were concentrated on the right part of the SMV6 - SMV5 wake. Moreover, due to wind fluctuations, the curtailment was not effective all the time during the total down-regulation period as sometimes the reference power went below the triggered values. This is shown on Figure 6.2 representing a time series recorder on December 22nd 2015. A second filtering must also be realized in order to select only the 10-min data points when SMV6 was effectively curtailed.

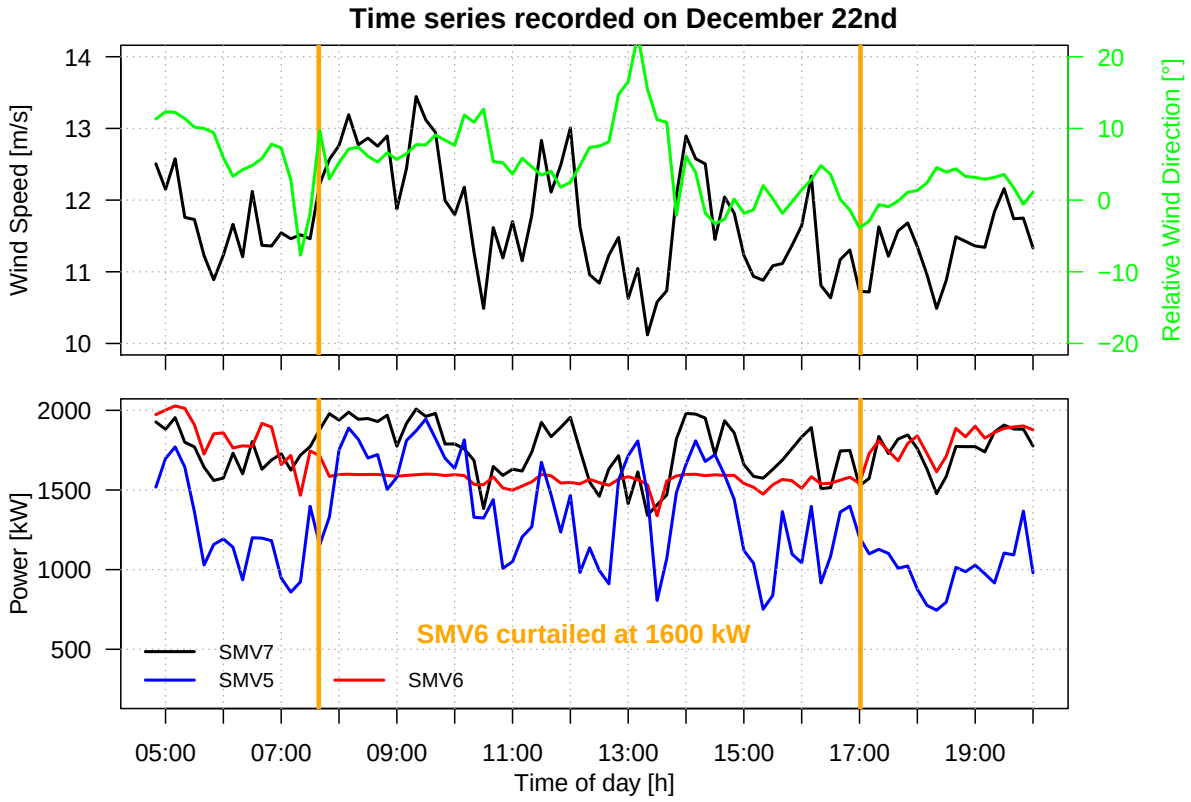

Figure 6.2: *The curtailment strategy implemented in the field test*

Combining these two issues, the error in the wind direction and the power filtering, considerably reduces the available data to be analyzed. Even though approximately 50 hours of curtailments were triggered in this first field test (17 h at 1200 kW, 33 h at 1600 kW), only 10 hours of down-regulation at 1600 kW and 30 minutes at 1200 kW can be used for the analysis. The latter are therefore left out of the study and the results evaluated on the following sections are only focused on a down-regulation at 1600 kW.

6.1.2 Impact on Power Production

The impact on the wind turbine power production of a curtailment at 1600 kW of the upwind wind turbine SMV6 is studied in this section. The change in the performance of the downwind turbine alone is first analyzed, and then the combined performance SMV5 + SMV6 is investigated. The data used to determine the reference power have been limited to the same time period December 2015 - April 2016 as when the curtailment periods where triggered in order to have similar external conditions between the two situations.

The SMV5 power curves in the sector [210; 220°] is represented on Figure 6.3a. This particular sector was chosen because the great majority of the available data points were concentrated here, as seen Figure 6.3b. In this last figure, the incoming wind speed were filtered to the interval 12 - 14 m/s for plotting the wake under normal operating conditions. Indeed, as seen on Section 4.2, the wake is deflecting with the wind speed so in order to analyze properly the impact of the down-regulation on the performance, it is needed to select the right wind speed range. Numerical values are presented on Table 6.1 and Table 6.2.

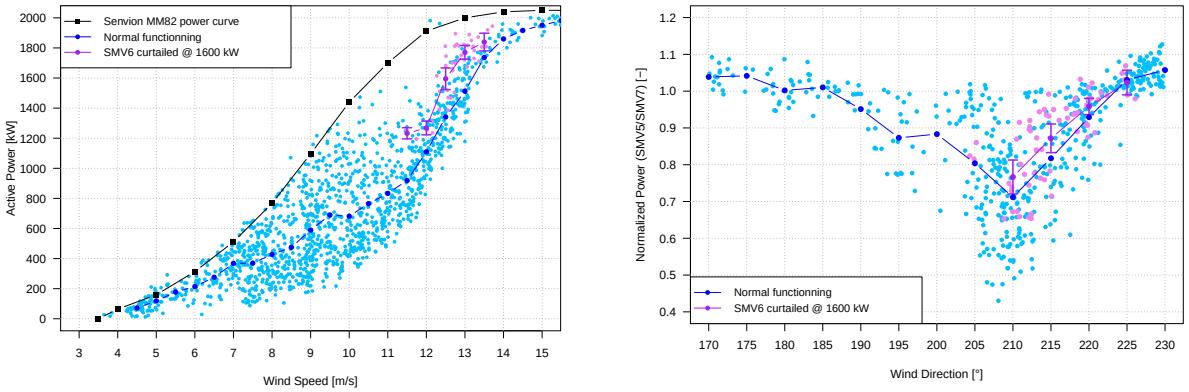

(a) *The power curve of SMV5 in the sector [210; 220°]* ***(b)*** *The SMV6 - SMV5 wake at 12 - 14 m/s*

Figure 6.3: *Impact of the down-regulation strategy on the power performance of SMV5. The error bars represents the 95% confidence interval. The wind speed is measured at the wind turbine SMV6 using the NTF*

Wind Speed [m/s]	Reference Power [kW]	SMV6 down-regulated at 1600 kW [kW]	Difference [%]
11.5	919	1232 ± 37	+34.0%
12.0	1109	1268 ± 45	+14.3%
12.5	1341	1595 ± 288	+18.9%
13.0	1512	1770 ± 182	+17.1%
13.5	1737	1839 ± 156	+5.9%

Table 6.1: *Impact of the curtailment in SMV5 power production in the sector [210; 220°]*

Wind Dir. [°]	Reference Normalized Power [-]	SMV6 down-regulated at 1600 kW [-]	Diff. [%]
210	0.71	0.77 ± 0.046	+8.5%
215	0.82	0.87 ± 0.039	+7.0%
220	0.93	0.96 ± 0.022	+3.2%
225	1.03	1.02 ± 0.033	-1.0%

Table 6.2: *Impact of the curtailment in SMV5 power production at 12 - 14 m/s*

As seen in Figure 6.3, the down-regulation of SMV6 has a positive impact on the power production of SMV5. This increase seems to be more or less regular, around 15 to 18%. The values at 11.5 and 12 have to be taken cautiously since they are only 3 data-points in those bins. There is also an uncertainty in assessing the wind speed and wind direction, since this is done with the nacelle anemometry of wind turbine SMV6. However, looking at Figure 6.3b, the augmentation in SMV5 power seems regular with a more important increase close to full wake conditions and a smaller one on the side of the wake.

A similar analysis is performed on the combined power production of SMV5 and SMV6. The power curves in the same sector and the impact on curtailment can be found on Figure 6.4. Numerical values are presented on Table 6.3 and Table 6.4.

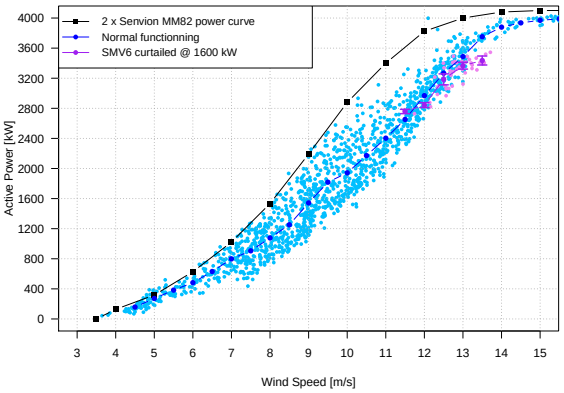

(a) The combined {SMV5+SMV6} power in the sector [210; 220°]

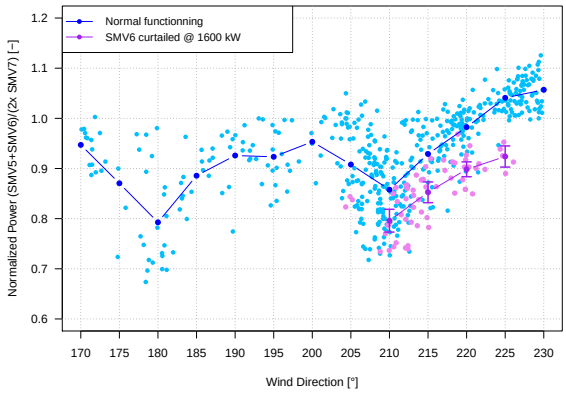

(b) Normalized SMV5 + SMV6 power as a function of the wind direction at 12 - 14 m/s

Figure 6.4: *Impact of the down-regulation strategy on the combined performance of SMV5 and SMV6. The error bars represents the 95% confidence interval. The wind speed is measured at the wind turbine SMV6 using the NTF*

Wind Dir. [°]	Reference Normalized Power [-]	SMV6 down-regulated at 1600 kW [-]	Diff. [%]
11.5	2652	2758 ± 29	+4.0%
12.0	2968	2843 ± 33	-4.2%
12.5	3267	3214 ± 73	-1.6%
13.0	3488	3339 ± 45	-4.3%
13.5	3752	3449 ± 60	-8.1%

Table 6.3: *Impact of the curtailment in the combined power production in the sector [210; 220°]*

Wind Dir. [°]	Reference Normalized Power [-]	SMV6 down-regulated at 1600 kW [-]	Diff. [%]
210	0.86	0.80 ± 0.023	-7.0%
215	0.93	0.85 ± 0.021	-8.6%
220	0.98	0.90 ± 0.015	-8.1%
225	1.04	0.92 ± 0.021	-11.5%

Table 6.4: *Impact of the curtailment in the combined power production at 12 - 14 m/s*

It can be seen that despite the hard curtailment strategy implemented on these first field tests, the losses of combined power production were very small (around 4 to 8% in all wind speed bins). This confirms the idea that the power lost at the upwind wind turbine is regained at the downwind wind turbine. As the wind speed increases, the combined power is expected to decrease since the curtailment of the SMV6 wind turbine becomes very important (close to 20%) and SMV5 is not expected to regain that much. In one wind speed bin, at 11.5 m/s, the combined power is 4% when the curtailment is applied. However for the reasons mentioned above, those values remain quite uncertain.

The Figure 6.4b is maybe most trustworthy as there are more data in each bin. In this graph can be seen a more or less constant loss of combined power of about 7 - 8%. This figure seems also to confirm that the curtailment strategy has a better impact close to full wake conditions, as the wake is the strongest in this region and therefore the potential gains more important. It is unfortunate that no data points could be recorded at smaller wind speed, around 10 and 11 m/s. The curtailment of the SMV6 wind turbine would have been much smaller at those wind speeds, and for wind directions close to full wake conditions, an increase in the combined power production might have been seen.

6.1.3 Impact on Wake Added Turbulence Intensity

The impact of the curtailment strategy on the wake added turbulence intensity is studied in this section. This parameter is interesting for two main reasons. First, from this parameter can be extracted an idea on the loading exerted on the downwind wind turbine. Second, turbulence intensity has an impact on the expansion of the wake emitted by the turbine, as seen in the re-calibrated Jensen model based on the local TI and developed on Chapter 5. In the case of a row of several wind turbines is studied, the changes in the wake-added TI should in theory be modeled to take into account the impact of the wind turbines curtailment.

The TI analyzed here is taken from the 10-min standard deviation coming from Nacelle wind speed SCADA signal, as in Figure 4.16. Similarly as in the previous section, the wake added TI during down-regulation of SMV6 is compared to the reference SMV5 TI. The ambient TI is assessed using the TI measured at the wind turbine SMV6 and shown on Figure 6.5. The impact of the SMV6 curtailment on the wake added TI is shown on Figure 6.6a for the variation against wind speed in the sector [210: 220°] and on Figure 6.6b for the variation against wind direction (for wind speeds between 12 and 14 m/s). Numerical values are presented on Table 6.7 and Table 6.8, respectively. Due to the high scatter of the experimental data, the 95 % confidence interval was computed for both the reference data and the curtailed data.

First, it seems that the curtailment periods were realized under more turbulent conditions, since the TI measured at the wind turbine SMV6 was between 1 and 2 % higher than the reference values. As a consequence it is difficult to compare the two measurements. However, and despite the important size of the error bars, the experimental data appear to underline a decrease in the wake added TI thanks to the curtailment of the upwind wind turbine. The two wind speed bins for which the SMV5 TI is seen to increase during the curtailment periods are the ones with the fewer data-points. In the other bins the reduction of TI is approximately 1 to 1.5%. This order of magnitude can be found also on the wind direction bins close to full wake conditions.

Consequently, a reduction in the downwind wind turbine loading can be expected by curtailing an upwind wind turbine. However, it must be reminded that the reduction measured here is related to a strong curtailment of the upwind wind turbine and thus a loss of power in the combined production. If a curtailment strategy is to be implemented for optimized power production, the down-regulation would be probably smaller and therefore so would be the decrease in the wake added TI. But in any case a reduction in TI is to be expected, and thus it can be expected that implementing an optimized curtailment strategy could lead to both an increase in combined power production and a decrease in the loading thanks to a drop in the wake added TI.

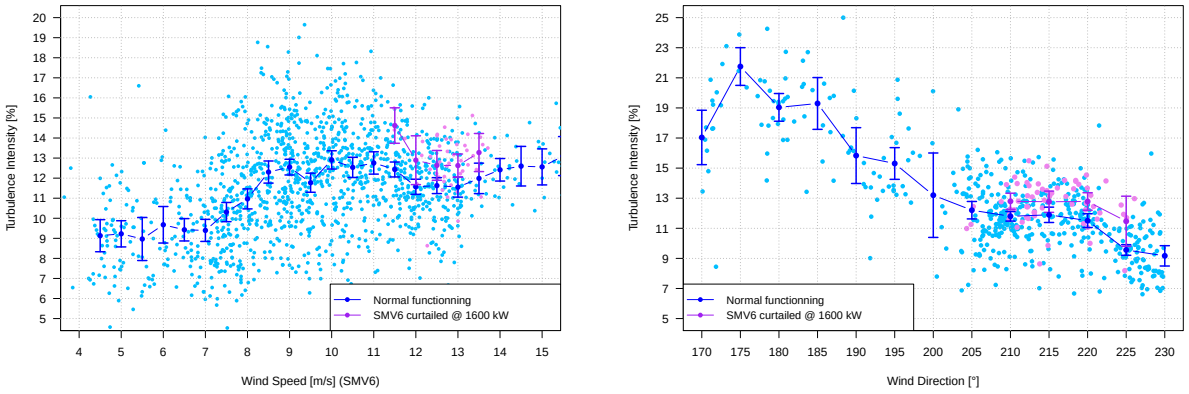

(a) SMV6 TI in the sector [210; 220°] *(b) SMV6 TI in the wake at 12 - 14 m/s*

Figure 6.5: *Ambient TI measured at wind turbine SMV6. The error bars represents the 95% confidence interval. The wind speed is measured at the wind turbine SMV6 using the NTF*

Wind Speed [m/s]	Reference TI [%]	TI under curtailment [%]	Difference in TI [%]
11.5	12.4 ± 0.4	14.6 ± 0.9	+2.2
12.0	11.6 ± 0.4	12.9 ± 1.2	+1.3
12.5	11.6 ± 0.4	12.6 ± 0.7	+1.0
13.0	11.6 ± 0.5	12.6 ± 0.6	+1.0
13.5	12.0 ± 0.7	13.3 ± 0.9	+1.3

Table 6.5: *Ambient TI measured at wind turbine SMV6 in the sector [210; 220°]*

Wind Dir. [°]	Reference TI [%]	TI under curtailment [%]	Difference in TI [%]
210	11.8 ± 0.3	12.8 ± 0.5	+1.0
215	11.9 ± 0.5	12.8 ± 0.7	+0.9
220	11.5 ± 0.5	12.8 ± 0.6	+1.3
225	9.6 ± 0.4	11.5 ± 1.7	+1.9

Table 6.6: *Ambient TI measured at wind turbine SMV6 at 12 - 14 m/s*

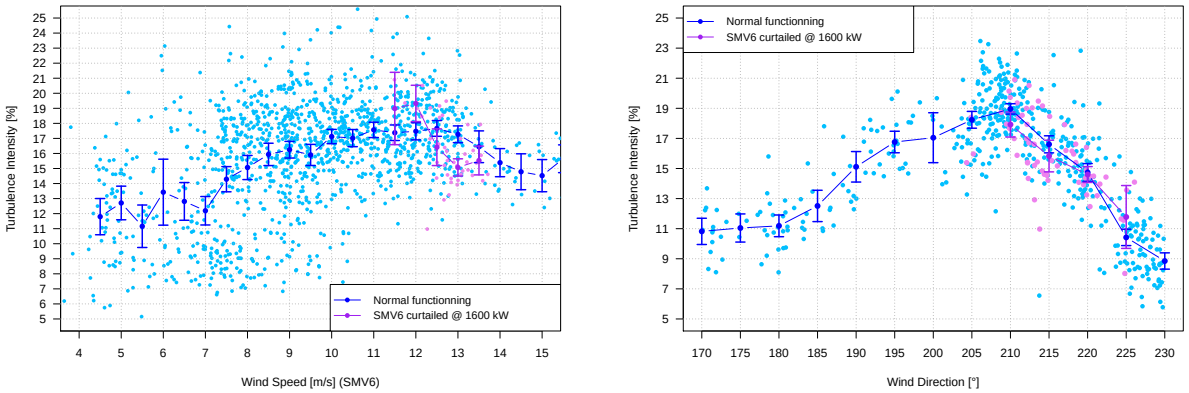

(a) SMV5 TI in the sector [210; 220°] *(b) SMV5 TI in the wake at 12 - 14 m/s*

Figure 6.6: *Impact of the down-regulation strategy on the wake added TI at wind turbine SMV5. The error bars represents the 95% confidence interval. The wind speed is measured at the wind turbine SMV6 using the NTF*

Wind Speed [m/s]	Reference TI [%]	TI under curtailment [%]	Difference in TI [%]
11.5	17.4 ± 0.5	19.0 ± 2.4	+1.6
12.0	17.5 ± 0.6	19.3 ± 1.2	+1.8
12.5	17.7 ± 0.5	16.4 ± 1.2	-1.3
13.0	17.3 ± 0.6	15.7 ± 0.6	-1.6
13.5	16.4 ± 1.1	15.5 ± 1.0	-0.9

Table 6.7: *Impact of the curtailment in the SMV5 TI in the sector [210; 220°]*

Wind Dir. [°]	Reference TI [%]	TI under curtailment [%]	Difference in TI [%]
210	19.0 ± 0.4	17.9 ± 0.8	-1.1
215	16.6 ± 0.6	15.8 ± 1.1	-0.8
220	14.7 ± 0.6	14.6 ± 0.5	-0.1
225	10.4 ± 0.5	11.8 ± 2.1	+1.4

Table 6.8: *Impact of the curtailment in the SMV5 TI at 12 - 14 m/s*

6.1.4 Summary of the Field Test Results

As a conclusion, the curtailment strategy implemented on this first field test campaign of the SMARTEOLE project did not achieve an increase in the combined power production of the two wind turbines SMV5 and SMV6. There are several reasons that contributed to this result. First, the power curve applied to the upwind turbine was maybe implicating a loss of power too significant to be regained downwind by SMV5. The wind conditions when the curtailment periods were triggered were also not adapted to this power curve: at 0.5 or 1 m/s lower an increase in combined power production might have been observed.

Second, the atmospheric conditions during the curtailment periods proved to be more turbulent than for the reference values; it is therefore difficult to compare the two cases as the data is influenced by two contradicting effects. On the one hand, a more important TI is responsible for a worse performance of the wind turbines. On the other the wake from SMV6 is expected to be less strong and thus the SMV5 power is expected to increase.

Finally, it must also be mentioned that a poor knowledge in the wind turbine operation, in particular in the calibration of the direction offset of the reference wind turbine SMV7, led to a significant loss of usable data and considerably reduced the available data in the wake sector.

In any case, this experiment underlines the difficulty to measure and highlight a gain in combined power production using only two turbines as it is the case here. Indeed, the combined gain are expected to be very small and the measure is quite uncertain, especially when using the nacelle anemometry. This uncertainty is also increased by the fact that the measurements between the two cases are not recorded at the same time, and thus under the same atmospheric conditions.

However, as already mentioned above, the objective of this first field test was not to really demonstrate an increase in the power production, but enlighten some phenomenons about wake behavior. In particular,

the increase in power production of the downwind turbine as a function of the curtailment of the upwind turbine could be underlined. It appears that even with a hard curtailment scenario the loss of combined power remains small. It is observed that this loss of combined power is increasing when the down-regulation of the upstream wind turbine is getting too important and the wind direction moves away from the full wake conditions. This confirms that in order to really obtain an increase in combined power production, the curtailment strategy must be adapted to each wind speed and wind directions. And therefore it also raises the issue of assessing accurately those wind conditions in real time to control the wind turbine correctly.

A reduction in the wake added turbulence intensity could also be measured. This decrease was assessed at approximately 1% at full wake conditions for the applied curtailment strategy, but it must be reminded that the ambient TI during the curtailment period was also higher than in the reference case. This information is of importance as it can be related to a reduced loading for the downwind turbine, even though the strain gauges installed at the blade roots were not installed at that time and thus cannot this loading reduction could not be quantified.

Finally, the data recorded in this first experiment can now be used to test and validate a Ct model that is to be an input into the Jensen model.

6.2 Derivation of a Ct Model

As developed in Chapter 5, the wake models generally all take as input the thrust coefficient of the upwind wind turbine. This thrust coefficient can be related to the extraction of the wind kinetic energy and is dependent on the aerodynamic properties of the wind turbine. Under normal operation condition, this Ct can be extracted from the ideal Ct curve provided by the manufacturer (see Figure 3.5), however when it comes to down-regulating the wind turbines these values are no longer valid.

As the upwind turbine is more and more curtailed, its aerodynamic properties are reduced and so is the Ct. But this decrease must be quantified as accurately as possible to estimate reliably the available downwind power using the wake model. Unfortunately, it is very difficult to measure the Ct coefficient of a wind turbine, contrary to the performance coefficient Cp which can be deduced from the active power signal. Measuring the thrust force exerted on the wind turbine can be an option, however no strain gauges were installed on the wind turbine tower to fulfill this role in SMARTEOLE. It was thus only possible to work with a Ct model.

In order to be able to optimize overall power production of a combined set of wind turbines, the Ct values derived from the model must also be related to equivalent Cp values. Indeed these two parameters are related and must be changed together.

Different approaches were investigated for that purpose. They are presented on Section 6.2.1 below. Then the experimental data analyzed on Section 6.1 are used for the validation of these models in Section 6.2.2.

6.2.1 Different Approaches for Modelling Ct

In order to be able to optimize the power production of the farm for all kind of external conditions, the constraints for this model are to be able to be used over the complete range of the wind turbine wind speed and for a large set of possible curtailments. It was first tried to derive a generic Ct model that would represent Ct as a function of two variables, the pitch angle θ and the tip-speed-ratio (TSR) λ. This led to the investigation of the REWS model and the NREL surfaces approaches developed below.

However these two attempts proved inconsistent with the Senvion MM82 wind turbine. Finally, a much simpler approach was followed. Considering three curtailed power curves provided by Senvion and used to reduce acoustic emissions, a correspondence between the Cp and the Ct could be established and used as a Ct model.

The REWS Approach

The first approach investigated is linked to the Cp model used for the calculation of the Rotor Effective Wind Speed (REWS) in Section 4.3. As this model proved to be working quite well for assessing the incoming wind speed to the wind turbine, especially under down-regulation, there was a fair chance that it could be extended into a Ct model as well.

Deriving a complete equation similar as Equation (4.2) would have been quite difficult and time consuming. Instead, the idea followed was to calculate first the value of Cp using the given equation and then convert this Cp into an equivalent Ct value. Indeed, according to BEM theory, these two parameters are linked together through the induction factor a and the very well-known equations:

$$C_t = 4a(1-a) \tag{6.2}$$

$$C_p = 4a(1-a)^2 \tag{6.3}$$

The modeled Cp value is thus calculated from Equation (4.2) (the coefficients c_1 and c_3 from Table 4.2 have been slightly modified to fit better the Senvion Cp curve), then Equation (6.3) is inverted to determine a which could then be used into Equation (6.2) to derive the corresponding Ct value. When obtaining a from Equation (6.3), the Cp modelled is normalized into a "Betz" Cp in order to get induction factors with the correct order of magnitude.

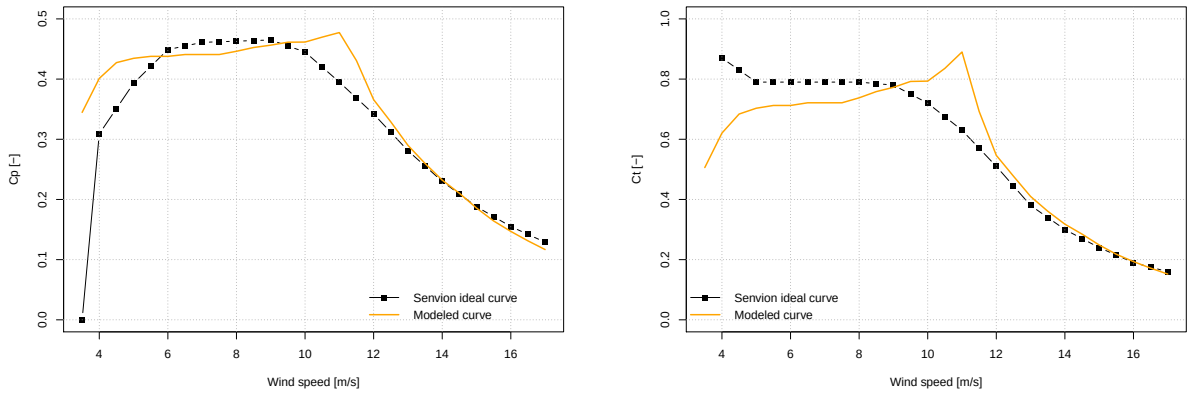

Figure 6.7: *Comparison of the modeled Cp and Ct curves using the REWS method with the Senvion ideal curves*

However, when compared with the Senvion ideal curves, both Cp and Ct are showing some discrepancies, in particular in the range 10 to 12 m/s where the wind turbine begins to pitch. This is due to an approximation in the Cp model equation which cannot consider negative pitch angles (the absolute value of the pitch is taken instead). Therefore when the turbine blades are pitched from -1° to 0° between 10 and 11 m/s, instead of the decrease in the actual Cp the Cp modeled shows an increase because as seen by the model equation the pitch angle is reduced from +1° to 0°.

Moreover, it can be observed that the modeled ct curve obtained using this method is not very well fitting with the ideal curve guaranteed by Senvion. As a consequence this model is finally not very suitable for optimization purposes.

The Ct Surface Approach

The second approach considered in this thesis was based on the Ct and Cp surfaces derived from the NREL 5 MW wind turbine [23]. Cp and Ct values for this reference wind turbine were tabulated against pitch angle and TSR using the toolbox from the Aeolus project [54]. They are represented on the Figure 6.8 below, with the position of the operating Senvion pitch angles and TSRs indicated.

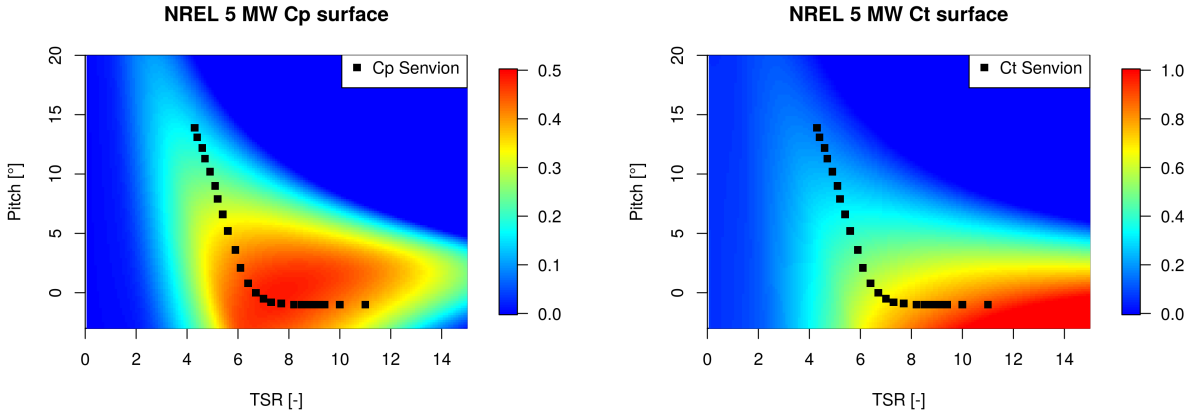

Figure 6.8: *Representation of the NREL 5 MW Cp and Ct surfaces with the location of the Senvion parameters*

These surfaces could not be used unchanged and had to be adapted to fit with the Senvion ideal curves. It proved that dividing the NREL Ct surface by a factor of 1.15 was enough to get a very similar curve as the one guaranteed by Senvion. This obtained Ct could thus used assuming that this factor of 1.15 could be apply for everywhere. However the shape of the NREL Cp curve proved to be quite different from the one from Senvion, and could not be easily modified to fit this latter curve. The comparison with Senvion ideal curves are shown on Figure 6.9 for both parameters. Due to this inconsistent Cp, this model is therefore not really suitable for optimization neither.

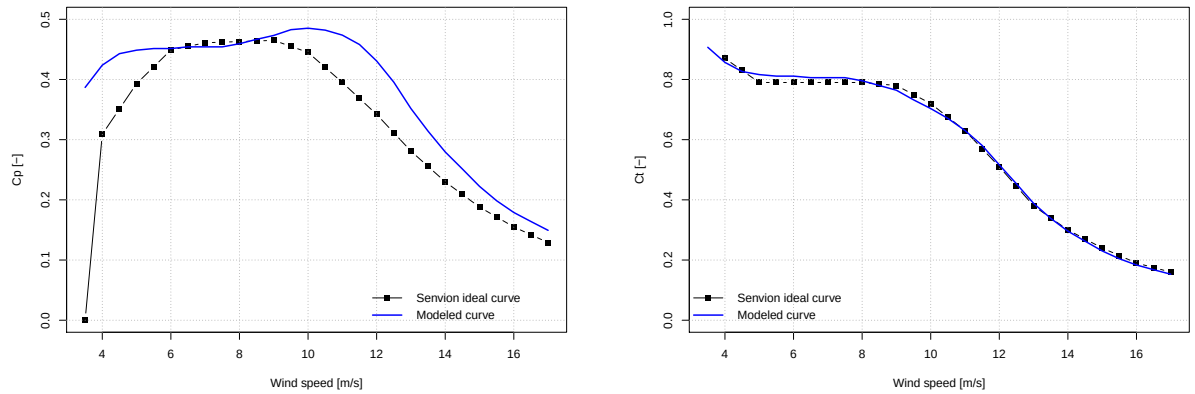

Figure 6.9: *Comparison of the modeled Cp and Ct curves using the modified NREL 5 MW surfaces with the Senvion ideal curves*

Derivation of Cp-based model

From the two approaches developed above, it proved difficult to derive a generic model based on pitch and TSR values that could be used reliably for the Senvion MM82 wind turbine. As a consequence it was finally decided to consider the Cp of the wind turbine as a given value and not a function of the two above parameters. Indeed, when the wind turbine is curtailed to a certain power value the Cp value can be easily computed knowing the incoming wind speed. The idea is now to convert this Cp into a Ct value.

To achieve that purpose, three curtailed power curves provided by Senvion were used. These curves are generally used to reduce acoustic emission to a certain level and comply with the regulation of the country where the turbines are installed. They are used in this section to identify a correspondence between the Cp and the Ct of the turbine.

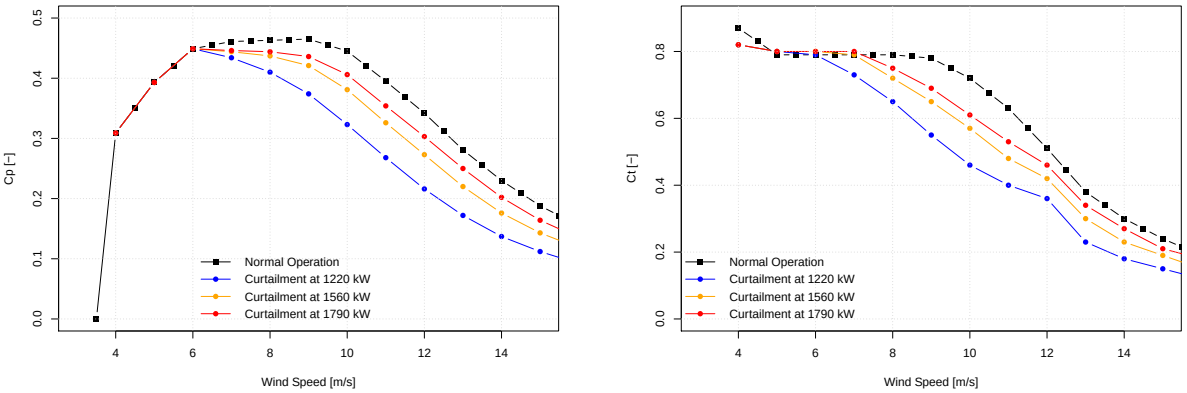

Figure 6.10: *The Senvion MM82 ideal Cp and Ct values as a function of the wind turbine down-regulation*

Their values for the three available down-regulation are represented on Figure 6.10. It can be seen that for a given wind speed both Cp and Ct are decreasing regularly when the down-regulation is increasingly important. However a more abrupt change can be observed in the Ct curves between 12 and 13 m/s, compared to the Cp curves. This is probably related to the fact that the rated wind speed is obtained at 12.5 m/s and therefore aerodynamic properties are slightly changing after this speed.

On Figure 6.11 is represented the correlation between the Cp and the Ct of the Senvion MM82 wind turbine. For each wind speed from 6 to 25 m/s, the Ct value is plotted against the wind turbine Cp (which is dependent on the down-regulation applied). Two regimes can easily be detected. Before rated wind speed, the relationship is convex and the Ct decreases more quickly than the Cp, especially around the maximum Cp value of ~ 0.45. On the contrary, once the rated wind speed has been reached, the variation is almost perfectly linear between the two parameters.

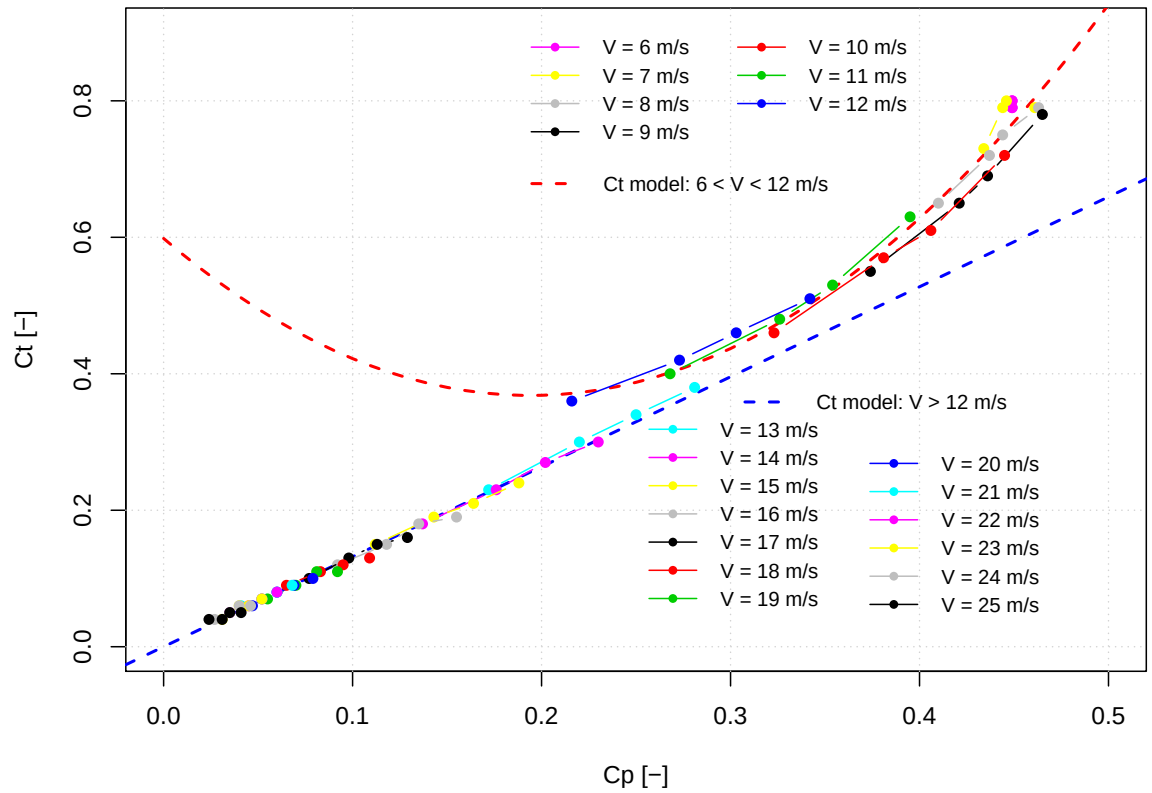

Figure 6.11: *Variation of the wind turbine Ct with the wind turbine Cp for several wind speed*

Based on these observations, a Ct model could be derived based on the wind turbine Cp value. The points below rated wind speed were fitted with a second order polynomial (only valid for Cp values above 0.2, as can be seen on Figure 6.11), while after rated wind speed a simple linear dependency was chosen. The Ct to be used as input into the wake model can therefore be simply expressed as a function of Cp using Equation (6.4) below.

$$\begin{cases} C_t = 6.1\,C_p^2 - 2.4\,C_p + 0.6 & \text{if } 6 < V < 12.5 \text{ m/s and } C_p > 0.2 \\ C_t = 1.3\,C_p & \text{if } V > 12.5 \text{ m/s} \end{cases} \tag{6.4}$$

6.2.2 Validation of the Model

The Ct model derived in the previous section is now validated using experimental data from the curtailment field test. This is done in order to make sure that the model can be relied on before launching the optimization process. The experimental power curve of SMV5 obtained during the SMV6 down-regulation period is compared with the values derived from the combination of the two models (Ct and Jensen).

The power curves are studied in the direction sector [210°; 220°] and are calculated based on the SMV6 nacelle wind speed measurement. The turbulence intensity used for the computation of the wake decay constant is taken directly from Table 6.7 for the SMV6 wind turbine and calculated similarly for SMV7. The wind direction considered is taken at 215° and corrected for each wind speed based on the wind turbine wake deflections as explained on Section 5.4. Finally the Cp of the wind turbine SMV6 needed for the derivation of the Ct value is calculated based on SMV6 measured power and nacelle wind speed. As the wind turbine SMV7 is working normally, its Ct is simply linearly interpolated from the ideal Ct curve and the wind speed measured at SMV6.

On Figure 6.12a are compared the modeled and the experimental power curves of SMV5 in both case. It can be seen that the modeled red curve is in fairly good agreement with the purple points corresponding to the experimental data. On Figure 6.12b the modeled and experimental data are compared directly on a XY graph. It can be observed that the points are scattered around the 1:1 line shown in red. When binning the data in 200 kW bins, it seems that the modeled is power is first over-estimated until ∼ 1500 kW and then under-estimated compare to the experimental data. This is also seen on the power curve graph where the modeled power curve during SMV6 curtailment is first above and then below the experimental curve. However as the model is also very sensitive to the value of wind speed and wind direction that are used to calculated the power, it is not identified to what extent this difference is due to the Ct model or to the uncertainty in measuring accurately the wind conditions. With the very small amount of available data points during the down-regulation of SMV6, it is difficult to completely validate the Ct model, but in any case it seems to give a power relatively close from the measurement.

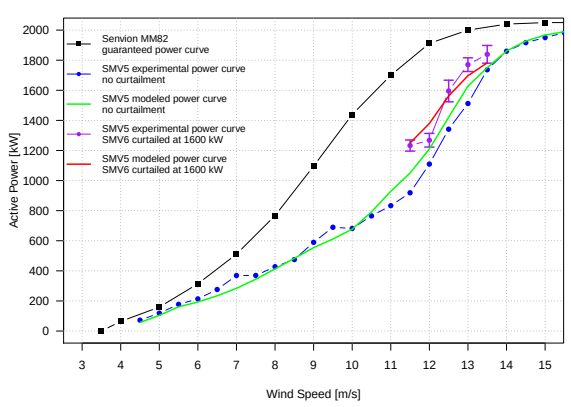

(a) Power curves in the sector [210; 220°]

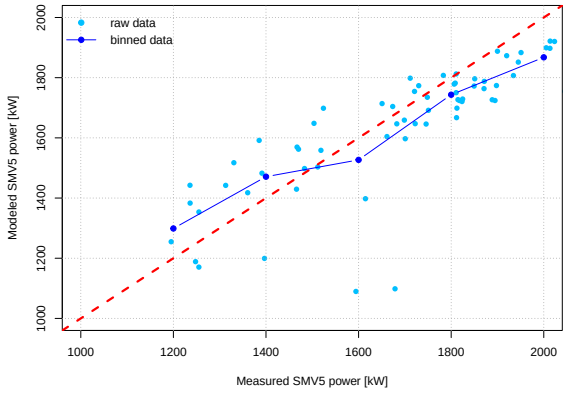

(b) Experimental VS modeled SMV5 power during SMV6 curtailment

Figure 6.12: *Validation of the Ct model*

6.3 Optimization of Wind Farm Power Production

Now that the different models have been validated, it is possible to focus on the optimization of the combined power production of the two turbines SMV5 and SMV6. The procedure followed for the optimization process is first described. Then the optimized power production of the wind turbines SMV5 and SMV6 is obtained considering idealized conditions: both wind turbines are supposed to follow the guaranteed power curve, and yaw errors or wake deflection are involved. Finally, the combined power production is optimized and for the real operating conditions and new curtailment strategies are suggested for the next measurement campaign of SMARTEOLE.

6.3.1 Description of the Optimization Process

As only two turbines are considered for the optimization of the combined power production, there is no need for implementing a fast-processing algorithm. All possible configuration of the upstream wind turbine can be studied and the combined power production calculated in each cases, and finally it will just be needed to choose the best one. Basically the optimization process can be summarized as follows:

- The optimization is realized in a given wind direction sector only. The wind direction angle has to be given and remains constant over the process. The TI distribution $TI(V)$ for this particular sector is also given as a function of the wind speed. The sector width in which this distribution is measured is 10°.
- The power curve of the wind turbine SMV6 in normal operating conditions must also be provided. This power curve is used to calculate the initial condition and then be modified during the process to be transformed in an optimized power curve. The power curves of SMV7 and SMV5 are also provided in order to calculate the contribution of SMV7 to the wake and the power production of SMV5 once the wake deficit has been found.
- Then for each wind speed V from 6 m/s to 15 m/s (the Ct model derived in Section 6.2 is only valid after 6 m/s, and after 15 m/s a curtailment is no longer needed), the optimal setting for the SMV6 wind turbine can be found as:
    1. The initial power coefficient value C_{p_0} of the SMV6 wind turbine in the normal operating conditions is calculated from the given power curve.
    2. A set of twenty different Cp values is created from this original C_{p_0}. In total the original Cp is allowed to be decreased up to 20%: $C_{p_1} = 0.99\,C_{p_0}$, $C_{p_2} = 0.98\,C_{p_0}$, ..., $C_{p_{20}} = 0.8\,C_{p_0}$.
    3. For each C_{p_i} value an equivalent C_{t_i} is calculated using the Ct model.
    4. The wind speed deficit U_{SMV5_i} at the wind turbine SMV5 is estimated for each C_{t_i} value using the re-calibrated Jensen model and the TI value at the given wind speed for the wind turbines SMV6 and SMV7. The Ct for the SMV7 wind turbine is simply interpolated from the guaranteed curve as this wind turbine is left unchanged.
    5. For each wind speed deficit U_{SMV5_i}, the corresponding SMV5 power production is calculated using the provided SMV5 power curve.
    6. The combined power production of SMV5 and SMV6, P_{comb_i}, is deduced for each case i and the one giving the best number is kept. That gives the optimal Cp setting $C_{p_{opt}}(V)$ for the given wind speed V.
- From the optimal Cp values at each wind speed, the SMV6 power curve realizing the maximum combined power production can then be deduced, and is finally given as output of the algorithm.

6.3.2 Optimization of Combined Power Production in Idealized Conditions

The combined power production of the two turbines is first optimized in idealized operating conditions. This is done in order to identify the precise sector where the curtailment strategy is profitable and to study its sensitivity to changes in wind directions. This should also give an idea of the maximum increase in power production that could be expected from this strategy.

In the optimization process described above in Section 6.3.1, the TI distributions taken for the wind turbines SMV6 and SMV7 corresponds the the measured TI for these two turbines in the full wake

sector: 205° ± 5°. Contrary to the real operating conditions, the power curves for all turbines are considered to be the Senvion MM82 guaranteed power curve.

The SMV6 power curve is first optimized in full wake conditions, i.e. considering a relative wind direction angle with the wind turbine alignment of 0°. The results are shown on Figure 6.13 below. The Figure 6.13a compares the two optimized power curves with the ones that would be obtained with no coordinated control. On Figure 6.13b is represented the expected relative increase in combined power production in each wind speed bin, along with the optimal reduction in Cp needed to achieve this performance.
It can be observed that the wind speed range where the coordinated control is really improving the combined power production is limited to 6 - 10 m/s. This corresponds to the range where both the Cp and the Ct of the wind turbine are almost constant and at their maximum value. As already mentioned in Section 2.3.2, in this region the Ct curve is much steeper than the Cp curve and therefore important reductions in Ct can be obtained with smaller reductions of Cp. This is also seen on the NREL surfaces on Figure 6.8. In the region at -1° pitch and a TSR of ~ 9, the Cp surface is seen to be much less sensitive to an increase of the pitch angle than the Ct surface.

As an illustration, the maximum relative increase in combined power production is 2.5% measured at 7 m/s. This gain is found by decreasing the Cp of the SMV6 wind turbine of 12%, i.e. from 0.46 to 0.405. Comparatively, the Ct of the wind turbine is reduced by approximately 20%, from 0.79 to 0.63 according to the considered Ct model. This significant reduction explains why an increased in combined power production can be obtained.

However, this relative gain decreases quickly with the wind speed: it is only $\sim 1\%$ at 9 m/s and $\sim 0.25\%$ at 10 m/s. As the more important gains are found at the low wind speeds, the absolute increase in power production remains very small, in the order of 20 kW only at 7 m/s. Consequently the total gain when average over all wind speed is almost imperceptible. When using a typical Weibull distribution measured for the 200 - 210° sector at SMV5 (A=8.5 m/s, k=2.5), the averaged gain over the complete wind speed range could be assessed at 0.6%.

And this value is only valid for a constant wind direction perfectly aligned with the two wind turbines. In case of a smaller deviation of this direction, the gain is expected to be even reduced. The impact of this changing wind direction is studied on Figure 6.14, where the expected gains are plotted for several relative wind directions.

It can be seen that the wind direction sector where the curtailment strategy is profitable is very narrow, only ± 8° each side of the perfect wind turbine alignment. Furthermore, for relative wind direction greater than ± 5°, the gains are so small (less than 0.75% in each wind speed bin) that they would probably be difficult to observe. Therefore it can be considered that the curtailment strategy is only profitable in a 10° sector centered around the full wake conditions.

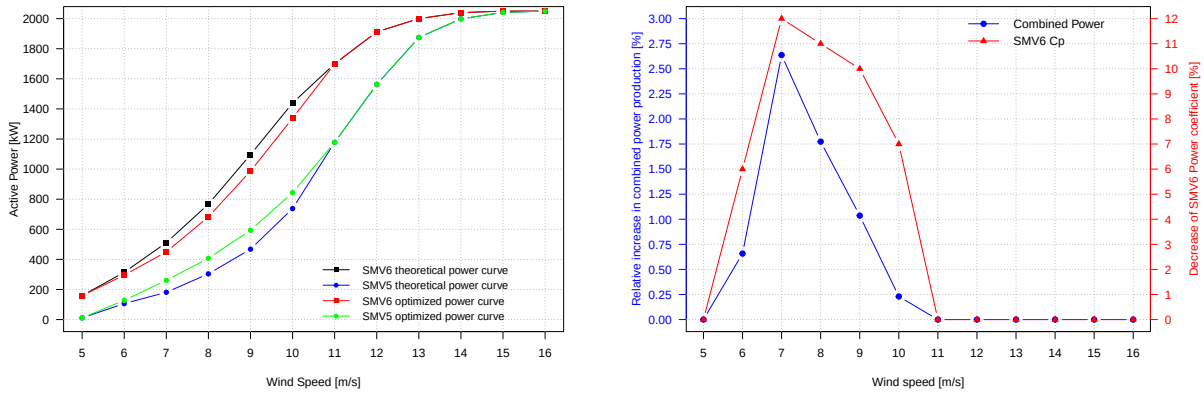

(a) *Optimized power curves of the two wind turbines in full wake conditions*

(b) *Relative increase in combined power production as a function of the wind speed*

Figure 6.13: *Optimization of the combined {SMV5 + SMV6} power production under full wake conditions*

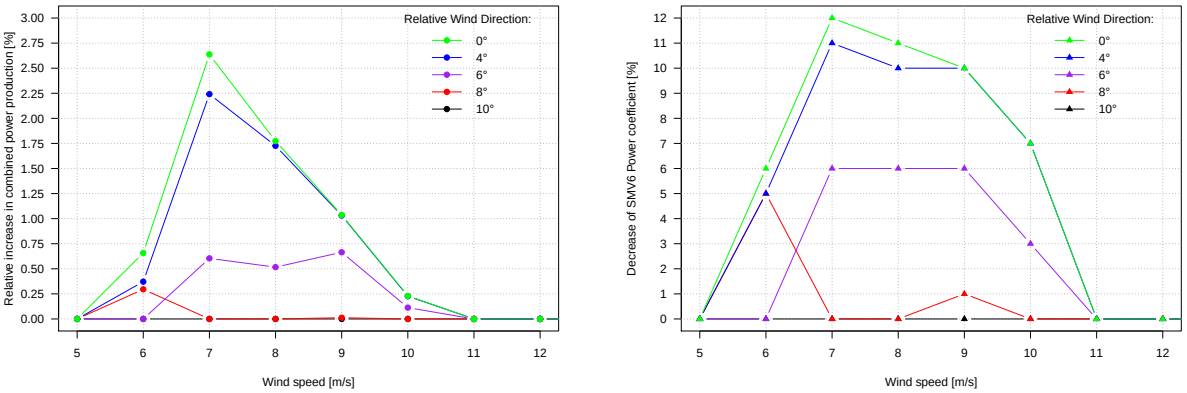

(a) Variation of the expected gains with the relative wind direction

(b) Variation of the optimal SMV6 Cp settings with the relative wind direction

Figure 6.14: *Sensitivity of the curtailment strategy to the wind direction for the SMV6 - SMV5 case*

6.3.3 Optimization of Combined Power Production in Real Conditions

The combined power production is now optimized in the real operating conditions. Compare to the previous section, this corresponds to two changes in the optimization process. First, the power curves considered are no longer the guaranteed power curve but the measured power curves of the wind turbine. For the wind turbine SMV6, the experimental curve obtained in Section 4.2 is used, and for SMV5 it is the measured SMV7 power curve in the relevant wind direction sector which is considered since this curve is the one that proved to give the best representation of the reality in Section 5.4.

Second, the yaw error of the SMV6 and SMV7 wind turbines is now considered, and that means that the relative wind direction given as input into the model must be corrected for each wind speed with the proper value as explained in Section 5.4.1. These real optimized power curves are only studied in the full wake sector as the analysis done in the previous section shew that the main gain of power were only realized close to the full wake conditions. They are represented on Figure 6.15 below.

Compare to the theoretical optimization realized in the previous section, it can be seen that the wind speed range where the coordinated control is interesting is reduced to 6 - 9 m/s. More important relative gains are obtained for the wind speed bin at 6 m/s. A relative gain of $\sim 9\%$ is measured, corresponding in an increase in the combined power production of 30 kW. However this increase is to be taken with caution since this big increase might only be due to sensitivity of the power curve used to convert the effective wind speed assessed at the SMV5 turbine into an equivalent power.

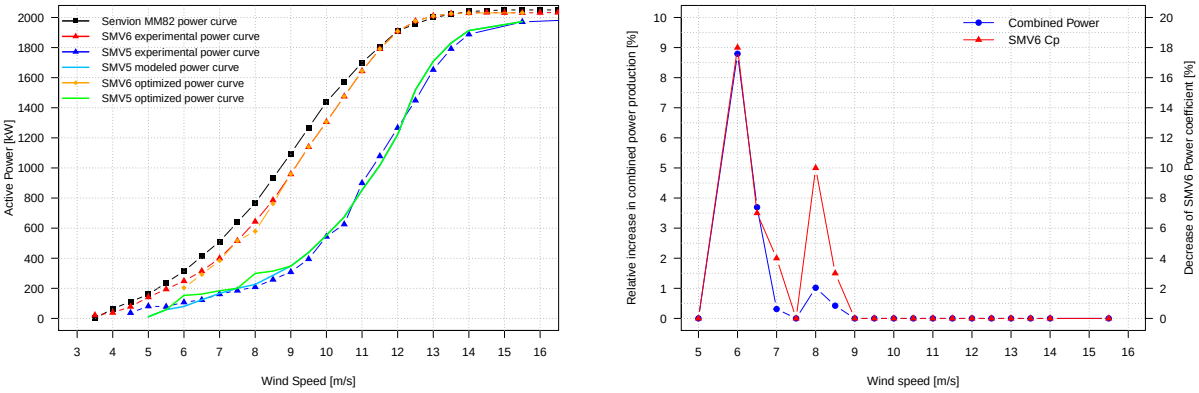

(a) Optimized SMV6 and SMV5 power curves in real operating conditions

(b) Expected combined gain from the implemented coordinated control

Figure 6.15: *Optimization of the combined {SMV5 + SMV6} power production under full wake conditions in the real case*

In all other wind speed bins, the expected gains in the real conditions are found to be smaller than the ones obtained for the idealized conditions. It is limited at $\sim 1\%$ at 8 m/s compared with the $\sim 1.75\%$ found in the previous section. Again this might be related to the power curve used to compute the SMV5 power. At these wind speeds, the wake deflection caused by the wind turbines yaw error is still small and do not have any influence on the results. This deflection becomes more important at wind speeds above 10 - 11 m/s but at these wind speeds the coordinated control is no longer needed.

Similarly as in the previous section, the total power production gain averaged over the complete wind speed range could be calculated using the same Weibull distribution. It could be assessed to 0.3 %, i.e. twice as small as the one obtained for the idealized conditions. This is explained by the fact that the range of applicable wind speeds for the application of the coordinated control has been reduced.

6.4 Summary and Discussion

The performance of the curtailment strategy for optimizing the combined power production of two wind turbines has been investigated in this chapter. This performance was first assessed based on experimental data and then at the end of an optimization process.

The analysis of the results of the first field test of SMARTEOLE shows that a gain in combined power production was not achieved during this campaign. This could be explained by the fact that the curtailment scenario implemented was not really adapted to this particular case, and that the wind conditions during the tests were also unfavorable.

Indeed, according to the optimization process realized on Section 6.3, the gains in combined power production are likely to be found between 6 and 10 m/s, and for wind conditions very close to full wake. The sector in which the coordinated control is profitable is quite narrow, in the order of 10° or so. Unfortunately, during the field tests only wind speeds above 11.5 m/s and wind directions above 210° could be measured. Despite these unfavorable conditions and the hard curtailment strategy implemented, the loss of combined power due to the down-regulation was kept small, in the order of 4 to 8%.

In these field tests a decrease in the wake-added turbulence intensity could also be measured. The order of magnitude of this reduction was about 1% with the implemented curtailment strategy. As a consequence a decrease in the downwind turbine dynamic loading can be expected. Also the data recorded during the campaign could be used to validate a Ct model based on the Senvion MM82 power curves.

The modeling involved in the optimization process could be trusted as it proved to be fitting quite well with the power curves in normal operation conditions. The results from the optimization process shows that an increase in combined power production of 1 to 2% can be expected for wind speeds between 6 and 10 m/s in full wake conditions. This increase is obtained by down-regulating the SMV6 wind turbine of about 5 to 10% in this wind speed range. This strategy is recommended to be implemented in the next measurement campaign of the SMARTEOLE project.

However, when averaged over the complete wind speed range with a relevant Weibull distribution, this gain is reduced to 0.3 - 0.5% only. These values are in line with the ones indicated in the literature, for example in [14] or [35]. It can therefore be concluded that using the curtailment strategy for the optimization of the combined power production of two wind turbines only is very limited. The gains that can be expected are relatively small and are restricted to full wake conditions only. Due to fluctuations of the incoming wind conditions, there is a high probability that implementing such a control will be responsible for production losses if the turbine is not able to react quickly to the changes in wind speed or direction.

This strategy has undoubtedly a much better potential when considering several wind turbines aligned in row. In that case the down-regulation of an upwind turbine will be profitable to all downwind turbines. The reduction of the fatigue loading will remain limited though. A decrease in the wake added TI for the second wind turbine can be observed, but as the TI is seen to be saturated very quickly (after the second or third turbine), it is much likely that the wind turbines further downwind will not experience any changes.

7 | The Yaw Offset Strategy

In this chapter is studied the impact of a yaw offset strategy in the combined power production of two and more wind turbines. It is therefore mainly focused on the experimental results obtained during the first measurement campaign which are presented and compared with models found in the literature. Contrary to the curtailment strategy and due to time constraints, optimization could not be done with the yaw offset.

7.1 Analysis of the Experimental Results

The results from the yaw offset field test, realized during the summer 2016, are studied in this section. The strategy set up during these tests is first presented, and then the data is analyzed.

7.1.1 Yaw Offset Strategy Implemented during the Field Test

The strategy implemented during this first measurement campaign was relatively simple. It only consisted to yaw the upstream wind turbine SMV6 and observe the consequences in the downwind SMV5 power. The SMV6 yaw error was artificially created by tricking the vane angle signal. There is a parameter in the Senvion control panel that allows to set the vane angle offset. This parameter can vary between 0 and 20°, and was initially set at 12°. It was observed that when this parameter was decreased to 0°, the yaw position signal of the wind turbine was also reduced by 12° (and respectively increased by 8° when the parameter was set to 20°).

The SMV6 wind turbine was thus submitted to two different yaw errors:

- -12° between 02.08.2016 and 12.08.2016, and
- +8° between 12.08.2016 and 08.09.2016.

The wind speed and direction occurrences during the tests are presented for both yaw error cases on Figure 7.1. Two different things are investigated during this measurement campaign. First the loss of the upwind power due to a yaw error. To that purpose the SMV6 power curves are drawn outside of any disturbing sector (the available data are represented in red), and compared with the normal functioning power curve calculated in Section 4.2. This is done in Section 7.1.2.

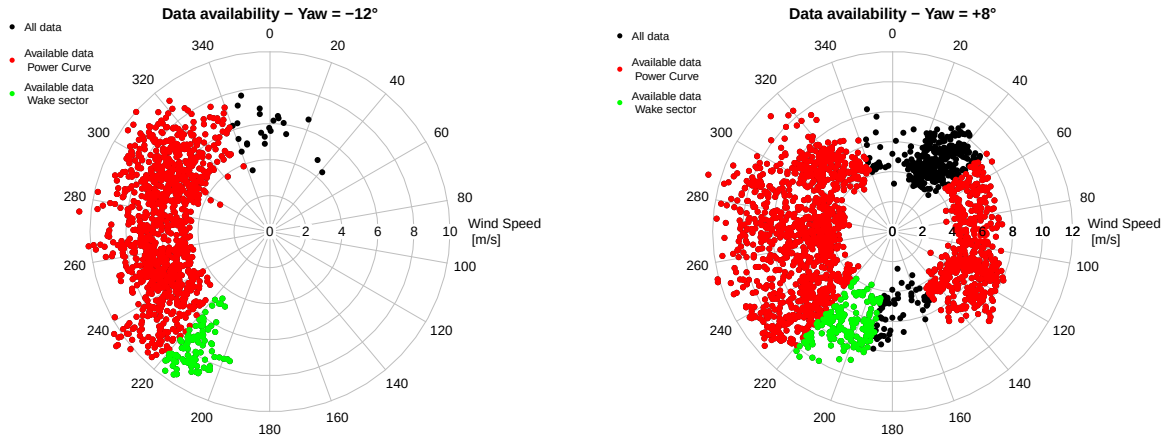

Figure 7.1: *Wind data roses during the yaw ofset experiment*

Then the deflection of the wind turbine wake is studied by looking at the changes in the SMV5 power. This must be done in the wake sector [190°; 220°], where the available data are shown in green. Despite the fairly long time period to which the yaw errors were maintained, the available data for the analysis of

a possible wake deflection proved to be quite reduced. Only 98 and 160 10-min data points were located in the SMV6 - SMV5 wake sector for the -12° and +8° yaw offset case, respectively. Also, as the test was carried out during the summer, the occurring wind speeds were quite low and limited to the range 4 - 10 m/s. This analysis is realized on Section 7.1.3.

Finally, it must be reminded that the SMV6 wind turbine has its own dynamic yaw error which varies with the wind speed, as seen on Section 4.2 and represented again on Figure 7.2 below. This must be considered and added to the static yaw error implemented during the measurement campaign. The misalignment was measured by the 5 beam lidar during the winter period (the data for this lidar during the summer period were only obtained after the analysis was done), and also contains an offset related to the alignment of the lidar with the wind turbine. It is therefore very difficult to analyze the results since the total yaw error is the result of two different effects that are either adding or compensating each other.

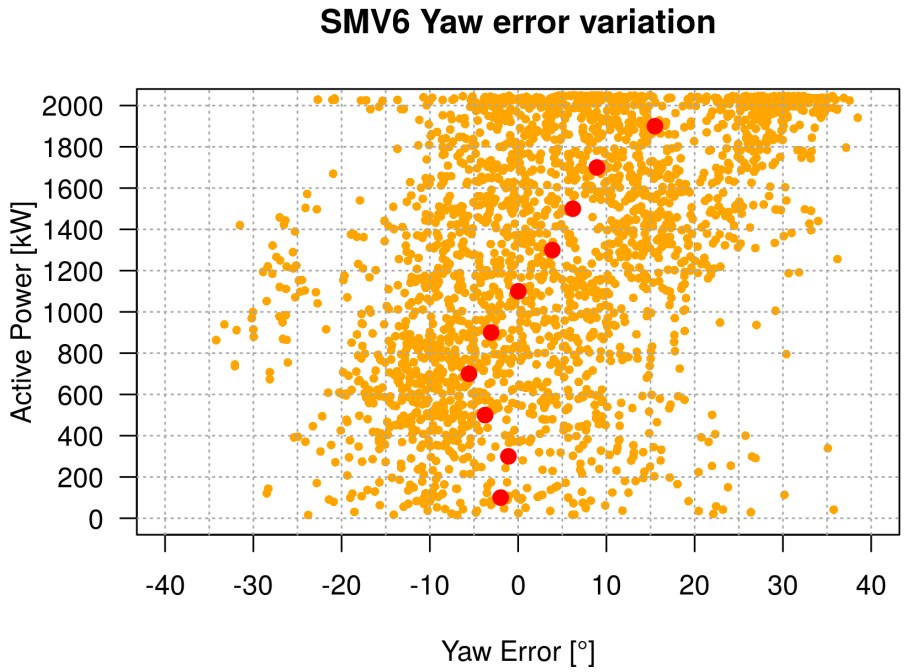

Figure 7.2: *Yaw error of the wind turbine SMV6 as a function of the active power production, measured by the 5 beam lidar*

7.1.2 Impact on Power Production

The impact of a yaw error on the wind turbine power production is analyzed in this section. The power curves of SMV6 during the two different yaw error periods is compared with the normal functioning curve on Figure 7.3a below. On Figure 7.3b is represented the difference between these power curves and the guaranteed power curve ensured by Senvion.

The behavior of these power curves seems consistent with the variation of the yaw error measured by the lidar. At low wind speeds (below 500 kW), the power production in the two yaw error cases is very similar. They are both below the power curve with no yaw error, but the power curve with -12° presents a better performance than the one at +8°. This tends to indicate that the wind turbine has initially a very slight positive yaw error, and therefore adding a negative yaw error is compensating a little while adding a positive yaw error is only making things worse.

Then, when the wind speed increases between 7 and 9 m/s (i.e. between 500 and 900 kW), this tendency is inverted and the power curve with +8° yaw becomes a bit better than the one with -12°. Similarly, at these power ranges the misalignment measured by the lidar is slightly going toward negative values.

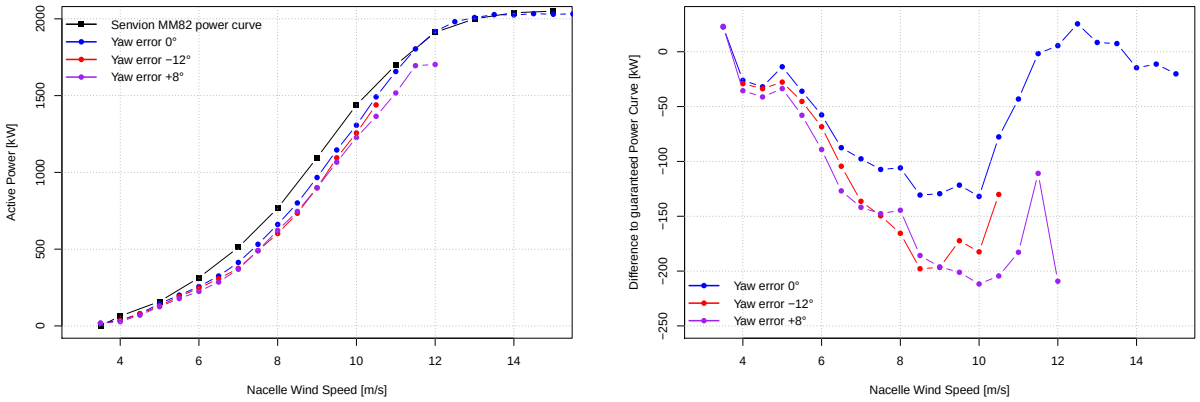

(a) *SMV6 power curves as a function of the yaw error* ***(b)*** *Difference to the guaranteed power curves*

Figure 7.3: *SMV6 power curves as a function of the yaw error*

Finally, when the wind speed and the power increase further, the situation becomes similar to the case at low wind speed with the power curve corresponding to the misalignment of -12° located between the two other ones. At even higher wind speeds, we might have observed the red curve going above the blue one, since the lidar measures a misalignment of approximately 10 to 15°. Therefore adding a negative yaw on top of this misalignment would have reoriented the wind turbine towards the correct wind direction.

The power coefficient of a wind turbine with a yaw error is generally modeled using a cosine law with an exponent [25]:

$$C_p(\gamma) = C_p(\gamma_0)\, cos(\gamma - \gamma_0)^{\beta} \tag{7.1}$$

where γ is the yaw error, β the exponent and $C_p(\gamma_0)$ the power coefficient measured at the optimal yaw position γ_0.

The more interesting parameter in Equation (7.1) is the exponent β as it drives the steepness of the cosine curve. The greater the coefficient, the steeper the curve and the more important the power loss due to the yaw error. Its order of magnitude is generally considered to be between 2 and 3 [36, 55]. In the field tests realized in [25], this parameter was found to vary between 1 and 5 depending on the wind speed and also the wind turbines considered.

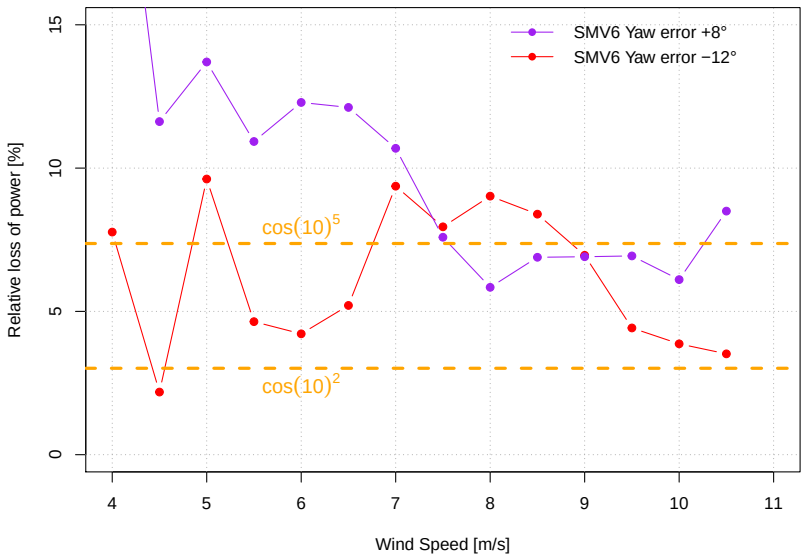

Figure 7.4: *Relative loss of power due to the two yaw error configurations compare to the normal functioning power production, as a function of the wind speed*

Due to the fact that the real yaw error could not be known for certain, and that only two different misalignment values were used during the tests, it was not possible to fit such a function with the experimental data. Instead, the relative loss of power of the two yaw error configurations compare to the normal functioning case is investigated and represented on Figure 7.4. The lines showing the expected loss of power for a misalignment of 10° and an exponent of 2 and 5 are also shown. It can be seen that for the -12° yaw error the relative loss is most of the time measured between these two lines. For the +8° yaw, it is slightly higher for the low wind speeds, probably because the wind turbine already has a residual positive yaw error and thus the total yaw error is bigger than 10°. It seems that the relative loss of power is decreasing with the increasing wind speed, this tendency was also noticed in [25].

7.1.3 Deflection of the Wind Turbine Wake

The performance of the downstream wind turbine power is now investigated to try to underline a deflection of the SMV6 wake. Looking back at Figure 2.4, when a wind turbine has a negative yaw error, the wake is deflected towards smaller wind direction (and inversely when there is a positive yaw error). Similarly as the study realized in Section 4.2, the performance of the wind turbine SMV5 is studied in three different sectors: [190°; 200°], [200°; 210°] and [210°; 220°].

The first sector corresponds to the left part of the wake. If the upwind wind turbine is yawed positively the wake should in theory be moving towards higher wind direction and therefore be deflected away from the downwind wind turbine. On the contrary, yawing the turbine negatively will only make things worse as the situation is expected to change from partial wake conditions to full wake conditions. As a consequence, a positive SMV6 yaw error for wind direction between 190° and 200° is supposed to improve the SMV5 performance while a negative yaw error will reduce the power production.

The situation is opposite in the third sector [210°; 220°] where a negative yaw error is expected to increase the power production and a positive yaw error decrease the performance. As the middle sector initially corresponds to the full wake situation, any kind of yaw error should change it into partial wake situation and thus an increase in the SMV5 performance can be hoped in both case.

The power production of the SMV5 wind turbine is shown on Figure 7.5, with the 95% confidence interval drawn for the two yaw error cases. As only two points were available for the -12° yaw case in the [190°; 200°], the power curve could not be calculated. The wind direction is assessed using the wind turbine SMV7 and the wind speed is measured at the wind turbine SMV6. The wake behavior is also investigated. The normalized power production and the turbulence intensity are represented against wind direction on Figure 7.6. For drawing the curves in the reference 0° yaw case, the data has been filtered to keep only the points for which the SMV7 power was below 1200 kW. This is done to consider the same order of magnitude for the active power as the one observed in the two yaw error cases. Also, at this power range, the impact of the SMV6 dynamic yaw error should remain limited

Unfortunately, these graphs do not seem to underline any real effect of the upstream wind turbine yaw error in the downstream wind turbine performance. All of them are characterized by an important scatter of data and no real tendencies can be extracted. The power curves are all very similar in each sector, and no particular wake deflection can be observed by looking either at the normalized power or at the turbulence intensity. Therefore, based on these field test results, no conclusions can be drawn regarding the impact of the yaw offset strategy on the increase of the downstream production.

There might be several explanations for this problem. First, the number of data points available in the wake sector during the SMV6 yaw error period are very reduced and it is difficult to have a good statistic representation of the tendencies. Second, the yaw offset campaign was realized during the summer while the power curves for the reference case are based on one year of data, so the atmospheric conditions might be different. There might also be some influence of the dynamic yaw error of the SMV6 downwind turbine. However, it can be seen that the maximum wind speeds measured during the misalignment period were in the order of magnitude of 10 m/s maximum. At those wind speed the SMV6 power production is approximately 1200 - 1300 kW. As seen on Figure 4.9b, the deflection of the wake for such power production is very small ($\sim 2°$ max) and thus this influence should not have a major impact. The deflection of the wake due to the dynamic yaw error would have been visible at higher wind speeds.

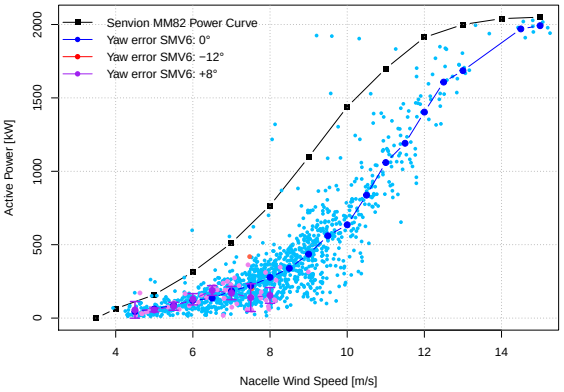

(a) Between 190° and 200°

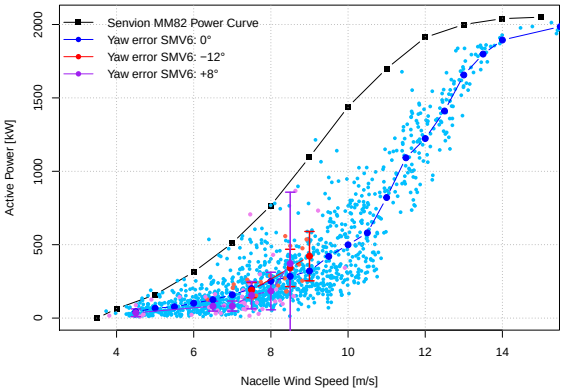

(b) Between 200° and 210°

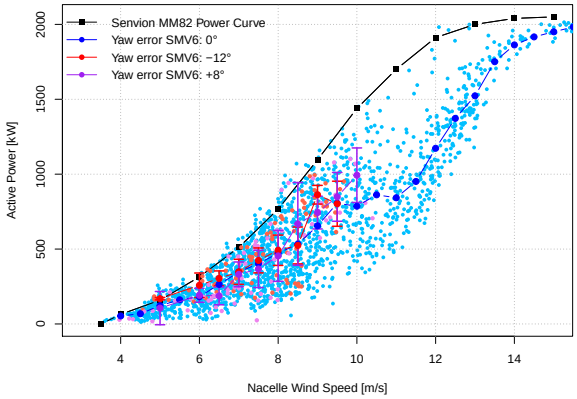

(c) Between 210° and 220°

Figure 7.5: *SMV5 power performance depending on the SMV6 yaw error for the three different wind direction sectors*

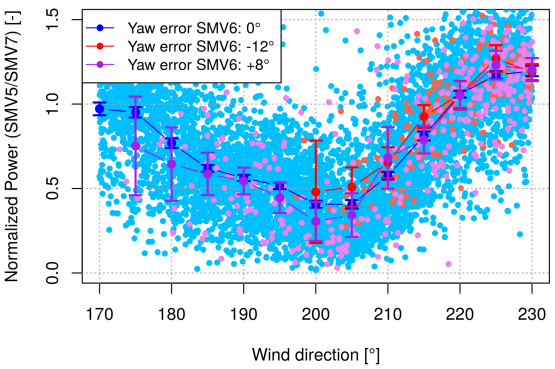

captionStudy of the normalized power

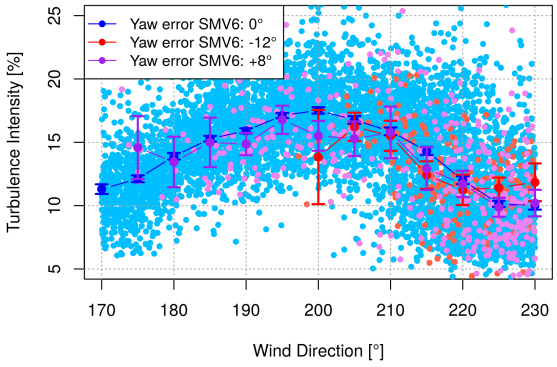

(a) Study of the turbulence intensity

Figure 7.6: *Behavior of the SMV6 - SMV5 wake as a function of wind direction for the different SMV6 yaw error case*

Finally, there might be a last issue related to the fact that the yaw error angles applied were too small to really observe a deflection in the downwind power. To discuss this point, the strategy and the results obtained during these field tests are compared to two different wake deflection models that could be

found in the literature. In the first one, developed in [26], the skew angle of the wake is seen as linearly dependent of the wind turbine yaw angle, with coefficient of proportionality in the order of 1.2 - 1.3. This means that the wake is deflected with a higher angle than the misalignment angle. Using this model with the given yaw error values of -12° and +8° would give skew angles of $\sim$ -15° and $\sim$ +10°, respectively. With these angles, an impact on the SMV5 performance would have surely been visible, since the power curves shown in Figure 4.9a proved that a deflection of $\sim$ 5° already had a visible effect. This model might only be applicable when the measurement is realized close to the yawed turbine, in the near wake region. The experimental measurement realized in [26] were indeed done at 1.8 D downstream only. When the distance to the upwind turbine increases further, the impact of the free stream flow becomes so significant that the wake is redirected towards the main wind direction and therefore the skew angle is considerably reduced.

The second wake deflection model, proposed in [55], is based on LES simulation and takes into account these considerations and is therefore more appropriate for the far wake region. In this model the wake skew angle θ can be assessed as a function of the upwind wind turbine misalignment angle γ and the downstream distance x using Equation (7.2):

$$\theta = \frac{\frac{C_t}{2} cos^2(\gamma) sin(\gamma)}{\left(1 + \beta \frac{x}{D}\right)} \tag{7.2}$$

where β drives the expansion of the skewed wake, similarly as the wake decay constant α in the Jensen model. Using this formula with a misalignment $\gamma = 10°$, an expansion coefficient $\beta = 0.1$ (order of magnitude of the recommended values in [55]) and with a thrust coefficient $C_t = 0.8$ at a downstream distance $x = 3.7\ D$ gives a wake skew angle of $\theta = 2°$. It is likely that such small angles are difficult to measure with only a hundred data points available in the disturbed sector.

The results from this model can also be confronted to the dynamic wake deflection of SMV6 measured in Section 4.2. The wake center position seen at SMV5 was displaced by 5 - 7° when the wind turbine misalignment measured by the 5 beam lidar was $\sim$ 15°. However, using Equation (7.2) with a Ct of 0.4 (corresponding value at the nominal wind speed) gives a skew angle of 1.5° only. As a consequence it seems that this model does not seem completely applicable for the SMV6 - SMV5 wake. This might be related to the fact that the distance between the two turbines is still small and probably quite close to the near wake region. The values for β found in [55] were obtained at a distance of 8 D, i.e. more than twice the distance between SMV6 and SMV5, and might therefore not be adapted to a distance of 3.7 D only.

7.2 Summary of the Field Test Results and Discussion

Unfortunately, the yaw offset measurement campaign did not provide as much results as could have been hoped. During the periods when the yaw error was implemented, the wind speeds were quite low and the wind did not blow in the right direction sector. The available data-set in the wake sector was therefore considerably reduced. Moreover, the turbines seem to have an initial yaw error varying with the wind speed and that was not properly calibrated or measured before the tests, as a consequence the effective yaw error implemented during the campaign are not known for certain.

Some results could nonetheless be obtained from this first field tests. A loss of power production in the yawed turbine could be measured, the fluctuations of these losses with the wind speed are consistent with the measured variations of yaw error realized with the nacelle lidar. The order of magnitude of the relative power losses due to the yaw error also seems in line with the values indicated in the literature.

However, no conclusions could be drawn regarding a possible wake deflection. As this parameter could only be measured at the downwind turbine, and considering the small amount of data points available in the wake sector, this is not surprising. There is also a question about whether the yaw error angles scenarios allowed big enough angles to really measure a wake deflection. An improvement of a wake deflection modelling seems also needed as the two wake deflection models studied here were not exactly giving the same results as the values obtained from the measured dynamic yaw errors.

The study of the results of the scanning lidar might provide some information about this point, as the behavior of the SMV6 wake can be investigated in other wind direction sectors where the amount of recorded data during the tests is more important. This work should be done by the PRISME during the next months. Another way to increase this amount of available data would be to analyze the dynamic yaw errors of the wind turbines of the farm. As these yaw errors are varying from one turbine to another, they could provide some interesting results. In any case calibrating the variations of yaw error with the wind speed and measuring as accurately as possible the initial setting seems necessary before the beginning the next field test campaign.

The measurements of the strain gauges installed in the wind turbine blades were not analyzed during this thesis. They could provide some interesting results about the changes in wind turbine loading when using the yaw offset strategy, both for the upstream wind turbine in yawed conditions and for the downstream wind turbine due to the wake deflection. In particular, the fluctuation of loading of the downstream turbine depending on the wake conditions (full-wake or partial wake) are of great interest since they will be giving the wind direction range when this strategy can be profitable.

Indeed, contrary to the curtailment strategy, the yaw offset strategy seems to have a very good potential for half wake situations mainly. In full wake conditions, it does not seem possible to deflect completely the wake away from a downstream turbine even with an important yaw error. Then it may not be very profitable to use this strategy to go from full wake to partial wake only. The blades will be facing very different wind conditions during their cycle and thus the loads can increase significantly for a small increase in power production. On the other hand, using this strategy during the partial wake situations to completely deflect the wake away from the wind turbine is expected to provide both a decrease in the loading and an increase in the production.

8 | Final Discussion and Conclusion

Wind energy is a very fast growing industry and becomes every year even more competitive with conventional power generation sources. In order to decrease even further the cost of wind energy, innovative control strategies are implemented at a wind farm scale with double objective: increase the overall wind farm power production and its lifetime thanks to a reduction in the fatigue loading of the wind turbines. This is achieved by controlling the wind turbines of the farm in such a way that aerodynamic interactions between them are minimized.

This topic has been increasingly investigated over the past years and simulation results indicate that gains in power production or reductions in wind turbine loading are indeed possible. However these results seem to be quite dependent on the models used during the process and generally consider ideal incoming wind conditions. They all underline the gains are highly sensitive to changes in these conditions.

Consequently, it appears difficult to reproduce these expected results in a full scale operating wind farm, where wind conditions are known to be very fluctuating. The French national project SMARTEOLE is one of the first attempts to achieve this goal. Two different strategies, the curtailment strategy and the yaw offset strategy, are being tested during two field tests carried out in an operating onshore wind farm, *La Sole du Moulin Vieux*, in the North of France.

This master thesis is based on the results of the first measurement campaign of SMARTEOLE, realized in 2016. The analysis of those results confirms the difficulty of achieving increase in power production considering actual operating conditions, in particular for the assessment of the real time incoming wind conditions.

In this first campaign, these conditions were mainly assessed by the SCADA measurements provided by the wind turbines. This practice is followed in most of the wind farms as SCADA are generally the only measurements available. However, in the case of SMV, the wind direction sensors were not calibrated properly and this led to a significant loss of available data for the curtailment experiment. A method to correct those values was used in this thesis so that this problem should not be repeated in the second campaign.

The question of the assessment of wind speed is harder as this parameter is fluctuating much more. In this thesis Nacelle Transfer Functions were derived with the help of the nacelle lidars installed during the first campaign in order to correct the SCADA measurements. This method seems good enough to analyze 10-min averaged data, however when it comes to assessing real time wind speed from second wise measurement it is probably not good enough. Indeed, the nacelle wind speed signal is seen to be oscillating constantly as it is located behind the rotor and thus exposed to a highly distorted flow.

Alternative ways of assessing wind speed must then be found. Remote sensing devices such as lidars could be one of them. Another one, the concept of Rotor Effective Wind Speed, was developed in the PossPOW project and tested in this thesis. It consists in assessing the wind speed from the SCADA signals of power, rotational speed and pitch angle, which are less fluctuating than the nacelle wind speed signal. Compared to the wind speed that can be derived from the measured power using the power curve, it can still be used once the rated power is reached or when the turbine is down-regulated. The results found in this thesis confirms that this method offers a reliable way of measuring the real time speed.

Finally, another particular problem was related to the singular behavior of the wind turbines of the SMV wind farm. These wind turbines were seen to have a yaw error that was increasing with the wind speed, causing a decrease in their performance but also a wake deflection. This wake deflection must be corrected otherwise the optimization of power production is made even more sensitive to changes in the wind conditions.

As already mentioned, one of the main issues when optimizing the wind farm power production is using a reliable wake model. Thanks to the available experimental data a trustworthy model could be derived based on a re-calibration of the Jensen model. The Jensen model is an old but very well known and

used wake model in the industry. Thanks to its simplicity and quickness of execution, it is generally considered for optimization purposes. In the original model, the wind speed deficit is calculated using a certain parameter, the wake expansion coefficient, which is dependent on the atmospheric conditions. In the common practice this parameter is taken constant for the whole wind farm. However when a wind turbine is under wake conditions, its own wake will be decaying much faster and therefore using the same constant as the most upwind turbine clearly over-estimate the wind speed deficit.

In the re-calibrated Jensen model presented here, the wake expansion coefficient is calculated at each wind turbine based on the turbulence intensity distribution measured by the nacelle wind speed. A linear dependency between these two parameters was used, and the best value for the proportional coefficient was found to be 0.55. In that way the wake added turbulence can be taken into account and thus a much better representation of the actual wind speed deficit can be obtained. This model proved to be very consistent with the experimental measurements.

Two strategies were tested during the SMARTEOLE first measurement campaign. Unfortunately a gain in combined power production could not be achieved in any of them. Regarding the curtailment strategy, this could be explained by the choice of a down-regulation slightly too high and unfavorable wind conditions. However the measured total loss of power proved to be limited. Moreover, a Ct model derived from the study of several power curves guaranteed by the manufacturer could be validated thanks to the data recorded during these tests.

This Ct model could then be used alongside with the re-calibrated Jensen model in order to find the maximum expected power production of two wind turbines. The gains are realized for wind speed between 6 and 10 m/s, which corresponds to the range where both Cp and Ct are high. At those wind speed, Ct is much more sensitive than Cp and therefore a significant reduction in Ct can be obtained with a much smaller reduction of Cp. However when considering only two turbines the increase in combined power production remains very limited. The maximum gains at a particular wind speed are found to be 2 to 3 % only, and when averaged over the complete wind speed range the total gains are in the order of 0.3 - 0.5%. Also the width of the direction sector in which this strategy is profitable could be assessed to 10° centered on the full wake conditions. The curtailment strategy is thus only applicable for the full wake conditions and is expected to be more profitable when several turbines in a row are considered, since the curtailment of the most upwind turbine will be beneficial to all downstream wind turbines.

The results about the yaw offset experiment were quite difficult to analyze due to the reduced amount of available data in the wake sector. Also, the fact that the initial yaw error of the turbines was not calibrated complicated the analysis. No wake deflection could be measured at the downwind turbine and therefore no conclusion could be drawn regarding a positive impact allowed by the misalignment of the upwind turbine. A loss of production due to the yaw error at the upwind turbine could be measured and seems to be in the same order of magnitude of reported values in a similar case.

The study of the wind turbine loading could not be realized during this thesis. This question is nonetheless very important as an increase in power production cannot be beneficial if at the same time the loads are significantly increased. This information is particularly important regarding the yaw offset strategy as it is not very known how the loading is varying with the yaw error and also the wake situation (partial or full wake). For the curtailment strategy a reduction in the fatigue loading can be expected for the second wind turbine of the row thanks to the decrease of the wake added turbulence intensity.

It is much likely that the two control strategies investigated in this thesis are not competing against each other but on the contrary being very complementary. Indeed, the curtailment strategy is only profitable in full wake conditions while the yaw offset strategy seems mainly beneficial in partial wake conditions, where the wake can be controlled and deflected away from the downwind turbine.

New scenarios about these two strategies will be tested during the second field test campaign of SMARTEOLE which is about to begin. They will hopefully show that an increase in power production can be effectively obtained in a full scale wind farm. However this result would only be the first step in the way of implementing a trustworthy control for power production optimization.

A second step consists in modeling in a reliable way the behavior of the wake when curtailing or yawing a

wind turbine. The modeling involved in this thesis was focused on the particular case of the SMARTEOLE project, and it is not known to what extent both the re-calibrated Jensen model and the Ct model can be applied in other wind farms and other wind turbine models, respectively. Some work is also needed for the derivation of a proper wind deflection model.

Finally, a last step would be the actual design of wind turbine controller able to meet all the requirements needed to realize the optimization of the power production at a wind farm scale. The most important constraints that would be imposed on such a controller are in particular the capacity of assessing with a high accuracy the incoming wind conditions of the farm, and of reacting in real time to fluctuations of these conditions. Eventually, it will be also required the ability of choosing at each instant the best control method among those available and calculate the optimal settings of each individual wind turbines of the farm.

Bibliography

[1] Wind Europe. *Wind in power – 2016 European statistics*. 2017.

[2] *Wind Europe website – Economics*. `https://windeurope.org/policy/topics/economics/`. Accessed: 2017-06-15.

[3] B Sanderse. *Aerodynamics of wind turbine wakes - Literature review*. Tech. rep. Energy research Center of the Netherlands, 2009.

[4] J Højstrup. "Spectral coherence in wind turbine wakes". In: *Journal of Wind Engineering and Industrial Aerodynamics* 80.1 (1999), pp. 137–146.

[5] LJ Vermeer, JN Sørensen, and A Crespo. "Wind turbine wake aerodynamics". In: *Progress in aerospace sciences* 39.6 (2003), pp. 467–510.

[6] T Burton, D Sharpe, N Jenkins, and EA Bossanyi. *Wind energy handbook*. John Wiley & Sons, 2001.

[7] PEJ Vermeulen. "An experimental analysis of wind turbine wakes". In: *3rd international symposium on wind energy systems*. 1980, pp. 431–450.

[8] A Crespo, J Hernandez, and S Frandsen. "Survey of modelling methods for wind turbine wakes and wind farms". In: *Wind energy* 2.1 (1999), pp. 1–24.

[9] T Ackermann. *Wind power in power systems*. John Wiley & Sons, 2005.

[10] JF Manwell, JG McGowan, and AL Rogers. *Wind energy explained: theory, design and application*. John Wiley & Sons, 2010.

[11] *IEC International Standard, IEC 61400–1: Wind turbines – Part 1: Design requirements*. 2005.

[12] EA Bossanyi. "Wind turbine control for load reduction". In: *Wind energy* 6.3 (2003), pp. 229–244.

[13] LY Pao and KE Johnson. "A tutorial on the dynamics and control of wind turbines and wind farms". In: *American Control Conference, 2009. ACC'09.* IEEE. 2009, pp. 2076–2089.

[14] T Knudsen, T Bak, and M Svenstrup. "Survey of wind farm control—power and fatigue optimization". In: *Wind Energy* 18.8 (2015), pp. 1333–1351.

[15] PA Fleming, PMO Gebraad, S Lee, J-W van Wingerden, K Johnson, M Churchfield, J Michalakes, P Spalart, and P Moriarty. "Evaluating techniques for redirecting turbine wakes using SOWFA". In: *Renewable Energy* 70 (2014), pp. 211–218.

[16] PA Fleming, PMO Gebraad, S Lee, J-W van Wingerden, K Johnson, M Churchfield, J Michalakes, P Spalart, and P Moriarty. "Simulation comparison of wake mitigation control strategies for a two-turbine case". In: *Wind Energy* 18.12 (2015), pp. 2135–2143.

[17] LAH Machielse, S Barth, ETG Bot, HB Hendriks, and GJ Schepers. *Evaluation of "heat and flux" farm control*. Tech. rep. Energy research Center of the Netherlands, 2007.

[18] JG Schepers and SP Van der Pijl. "Improved modelling of wake aerodynamics and assessment of new farm control strategies". In: *Journal of Physics: Conference Series*. Vol. 75. 1. IOP Publishing. 2007, p. 012039.

[19] F Heer, PM Esfahani, M Kamgarpour, and J Lygeros. "Model based power optimisation of wind farms". In: *Control Conference (ECC), 2014 European*. IEEE. 2014, pp. 1145–1150.

[20] KE Johnson and G Fritsch. "Assessment of extremum seeking control for wind farm energy production". In: *Wind Engineering* 36.6 (2012), pp. 701–715.

[21] *ECN Wind Turbine Test Site Wieringermeer*. `https://www.ecn.nl/extranet/ewtw/index.html`. Accessed: 2017-06-05.

[22] M Soleimanzadeh, R Wisniewski, and S Kanev. "An optimization framework for load and power distribution in wind farms". In: *Journal of Wind Engineering and Industrial Aerodynamics* 107 (2012), pp. 256–262.

[23] J Jonkman, S Butterfield, W Musial, and G Scott. *Definition of a 5-MW reference wind turbine for offshore system development*. Tech. rep. National Renewable Energy Laboratory, 2009.

[24] MS Adaramola and P-Å Krogstad. "Experimental investigation of wake effects on wind turbine performance". In: *Renewable Energy* 36.8 (2011), pp. 2078–2086.

[25] K Boorsma. *Power and loads for wind turbines in yawed conditions*. Tech. rep. Energy research Center of the Netherlands, 2012.

[26] JW Wagenaar, L Machielse, and J Schepers. "Controlling wind in ECN's scaled wind farm". In: *Proc. Europe Premier Wind Energy Event* (2012), pp. 685–694.

[27] *Agence Nationale pour la Recherche, the SMARTEOLE national project*. `http://www.agence-nationale-recherche.fr/?Project=ANR-14-CE05-0034`. Accessed: 2017-05-01.

[28] S Emeis. *Wind energy meteorology: atmospheric physics for wind power generation*. Springer Science & Business Media, 2012.

[29] L Landberg. *Meteorology for wind energy: an introduction*. John Wiley & Sons, 2015.

[30] C Braud and E Guilmineau. "Jet flow control at the blade scale to manipulate lift". In: *Journal of Physics: Conference Series*. Vol. 753. 2. IOP Publishing. 2016, p. 022031.

[31] S Baleriola, A Leroy, S Loyer, P Devinant, and S Aubrun. "Circulation control on a rounded trailing-edge wind turbine airfoil using plasma actuators". In: *Journal of Physics: Conference Series*. Vol. 753. 5. IOP Publishing. 2016, p. 052001.

[32] A Leroy, C Braud, S Baleriola, S Loyer, P Devinant, and S Aubrun. "Comparison of flow modification induced by plasma and fluidic jet actuators dedicated to circulation control around wind turbine airfoils". In: *Journal of Physics: Conference Series*. Vol. 753. 2. IOP Publishing. 2016, p. 022012.

[33] F Guillemin, D Di Domenico, N Nguyen, G Sabiron, M Boquet, N Girard, and O Coupiac. "Nacelle LiDAR online wind field reconstruction applied to feedforward pitch control". In: *Journal of Physics: Conference Series*. Vol. 753. 5. IOP Publishing. 2016, p. 052019.

[34] S Aubrun, E Torres Garcia, M Boquet, O Coupiac, and N Girard. "Wind turbine wake tracking and its correlations with wind turbine monitoring sensors. Preliminary results". In: *Journal of Physics: Conference Series*. Vol. 753. 3. IOP Publishing. 2016, p. 032003.

[35] T Ahmad, O Coupiac, A Petit, S Guignard, N Girard, B Kazemtabrizi, and PC Matthews. "Field implementation and trial of coordinated control of wind farms". In: *IEEE Transactions on Sustainable Energy* (2017). (submitted).

[36] F Zahle and NN Sørensen. "Characterization of the unsteady flow in the nacelle region of a modern wind turbine". In: *Wind Energy* 14.2 (2011), pp. 271–283.

[37] *IEC International Standard, IEC 61400–12-2, Wind Turbines – Part 12-2: Power performance of electricity producing wind turbines based on nacelle anemometry*. 2013.

[38] T Göçmen. "Possible Power Estimation of Down-Regulated Offshore Wind Power Plants". PhD thesis. 2016.

[39] S Heier. *Grid integration of wind energy conversion systems*. 1998.

[40] K Raiambal and C Chellamuthu. "Modeling and simulation of grid connected wind electric generating system". In: *TENCON'02. Proceedings. 2002 IEEE Region 10 Conference on Computers, Communications, Control and Power Engineering*. Vol. 3. IEEE. 2002, pp. 1847–1852.

[41] T Göçmen, G Giebel, NK Poulsen, and M Mirzaei. "Wind speed estimation and parametrization of wake models for downregulated offshore wind farms within the scope of PossPOW project". In: *Journal of Physics: Conference Series*. Vol. 524. 1. IOP Publishing. 2014, p. 012156.

[42] T Göçmen and G Giebel. "Estimation of turbulence intensity using rotor effective wind speed in Lillgrund and Horns Rev-I offshore wind farms". In: *Renewable Energy* 99 (2016), pp. 524–532.

[43] T Göçmen, P Van der Laan, P-E Réthoré, A Peña, GC Larsen, and S Ott. "Wind turbine wake models developed at the technical university of Denmark: A review". In: *Renewable and Sustainable Energy Reviews* 60 (2016), pp. 752–769.

[44] NO Jensen. *A note on wind generator interaction*. 1983.

[45] I Katic, J Højstrup, and NO Jensen. "A simple model for cluster efficiency". In: *European Wind Energy Association Conference and Exhibition*. 1986, pp. 407–410.

[46] GC Larsen. *A simple wake calculation procedure*. 1988.

[47] GC Larsen. *A simple stationary semi-analytical wake model*. Tech. rep. Risø National Laboratory for Sustainable Energy, Technical University of Denmark, 2009.

[48] NG Mortensen, L Landberg, I Troen, E Lundtang Petersen, O Rathmann, and M Nielsen. *Wind Atlas Analysis and Application program (WAsP): vol. 3: Utility programs*. Tech. rep. Risø National Laboratory, 1999.

[49] P Nielsen, J Villadsen, J Kobberup, ML Thørgersen, MV Sørensen, T Sørensen, et al. *Windpro: Software and manual*. 2003.

[50] A Peña and O Rathmann. "Atmospheric stability-dependent infinite wind-farm models and the wake-decay coefficient". In: *Wind Energy* 17.8 (2014), pp. 1269–1285.

[51] A Peña, P-E Réthoré, and MP Laan. "On the application of the Jensen wake model using a turbulence-dependent wake decay coefficient: the Sexbierum case". In: *Wind Energy* (2015).

[52] T Ahmad, N Girard, B Kazemtabrizi, and PC Matthews. "Analysis of two onshore wind farms with a dynamic farm controller." In: *EWEA Paris France*. 2015.

[53] U Hassan. *A wind tunnel investigation of the wake structure within small wind turbine farms*. Harwell Laboratory, Energy Technology Support Unit, 1993.

[54] JD Grunnet, M Soltani, T Knudsen, MN Kragelund, and T Bak. "Aeolus toolbox for dynamics wind farm model, simulation and control". In: *The European Wind Energy Conference & Exhibition, EWEC 2010*. 2010.

[55] Á Jiménez, A Crespo, and E Migoya. "Application of a LES technique to characterize the wake deflection of a wind turbine in yaw". In: *Wind energy* 13.6 (2010), pp. 559–572.

A | Data Calibration

A.1 Direction Offset Calibration Results and Figures

SMV1

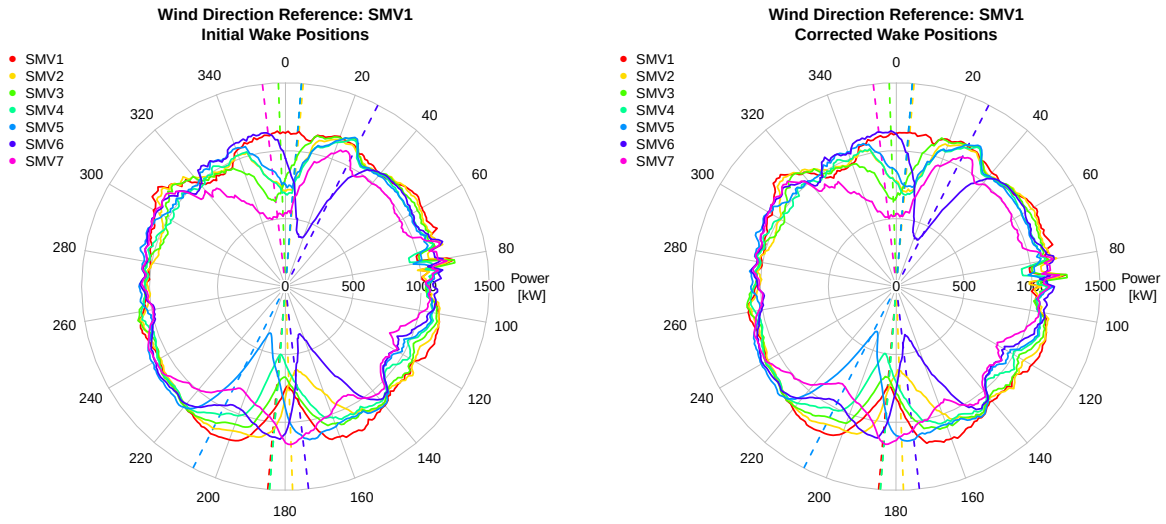

Figure A.1: *SMV1 wake rose before (left) and after (right) offset calibration*

Table A.1: *Direction offset calibration for SMV1*

Wake			Before calibration		After calibration	
From	To	Theoretical position [°]	Real Position [°]	Error [°]	Final Position[°]	Residual Error [°]
SMV1	SMV2	5	359.9	-5.1	5.4	0.4
SMV2	SMV1	185	179.0	-6.0	184.5	-0.5
SMV2	SMV3	358	352.9	-5.1	358.4	0.4
SMV3	SMV2	178	173.4	-4.6	178.9	0.9
SMV3	SMV5	4.5	0.6	-3.9	6.1	1.6
SMV4	SMV3	184.5	181.3	-3.2	186.8	2.3
SMV4	SMV5	4.5	3.7	-0.8	9.2	4.7
SMV5	SMV4	184.5	184.4	-0.1	189.9	5.4
SMV5	SMV6	27	18.5	-8.5	24	-3
SMV6	SMV5	207	197.7	-9.3	203.2	-3.8
SMV6	SMV7	353.5	348.7	-4.8	354.2	0.7
SMV7	SMV6	173.5	164.7	-9.3	169.7	3.8

SMV2

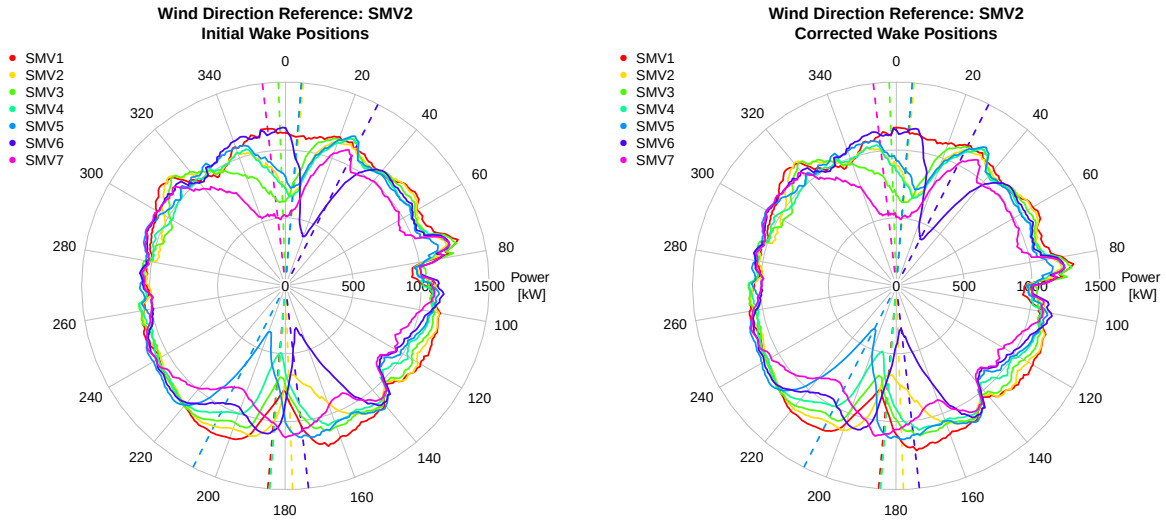

Figure A.2: *SMV2 wake rose before (left) and after (right) offset calibration*

Table A.2: *Direction offset calibration for SMV2*

Wake			Before calibration		After calibration	
From	To	Theoretical position [°]	Real Position [°]	Error [°]	Final Position[°]	Residual Error [°]
SMV1	SMV2	5	2.7	-2.3	10.7	5.7
SMV2	SMV1	185	181.0	-4.0	189	4.0
SMV2	SMV3	358	356.7	-1.3	4.7	6.7
SMV3	SMV2	178	177.4	-0.6	185.4	7.4
SMV3	SMV5	4.5	2.7	-1.8	10.7	6.2
SMV4	SMV3	184.5	182.8	-1.7	190.8	6.3
SMV4	SMV5	4.5	3.7	-0.8	11.7	7.2
SMV5	SMV4	184.5	184.2	-0.3	192.2	7.7
SMV5	SMV6	27	19.4	-7.6	27.4	0.4
SMV6	SMV5	207	198.5	-8.5	206.5	-0.5
SMV6	SMV7	353.5	355.1	1.6	3.1	9.6
SMV7	SMV6	173.5	165.7	-7.8	173.7	0.2

SMV3

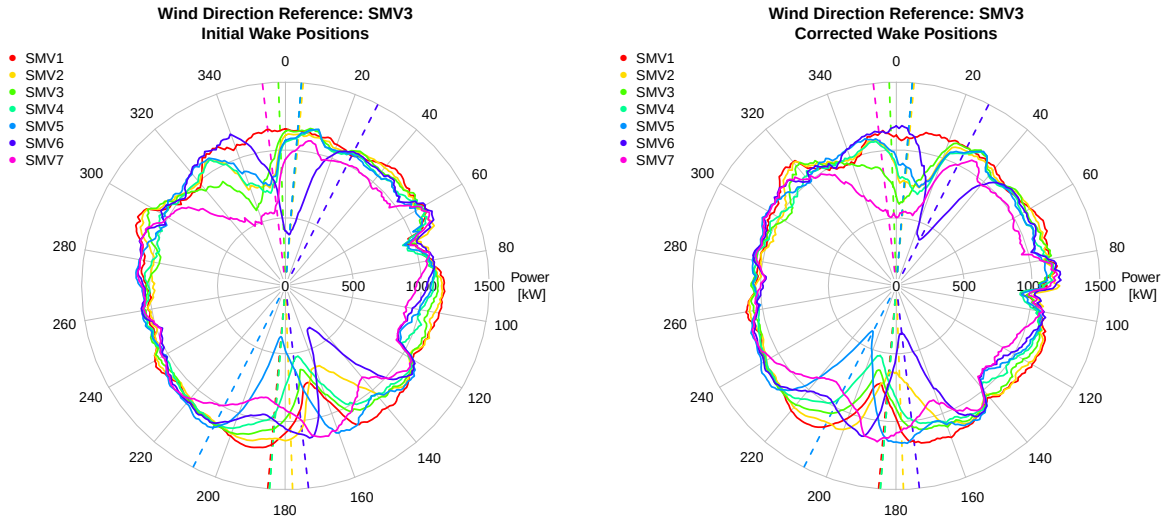

Figure A.3: *SMV3 wake rose before (left) and after (right) offset calibration*

Table A.3: *Direction offset calibration for SMV3*

Wake			Before calibration		After calibration	
From	To	Theoretical position [°]	Real Position [°]	Error [°]	Final Position[°]	Residual Error [°]
SMV1	SMV2	5	351.0	-14.0	13.5	8.5
SMV2	SMV1	185	166.7	-18.3	189.2	4.2
SMV2	SMV3	358	338.9	-19.1	1.4	3.4
SMV3	SMV2	178	159.3	-18.7	181.8	3.8
SMV3	SMV5	4.5	350.7	-13.8	13.2	8.7
SMV4	SMV3	184.5	170.0	-14.5	192.5	8.0
SMV4	SMV5	4.5	350.5	-14.0	13.0	8.5
SMV5	SMV4	184.5	170.2	-14.3	192.7	8.2
SMV5	SMV6	27	3.9	-23.1	26.4	-0.6
SMV6	SMV5	207	185.2	-21.8	207.7	0.7
SMV6	SMV7	353.5	333.9	-14.6	1.4	7.9
SMV7	SMV6	173.5	150.9	-22.6	173.4	-0.1

SMV4

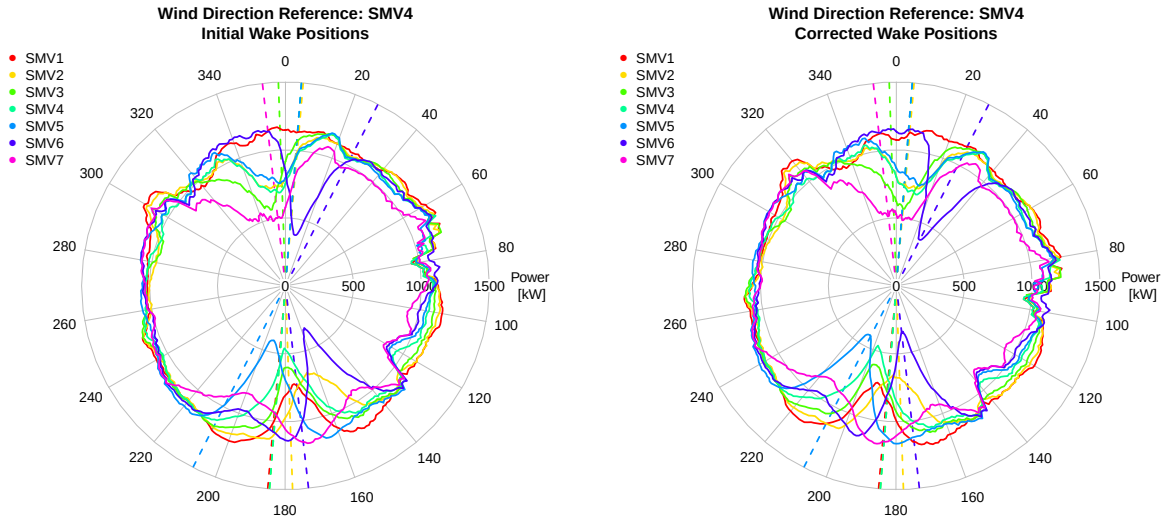

Figure A.4: *SMV4 wake rose before (left) and after (right) offset calibration*

Table A.4: *Direction offset calibration for SMV4*

Wake			Before calibration		After calibration	
From	To	Theoretical position [°]	Real Position [°]	Error [°]	Final Position[°]	Residual Error [°]
SMV1	SMV2	5	351.5	-13.5	7.5	2.5
SMV2	SMV1	185	175.4	-9.6	191.4	6.4
SMV2	SMV3	358	350.1	-7.9	6.1	8.1
SMV3	SMV2	178	165.8	-12.2	181.8	3.8
SMV3	SMV5	4.5	357.7	-6.8	13.7	9.2
SMV4	SMV3	184.5	178.3	-6.2	194.3	9.8
SMV4	SMV5	4.5	358.6	-5.9	14.6	10.1
SMV5	SMV4	184.5	180.8	-3.7	196.8	12.3
SMV5	SMV6	27	11.7	-15.3	27.7	0.7
SMV6	SMV5	207	192.3	-14.7	208.3	1.3
SMV6	SMV7	353.5	350.5	-3.0	6.5	13.0
SMV7	SMV6	173.5	156.0	-17.5	172.0	-1.5

SMV5

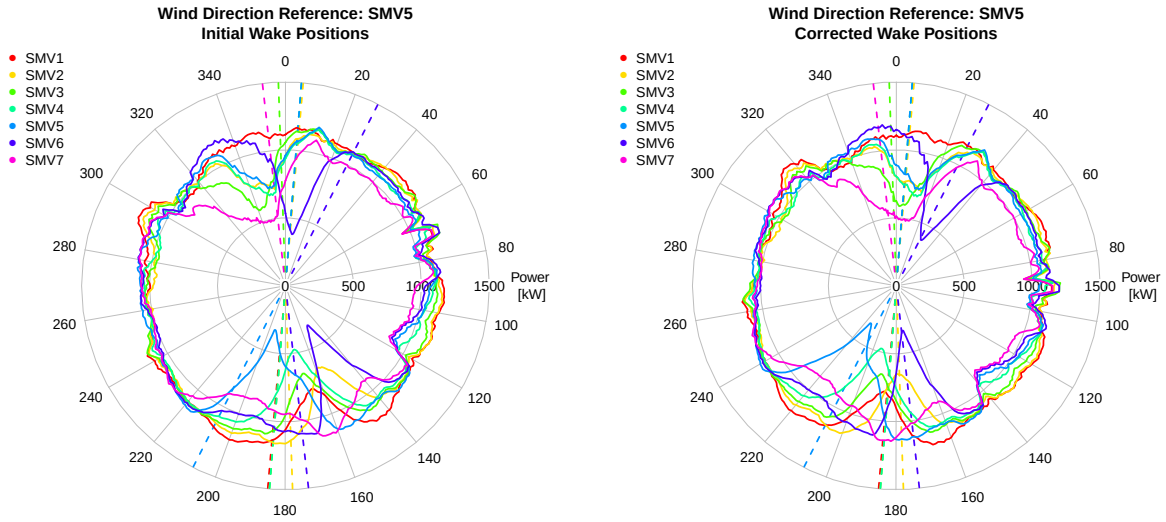

Figure A.5: *SMV5 wake rose before (left) and after (right) offset calibration*

Table A.5: *Direction offset calibration for SMV5*

Wake			Before calibration		After calibration	
From	To	Theoretical position [°]	Real Position [°]	Error [°]	Final Position[°]	Residual Error [°]
SMV1	SMV2	5	353.8	-11.2	14.9	9.9
SMV2	SMV1	185	166.6	-18.4	187.6	2.6
SMV2	SMV3	358	341.8	-16.2	2.8	4.8
SMV3	SMV2	178	157.4	-20.6	178.4	0.4
SMV3	SMV5	4.5	351.5	-13.0	12.5	8.0
SMV4	SMV3	184.5	168.2	-16.3	189.2	4.7
SMV4	SMV5	4.5	351.5	-13.0	12.5	8.0
SMV5	SMV4	184.5	172.2	-12.3	193.2	8.7
SMV5	SMV6	27	7.0	-20.0	28.0	1.0
SMV6	SMV5	207	193.2	-13.8	214.2	7.2
SMV6	SMV7	353.5	348.6	-4.9	9.6	16.1
SMV7	SMV6	173.5	151.3	-22.2	172.3	-1.2

SMV6

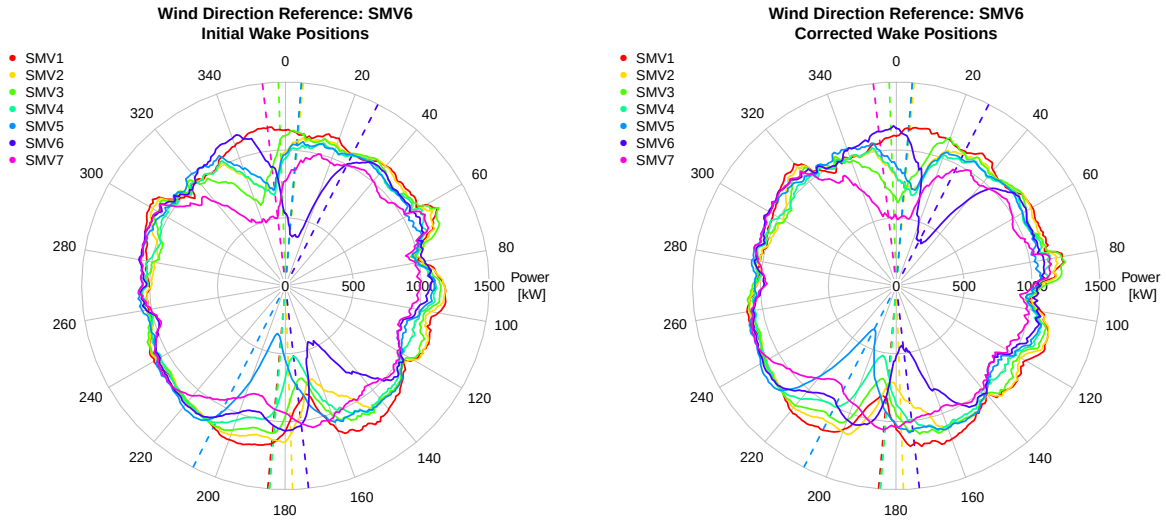

Figure A.6: *SMV6 wake rose before (left) and after (right) offset calibration*

Table A.6: *Direction offset calibration for SMV6*

Wake			Before calibration		After calibration	
From	To	Theoretical position [°]	Real Position [°]	Error [°]	Final Position[°]	Residual Error [°]
SMV1	SMV2	5	352.6	-12.4	10.1	5.1
SMV2	SMV1	185	170	-15.0	187.5	2.5
SMV2	SMV3	358	343.4	-14.6	0.9	2.9
SMV3	SMV2	178	164.2	-13.8	181.7	3.7
SMV3	SMV5	4.5	352.6	-11.9	10.1	5.6
SMV4	SMV3	184.5	170.0	-14.5	187.5	3.0
SMV4	SMV5	4.5	353.0	-11.5	10.5	6.0
SMV5	SMV4	184.5	173.9	-10.6	191.4	6.9
SMV5	SMV6	27	7.9	-19.1	25.4	-1.6
SMV6	SMV5	207	189.4	-17.6	206.9	-0.1
SMV6	SMV7	353.5	343.3	-10.2	0.8	7.3
SMV7	SMV6	173.5	157.9	-15.6	175.4	1.9

SMV7

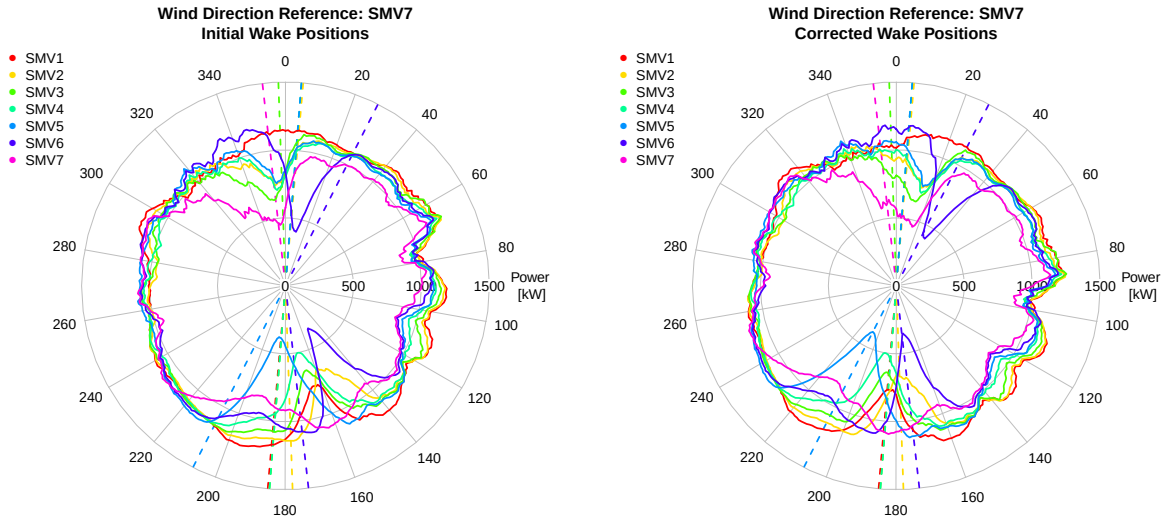

Figure A.7: *SMV7 wake rose before (left) and after (right) offset calibration*

Table A.7: *Direction offset calibration for SMV7*

Wake			Before calibration		After calibration	
From	To	Theoretical position [°]	Real Position [°]	Error [°]	Final Position[°]	Residual Error [°]
SMV1	SMV2	5	354.0	-11.0	14.0	9.0
SMV2	SMV1	185	161.7	-2.3	181.7	-3.3
SMV2	SMV3	358	352.4	-5.6	12.4	14.4
SMV3	SMV2	178	158.9	-19.1	178.9	0.9
SMV3	SMV5	4.5	354.9	-9.6	14.9	10.4
SMV4	SMV3	184.5	166.1	-18.4	186.1	1.6
SMV4	SMV5	4.5	354.9	-9.6	14.9	10.4
SMV5	SMV4	184.5	169.4	-15.1	189.4	4.9
SMV5	SMV6	27	10.2	-16.8	30.2	3.9
SMV6	SMV5	207	186.6	-20.4	206.6	-0.4
SMV6	SMV7	353.5	355.7	2.2	15.7	22.2
SMV7	SMV6	173.5	151.7	-21.8	171.7	-1.8

Met-mast Ablaincourt

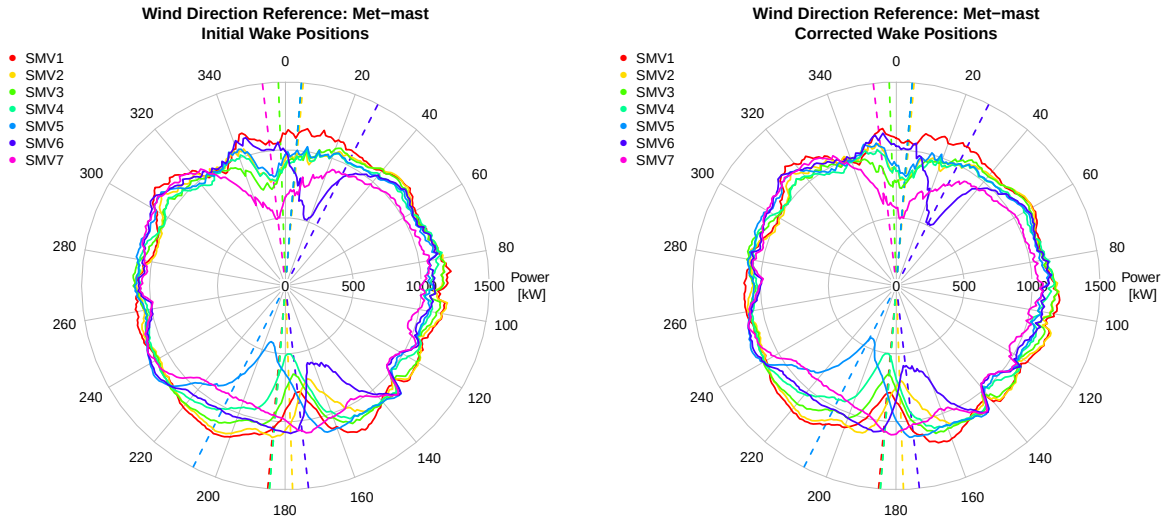

Figure A.8: *Met-mast wake rose before (left) and after (right) offset calibration*

Table A.8: *Direction offset calibration for the met-mast*

Wake			Before calibration		After calibration	
From	To	Theoretical position [°]	Real Position [°]	Error [°]	Final Position[°]	Residual Error [°]
SMV1	SMV2	5	354.8	-10.2	5.7	0.7
SMV2	SMV1	185	172.9	-12.1	183.4	-1.6
SMV2	SMV3	358	352.0	-6.0	2.5	4.5
SMV3	SMV2	178	167.2	-10.8	177.7	-0.3
SMV3	SMV5	4.5	354.7	-9.8	5.7	1.2
SMV4	SMV3	184.5	174.5	-10.0	185.0	0.5
SMV4	SMV5	4.5	354.7	-9.8	5.7	1.2
SMV5	SMV4	184.5	176.4	-8.1	186.9	2.4
SMV5	SMV6	27	17.4	-9.6	27.9	0.9
SMV6	SMV5	207	194.1	-12.9	204.6	-2.4
SMV6	SMV7	353.5	355.2	1.7	5.7	12.2
SMV7	SMV6	173.5	161.9	-11.6	172.4	-1.1

Windcube (position1)

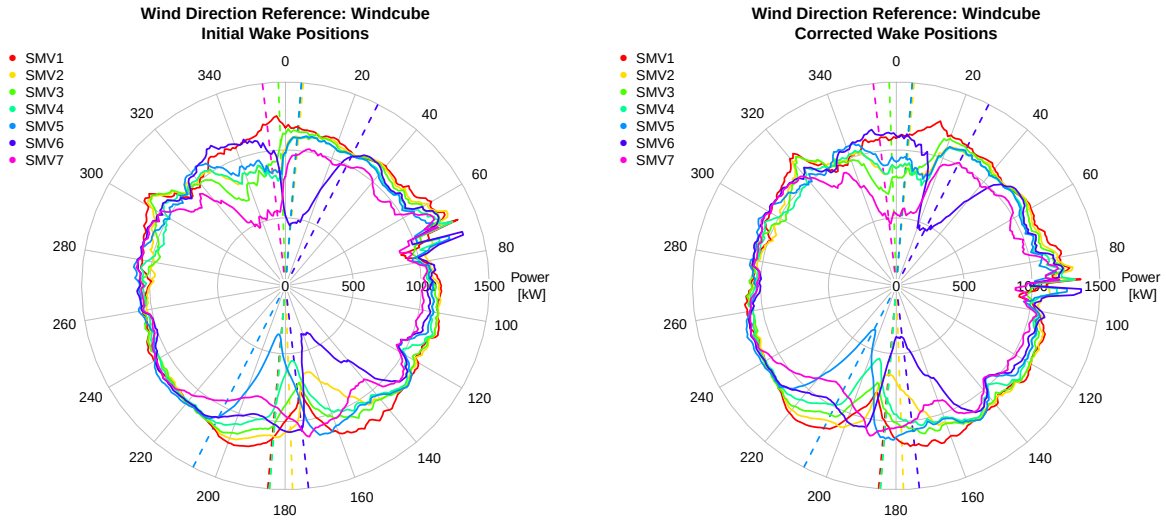

Figure A.9: *Windcube wake rose before (left) and after (right) offset calibration*

Table A.9: *Direction offset calibration for the windcube*

Wake			Before calibration		After calibration	
From	To	Theoretical position [°]	Real Position [°]	Error [°]	Final Position[°]	Residual Error [°]
SMV1	SMV2	5	337.0	-28.0	355.5	-9.5
SMV2	SMV1	185	172.1	-12.9	190.6	5.6
SMV2	SMV3	358	336.2	-21.8	354.7	-3.3
SMV3	SMV2	178	165.9	-12.1	184.4	6.4
SMV3	SMV5	4.5	357.8	-6.7	14.0	9.5
SMV4	SMV3	184.5	172.2	-12.3	190.7	6.2
SMV4	SMV5	4.5	357.8	-6.7	14.0	9.5
SMV5	SMV4	184.5	174.5	-10.0	192.9	8.4
SMV5	SMV6	27	3.9	-23.1	22.4	0.9
SMV6	SMV5	207	187.5	-19.5	206.0	-4.6
SMV6	SMV7	353.5	336.2	17.3	354.7	1.2
SMV7	SMV6	173.5	161.9	-11.6	180.4	6.9

A.2 Derivation of NTF: Procedure and Results

The procedure followed for the identification of the NTF is based on the recommendations of the IEC standard IEC 61400-12-2:2013 Annex D, with a major difference in that the reference free wind speed is given by a nacelle mounted lidar instead of a neighbouring met mast. The free wind speed is measured 200 m upwind (corresponding to a distance L = 2.5 D for the given wind turbines).

The reference wind direction is taken from the nacelle wind vane and is not corrected for offsets. The valid measurement sectors are identified by looking at mean and standard deviation of the ratio between the free wind speed and the nacelle wind speed $V_{free}/V_{nacelle}$ as recommended by the standard. Free wind speed data is then binned against the nacelle wind speed, with a bin width of 0.5 m/s). The NTF is then obtained by the mean value of the free wind speed measured for each wind speed bin.

Uncertainties were not calculated, instead the 95% confidence interval for each bin is indicated by the error bars.

SMV5

The available data for the calculation of the NTF of turbine SMV5 consists of 21314 10-min average wind speed values recorded between 28.10.2015 and 26.04.2016 (combined available data between the Wind Iris lidar and SCADA for SMV5). The data is then reduced to the valid measurement sector and when the turbine is operating (active power > 10 kW). The final filtered dataset corresponds to 1650 hours of measurements (9918 points). The valid measurement sector is [30°; 170°] & [240°; 330°] based on SMV5 wind direction, corrected for offset.

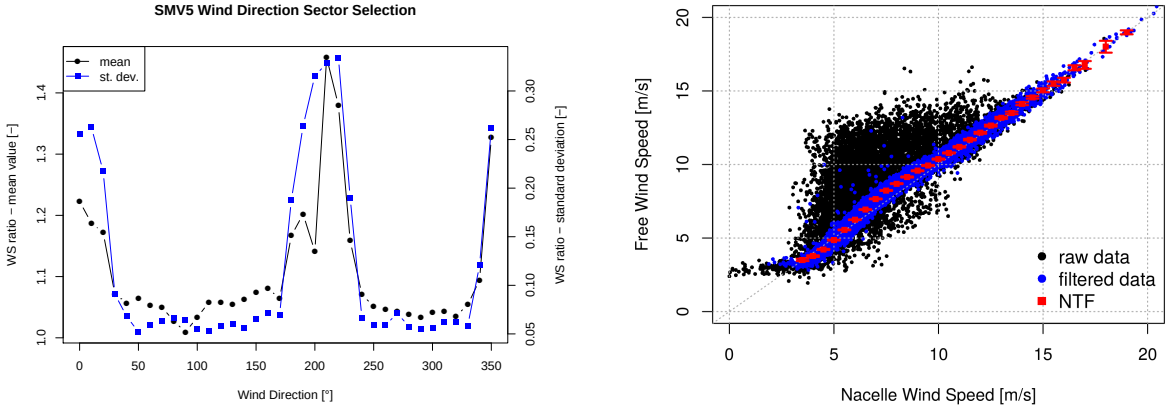

(a) Valid measurement sector determination

(b) Derivation of the NTF

Figure A.10: *Derivation of the NTF for SMV5*

SMV6

The available data for the calculation of the NTF of turbine SMV6 consists of 6169 10-min average wind speed values recorded between 26.11.2015 and 01.04.2016 (combined available data between the 5 beams lidar and SCADA for SMV6, with a break between 01.01.2016 and 23.02.2016). The data is then reduced to the valid measurement sector and when the turbine is operating (active power > 10 kW). The final filtered dataset corresponds to 310 hours of measurements (1872 points). The valid measurement sector is [60°; 140°] & [210°; 290°] based on SMV6 wind direction, corrected for offset. The axes on Figure A.11b have been removed for confidentiality issues.

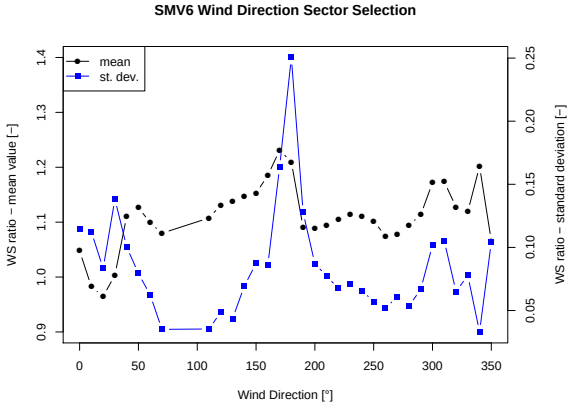

(a) Valid measurement sector determination

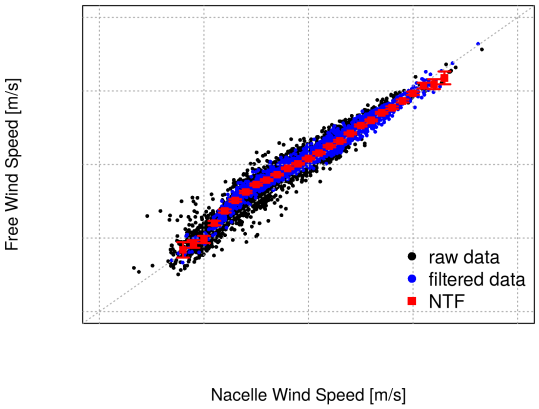

(b) Derivation of the NTF

Figure A.11: *Derivation of the NTF for SMV6*

SMV2

Another NTF is determine on SMV2 based on the wind speed measurement from the windcube located nearby. The available data for this calculation consists of 59939 10-min average wind speed values recorded between 15.06.2015 and 03.05.2016. The data is then reduced to the valid measurement sector and when the turbine is operating (active power $>$ 10 kW). The final filtered dataset corresponds to 2780 hours of measurements (16681 points). The valid measurement sector is [50°; 140°] & [210°; 310°] based on SMV2 wind direction, corrected for offset.

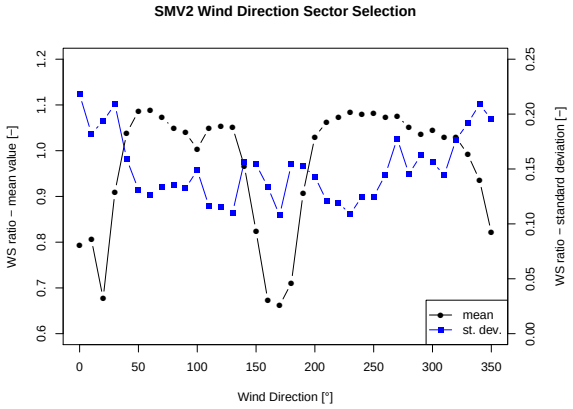

(a) Valid measurement sector determination

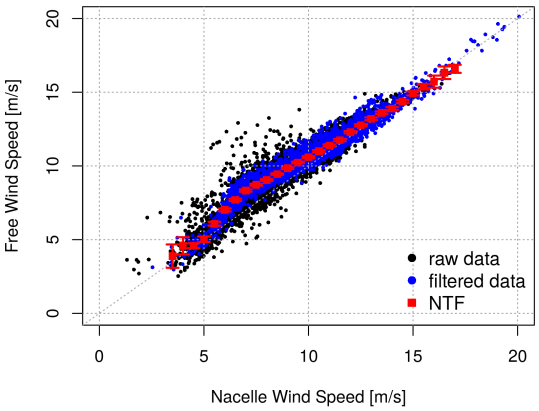

(b) Derivation of the NTF

Figure A.12: *Derivation of the NTF for SMV2*

B | Model Implementations in R

B.1 REWS: Calculation Process

As mentioned on Section 4.3, the Rotor Effective Wind Speed is calculated using a Newton-Raphson algorithm to solve iteratively the system of equations (4.2) - (4.4). The principle of a Newton-Raphson is illustrated on Appendix B.1 below. Guessing a first value x_0 as the root of a certain function f, the following value at the second iteration is given by:

$$x_1 = x_0 - \frac{f(x_0)}{f'(x_0)} \tag{B.1}$$

This mechanism ensures a quadratic convergence towards the researched root of f. The main constraints to be able to use this algorithm is that the function f must be derivable and that its derivative is different than 0. Also the first guess x_0 must also be close enough to the actual root, otherwise the algorithm cannot converge.

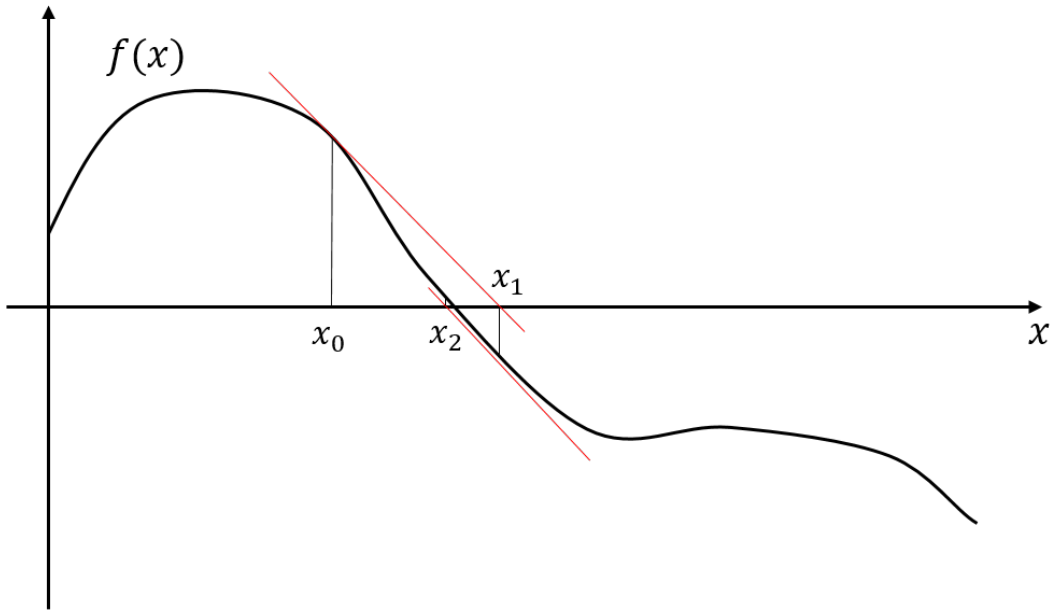

Figure B.1: *The Newton-Raphson convergence mechanism*

In this particular case, the objective function considered is:

$$f(\lambda) = P_{mod}(\lambda) - P_{SCADA} \tag{B.2}$$

with:

$$P_{mod}(\lambda) = \frac{1}{2}\rho\, C_p(\lambda,\theta)\,\pi\, R^2\, U^3(\lambda) \tag{B.3}$$

and:

$$\begin{cases} C_p(\lambda,\theta) & = c_1\left(\frac{c_2}{\lambda_i(\lambda)} - c_3\theta - c_4\theta^{c_5} - c_6\right) exp\left(\frac{-c_7}{\lambda_i(\lambda)}\right) \\ \lambda_i(\lambda) & = \left[\left(\frac{1}{\lambda+c_8\theta}\right) - \left(\frac{c_9}{\theta^3+1}\right)\right]^{-1} \\ U(\lambda) & = \frac{\omega R}{\lambda} \end{cases} \tag{B.4}$$

where the c_i are the coefficients tabulated in Table 4.2, and the rotational speed ω and pitch angle θ are known from the SCADA measurement. In Equation (B.4), there might be some issues when θ is negative, in particular when $\theta \simeq -1$ in the variable speed region. As a consequence, θ is converted into its absolute value whenever it is negative.

The expression for the derivative of the objective function can thus be developed as:

$$f(\lambda) = P'_{mod}(\lambda) = \frac{1}{2}\rho\pi R^2 \left(C'_p(\lambda,\theta)U^3(\lambda) + C_p(\lambda,\theta)3U'(\lambda)U^2(\lambda)\right) \tag{B.5}$$

with:

$$\begin{cases} C'_p(\lambda,\theta) & = c_1 exp\left(\frac{-c_7}{\lambda_i(\lambda)}\right)\frac{\lambda'_i(\lambda)}{\lambda_i^2(\lambda)}\left(-c_2 + c_7\left(\frac{c_2}{\lambda_i(\lambda)} - c_3\theta - c_4\theta^{c_5} - c_6\right)\right) \\ \lambda'_i(\lambda) & = \frac{1}{(\lambda+c_8\theta)^2}\left[\left(\frac{1}{\lambda+c_8\theta}\right) - \left(\frac{c_9}{\theta^3+1}\right)\right]^{-2} \\ U'(\lambda) & = -\frac{\omega R}{\lambda^2} \end{cases} \tag{B.6}$$

The final value of lambda is thus obtained as follow:

1. Knowing P_{SCADA}, ω and θ from the 1-sec SCADA measurement, an initial value λ_0 is guessed for the TSR. This guess is taken at 9 as it is the optimal TSR value in variable speed region.
2. The following value of the TSR is given by the Newton-Raphson expression: $\lambda_1 = \lambda_0 - \frac{f(\lambda_0)}{f'(\lambda_0)}$, using the objective function and the expressions defined above.
3. The difference between the two values $|\lambda_1 - \lambda_0|$ is calculated, if this difference is above a certain threshold then a new iteration of the Newton-Raphson algorithm is launched using λ_1 instead of λ_0. The threshold criteria is taken as 10^{-3}.
4. Finally once the algorithm has converged and the final value for the TSR λ_{conv} has been found, the REWS is simply given by: $U_{REWS} = \frac{\omega R}{\lambda_{conv}}$.

B.2 Implementation of the Wake Models

B.2.1 Jensen Model

In this section is presented the different equations and the procedure used to compute the wind speed deficit as a function of the distance l between the two turbines and the relative wind direction θ, as presented in Figure B.2 below.

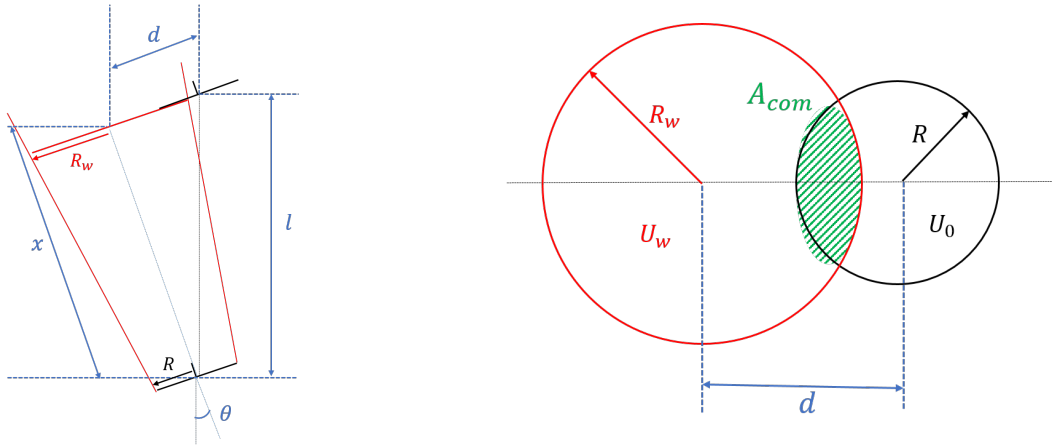

Figure B.2: *Sketch of the problem with the different parameters used for the equations*

The other inputs for the calculation procedure are the upwind wind turbine radius R (which is kept constant at 41 m all over the study) and thrust coefficient C_t, and the wake decay constant α. Then the different steps are followed:

1. The wake radius R_w and wind speed deficit δ_w are calculated at the distance $x = l\cos\theta$ using Equation (5.1) and Equation (5.3).
2. The distance between the downwind rotor center position and wake center $d = x\tan\theta$ is computed.
3. The combined swept area A_{com} between the wake radius and downstream radius is obtained using the following conditions:
   - if $d < R_w - R$, then $A_{com} = \pi R^2 = A_{rot}$
   - if $d > R_w + R$, then $A_{com} = 0$
   - else,

$$A_{com} = R_w^2 \arccos\left(\frac{d^2 + R_w^2 - R^2}{2dR_w}\right) + R^2 \arccos\left(\frac{d^2 + R^2 - R_w^2}{2dR}\right) - \frac{1}{2}\sqrt{(-d+R+R_w)(d+R-R_w)(d-R+R_w)(d+R+R_w)}$$

4. Finally, the effective wind deficit at the downstream rotor is calculated by integrating the point-wise wind speed over the whole area of the rotor and assuming a balance of momentum:

$$U_{eff} = \sqrt{\frac{1}{A_{rot}}\int_{A_{rot}} U^2 dA} \tag{B.7}$$

Considering a constant inflow wind speed U_0 and a constant wind speed inside the wake, the effective wind speed equation at the downstream rotor can be expressed simply as:

$$U_{eff} = U_0\sqrt{\frac{A_{com}}{A_{rot}}(1-\delta_w)^2 + \left(1 - \frac{A_{com}}{A_{rot}}\right)} \tag{B.8}$$

B.2.2 Larsen Model

The Larsen model is a bit more difficult to implement as the wake deficit in the wake is no longer constant but is now a function of the radius r from the axis of symmetry.

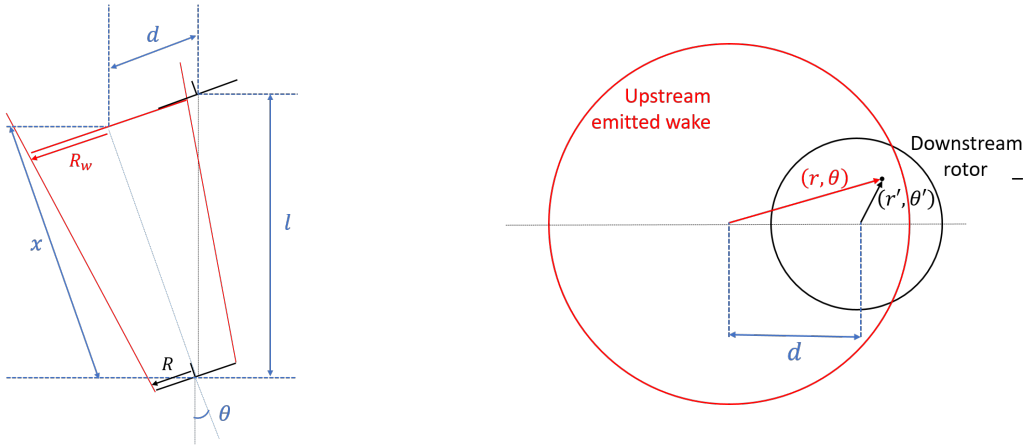

Figure B.3: *Sketch of the problem for the integration of the Larsen model*

Considering the situation as presented on Figure B.3, the point-wise wake deficit $U_x(x,r)$ can be calculated using the Equation (5.12) presented in Section 5.2 (the radial perturbation is not taken into account). To calculate the effective over the complete area of the rotor, it is thus needed to integrate this point-wise deficit over the area. As already mentioned, Larsen proposed two ways of realizing this integration but only the linear approach is used here and written again on Equation (B.9) below.

$$U_{x,eff}(x) = \frac{1}{A_{rot}} \int_{A_{rot}} U dA = \frac{1}{A_{rot}} \int_{\theta'=0}^{2/pi} \int_{r'=0}^{R} U_x(x,r') dr d\theta \tag{B.9}$$

As integrals are generally not very convenient to implement into numerical models, Larsen proposed in is later version of the model [47] an efficient way to compute Equation (B.9) using 4-point Gauss integration. Introducing the transformation variable:

$$\begin{aligned} \tilde{r} &= \frac{2r}{R} - 1 \\ \tilde{\theta} &= \frac{2\theta}{2\pi} - 1 \end{aligned} \tag{B.10}$$

the above equation can be approximated by the following expression:

$$U_{x,eff}(x) \simeq \frac{\pi R^2}{4A_{rot}} \sum_{j=1}^{4} \sum_{i=1}^{4} w_i w_j U_x \left(x, \frac{R(\tilde{r}_i + 1)}{2} \right) (\tilde{r}_i + 1) \tag{B.11}$$

where $(\tilde{r_i}, \tilde{\theta_1})$ and w_i are the Gauss coefficients and weights indicated on Equation (B.12) below.

$$\begin{cases} \tilde{r_1} = \tilde{\theta_1} = -0.339981043584856, & w_1 = 0.652145154862546 \\ \tilde{r_2} = \tilde{\theta_2} = -0.861136311594053, & w_2 = 0.347854845137454 \\ \tilde{r_3} = \tilde{\theta_3} = 0.339981043584856, & w_3 = 0.652145154862546 \\ \tilde{r_4} = \tilde{\theta_4} = 0.861136311594053, & w_4 = 0.347854845137454 \end{cases} \tag{B.12}$$

Equations (B.9) and (B.11) are valid only for full wake situation, when the downstream rotor the upstream emitted wake are perfectly aligned. When it is not the case, as presented on Figure B.3, a transformation between the (r,θ) and (r',θ') coordinate system must be done. Assuming that the wake and rotor center are at the same altitude and separated by a distance d, it can be written:

$$\begin{aligned} rcos(\theta) &= d + r'cos(\theta') \\ rsin(\theta) &= 0 + r'sin(\theta') \\ \Rightarrow r^2 &= d^2 + (r')^2 + 2dr'cos(\theta') \end{aligned} \tag{B.13}$$

Applying again the 4-point Gauss integration with the same variable transformation of Equation (B.10), the final expression for effective wake deficit at the upstream rotor can be derived as:

$$\begin{aligned} U_{x,eff}(x) &\simeq \frac{\pi R^2}{4A_{rot}} \sum_{j=1}^{4} \sum_{i=1}^{4} w_i w_j U_x\left(x, \tilde{r_{ij}}\right)(\tilde{r_i}+1) \\ \text{with} \quad \tilde{r_{ij}} &= \sqrt{d^2 + \frac{R^2(\tilde{r_i}+1)^2}{4} + d(\tilde{r_i}+1)Rcos(\pi(\tilde{\theta_j}+1))} \end{aligned} \tag{B.14}$$

with the same Gauss coefficients and weights and taking into account the following condition:

$$U_x\left(x, \tilde{r_{ij}}\right) = 0 \quad \text{if} \quad \tilde{r_{ij}} > 0 \tag{B.15}$$

The procedure followed for the implementation of Larsen model is thus developed below:

1. Calculate the values of the parameters x_0 and c_1 with the equation defined in [47]:

$$x_0 = \frac{9.6D}{\left(\frac{2R_{9.6D}}{d_1 D}\right)} \tag{B.16}$$

$$\text{with} \quad d_1 = \sqrt{\frac{1 + 1/\sqrt{1 - C_t}}{2}} \tag{B.17}$$

$$\text{and} \quad R_{9.6D} = a_1 exp(a_2 C_t^2 + a_3 C_t + a_4)(b_1 I_a + 1)D \tag{B.18}$$

$$c_1 = \left(\frac{d_1 D}{2}\right)^{5/2} \left(\frac{105}{2\pi}\right)^{-1/2} (C_t A x_0)^{-5/6} \tag{B.19}$$

   where a_i and b_1 are empirical coefficients tabulated in [47] and I_a the ambient turbulence intensity.

2. Calculate the distance d between the wake center and downwind rotor center: $d = x \tan\theta$.

3. Determine the wake radius at the distance x using Equation (5.11).

4. Apply Equations (B.14) and (B.15) to realize the 4-point Gauss integration.

5. Finally deduce the effective inflow wind speed as:

$$U_{eff} = 1 + \frac{U_{x,eff}}{U_0} \tag{B.20}$$